Study of dense partonic systems in Quantum Chromodynamics

Javier López Albacete
Departamento de Física Teórica y del Cosmos
Universidad de Granada

May 16, 2005

Editor: Editorial de la Universidad de Granada
Autor: Javier López Albacete
D.L.: Gr. 921 - 2005
ISBN: 84-338-3414-2

Trabajo presentado para su aceptación como tesis doctoral y la obtención del grado de Doctor en Física por la Universidad de Granada.

Abstract

This thesis is concerned with the high-energy, small-x domain of Quantum Chromodynamics. The relevant physics is that of dense partonic systems, for which the interactions between partons cannot be neglected. These interactions lead, in the case of nuclear collisions, to coherence phenomena that shadow the structure function of a nucleus with respect to that of its constituents nucleons. A phenomenological model for nuclear shadowing based on its relation with diffractive processes, given by the Abramovsky-Gribov-Kancheli cutting rules, is presented in the first part of the thesis. Comparison with experimental data, as well as predictions for the reduction of multiplicities at the LHC experimental program on heavy ion collisions, are given.

The second part of the thesis is dedicated to the study of small-x non-linear evolution. At high energies, the fast growth of gluon densities predicted by linear evolution is expected to be slowed down by gluon recombination processes. This phenomenon, known as saturation of the hadron wavefunction, is one of the main features of high-energy evolution and is expected to restore unitarity of hadronic cross sections at ultra-high energies. The discussion is centered on the Balitsky-Kovchegov equation in the local approximation as the simplest, most basic non-linear evolution equation, both in coordinate and momentum representation. Numerical solutions and analytical estimates for the Balitsky-Kovchegov equation are provided, including in an effective way next-to-leading logarithmic corrections emerging from the running of the coupling. A detailed study of the geometric scaling property of the solution, found both in fixed and running coupling evolution, as well as the energy and nuclear size dependence of the saturation scale, are given.

Finally, the behaviour of the Cronin effect —the observed enhancement in the particle yield at intermediate transverse momenta in proton-nucleus collisions with respect to proton-proton collisions— is studied. It is shown that small-x evolution erases any such enhancement present in the initial condition, turning into a relative suppression with increasing rapidity.

Contents

Acknowledgments

En primer lugar quiero manifestar mi más sincero agradecimiento a Néstor, mi director de tesis. Trabajar junto a él ha sido una experiencia enormemente enriquecedora, de gran aprendizaje y maduración como científico. Además, sin su apoyo incondicional y su paciencia infinita hubiese sido del todo imposible la culminación de esta tesis doctoral.

Este trabajo tiene un cierto aire nómada por los muchos sitios en los que trabajé y viví para poder hacerlo, lo que hace que, afortunadamente, deba gratitud a muchas personas que conocí y me ayudaron en este peregrinar. En primer lugar, siguiendo el orden cronológico de mis viajes, quiero agradecer la cálida acogida que recibí en el Departamento de Física Teórica y del Cosmos de la Universidad de Granada, en el que me sentí como en casa desde el primer día, gracias especialmente a Jose Ignacio Illana y a Paco del Águila. Luego siguió la división de Teoría del CERN, que me brindó todos los medios para pasar allí un excelente año y medio. Ha sido todo un lujo el poder trabajar y, sobre todo, aprender junto a Carlos Salgado, Urs Wiedemann, Alex Kovner y Guilherme Milhano. Especial mención merecen los amigos que allí hice: Nilo, mi salvador tantas veces, Inma, Abraham, Manolo, Cibrán, Sara, Sonia, Teresa, Ana... sin los cuales la vida allí hubiese sido mucho más difícil, y mucho más aburrida. La última parte de la escritura del trabajo la hice en el Departamento de Física de Partículas de la Universidad de Santiago de Compostela, donde fui recibido con la máxima hospitalidad. Finalmente quiero agradecer al Departamento de Física de la Universidad de Córdoba por todas las facilidades que me ha dado y por su comprensión hacia mi sempiterna ausencia.

No puedo olvidarme de mis amigos, de los que, muy a mi pesar, he tenido que separarme para poder hacer esta tesis, pero que siempre han estado a mi lado. Gracias a Jorge, a Javi, a Víctor, a Rubén, a Carlos, a Pepe ...

Este trabajo ha sido financiado por el Ministerio de Educación y Ciencia mediante la concesión de una beca FPU (referencia AP-3333-2001). Las estancias en el CERN fueron posibles gracias a los beneficios complementarios de dicha beca: ayudas para estancias breves, de febrero a agosto del 2003, y al traslado temporal de la beca a dicho centro durante el año 2004. Las estancias en la Universidad de Granada para cursar

el Programa de Doctorado Fisymat fueron posibles gracias a la concesión de una beca de movilidad para alumnos de tercer ciclo por parte del Ministerio de Educación y Ciencia.

Quiero dedicar esta tesis a mis padres, Javier y Caridad, y a mis hermanas, Itziar y Rocio. Siempre habrá mucho de ellos en todo lo bueno que sea capaz de hacer en mi vida.

1 Introduction

The full understanding of the internal structure of hadrons is one of the most fundamental unresolved problems in the physics of elementary interactions. Quantum Chromodynamics (QCD) is the relativistic quantum field theory for strong interactions. It is formulated in terms of quarks and gluons, both of them carriers of strong charge, as the fundamental degrees of freedom.

One of the most remarkable properties of QCD is that of asymptotic freedom, by which the strong coupling diminishes at small distances. This makes perturbative methods well suited for the study of processes involving large momentum transfers i.e. those dominated by small distance phenomena. Indeed, all available experimental data for such processes: DIS at moderate Bjorken-x, Drell-Yan and jet production are consistently described with great accuracy.

However, the study of hadron structure cannot be directly addressed by perturbative techniques, since it is determined by long-range (small momentum) physics, where the strong coupling is large, making meaningless the perturbative expansion. Moreover, there is no fundamental explanation for the problem of confinement: Although QCD is expressed in terms of quarks and gluons as the fundamental degrees of freedom of the theory, only hadrons – colourless combinations of quarks and gluons – are experimentally observed.

Despite this relative failure, perturbative QCD is very successful in determining the evolution of hadron structure. Perturbative evolution equations resum quantum corrections emerging from the variation of energy and momentum scales of the collisions in deep inelastic scattering experiments, where the hadron structure is measured.

So far, the best known and most oftenly used in practical applications, are linear evolution schemes in which the evolution is driven just by radiative processes. This is the case of DGLAP and BFKL evolution equations. However, at sufficiently large energies the hadron becomes a dense system, due to the increasing number of partons added to its wavefunction, and the possibility of gluon recombination processes has to be accounted for. This amounts to include non-linear terms in evolution equations. The role of the non-linearities is to tame the fast increase of gluon densities predicted by linear evolution. They reflect the fact that gluon occupation numbers reach a

maximum value beyond which further growth is suppressed by gluon self-interactions. This phenomenon is commonly refered to as saturation of the hadron wavefunction.

This aim has been largely pursued in the last years in different frameworks. Noticeably, all the approaches to the understanding of the saturation phenomenon converge in the Balitsky-Kovchegov equation, which has been established as the starting point for the study of high-density, saturation effects in high-energy QCD. Its solutions and properties, as well as phenomenological applications, will be discussed in detail all along this thesis.

The need for considering saturation effects is more evident in the case of nuclear collisions, where a large number of gluons is present already at moderate energies. Besides, high-energy nuclear collisions let us study the space-time development of the underlying microscopic processes as well as the presence of coherent collective effects. This is due to the composite nature of nuclei and would be an impossible task in the case of simpler objects i.e. isolated nucleons. One of these collective effects is nuclear shadowing, by which the small-x components of nuclear distribution functions are suppressed with respect to that of its constituent nucleons. A phenomenological model based on its relation with diffractive processes will be presented.

The interest in the small-x domain of QCD has been largely enhanced by two large experimental programs, small-x Deep Inelastic Scattering (DIS) at HERA[1] and nuclear collisions at RHIC[2] and the LHC[3]. In them, the kinematical region in which the saturation phenomenon may show up becomes experimentally accessible.

This memory is structured as follows: In section 2, the basics of the QCD formalism, DIS experiments and the parton model are reviewed, considering the nuclear processes and nuclear shadowing as a particular case. In section 3, the concept of perturbative evolution and standard DGLAP and BFKL schemes are presented, making special emphasis in the small-x problem, as a motivation for the need of non-linear extensions of linear evolution. Section 4 is dedicated to present the different approaches to the study of the small-x, non-linear regime of QCD. Special attention is paid to the BK

[1]Electron-proton collider at the Deutsches Elektronnen-Synchrotron (DESY) in Hamburg, Germany.

[2]Relativistic Heavy Ion Collider at the Brookhaven National Laboratory in Upton NY, USA.

[3]Large Hadron Collider at the European Organization for Nuclear Research (CERN) in Geneva, Switzerland.

equation, its physical content and analytical properties. In the last section current phenomenological applications of the saturation-based formalisms are discussed. Then I present the conclusions of this work. Finally, in the appendix A the Abramovsky-Gribov-Kancheli cutting rules, a key ingredient in the model for nuclear shadowing, are explained.

Three articles published in refereed journals are attached at the end of the memory. In them, the results of the research work that have led to this doctoral thesis, are presented and discussed.

2 QCD, DIS and the parton model

2.1 Quantum Chromodynamics

Quantum Chromodynamics is the theory of strong interactions. For a general reference see e.g. [1]. It is a non-abelian gauge field theory. The gauge symmetry group is $SU(N_c)$, $N_c = 3$. QCD describes the dynamics of adjoint gauge bosons (gluons), coupled to coloured fundamental fermions (quarks), and is defined by the Lagrangian density:

$$\mathcal{L}_{\mathcal{QCD}} = -\frac{1}{4} F_{\mu\nu,a} F^{\mu\nu,a} + \sum_f \bar{\psi}_{i,f} (i\gamma_\mu D^\mu - m_f)_{ij} \psi_{j,f}. \tag{1}$$

Here, the quark fields ψ of flavour f[4] and mass m_f are labeled by colour indexes $i, j = 1, 2, 3$[5]. The covariant derivative is $D^\mu = \partial^\mu + igt_a A^\mu_a$, where g is the QCD coupling constant, and the t_a are the generators of $SU(3)$ in the fundamental representation ($a = 1, ..., 8$). The gluon field strength tensor is $F^{\mu\nu}_a = \partial^\mu A^\nu_a - \partial^\nu A^\mu_a - g f_{abc} A^\mu_b A^\nu_c$, where f_{abc} are the $SU(3)$ structure constants that determine the t_a commutation relations: $[t_a, t_b] = i f_{abc} t_c$.

As in any renormalizable field theory, the strength of QCD interactions depends on the energy scale. Noticeably, in QCD the renormalized coupling diminishes with increasing momentum transfer. This property, known as asymptotic freedom [2,3], allows for perturbative methods to be used reliably in the computation of high-energy QCD processes. The running of the strong coupling, to leading order, is given by

$$\alpha_s(Q^2) = \frac{g^2_{ren}}{4\pi} = \frac{4\pi}{b_0 \ln(Q^2/\Lambda^2)}, \tag{2}$$

where $b_0 = (11N_c - 2N_f)/3N_c$. N_f is the number of quark flavours which can be assumed massless at the energy scale Q^2. Λ is the scale introduced by the renormalization procedure. Its magnitude is set by the typical size of a hadron, $\Lambda \sim 200$ MeV.

[4] f=(u)p, (d)own, (c)harm, (s)trange, (b)ottom, (t)op.

[5] Alternatively, (R)ed, (G)reen, (B)lue.

2.2 Deep Inelastic Scattering

The electromagnetic interaction of leptons is very well understood, making lepton-hadron experiments, Figure 1, the cleanest and most obvious ground for probing the structure of hadrons. The effective probe is the exchanged vector boson of momentum $q = k - k'$. The resolution scale of the probe can be estimated from the uncertainty principle[6]:

$$\lambda \sim \frac{1}{Q}, \qquad \text{with} \quad Q^2 = -q^2 > 0. \tag{3}$$

In Deep Inelastic Scattering (DIS) experiments a lepton is scattered off a hadronic target[7] [4]:

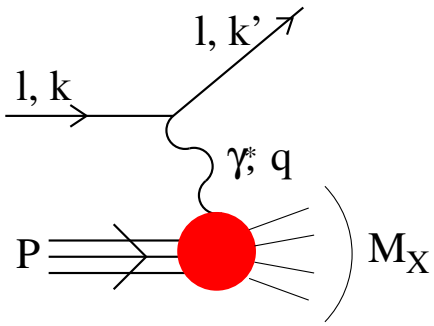

Figure 1: Picture of a DIS process.

Here, k (k') is the momentum of the incoming (outgoing) lepton. The momentum of the virtual exchanged photon is $q = k - k'$, P is the momentum of the hadronic target of mass M, and $p_X = P + q$ the momentum of the final state hadronic system.
This process is best described in term of the following Lorentz invariants:

$$s = (P + k)^2, \tag{4}$$

the center-of-mass energy squared;

[6] In what follows natural units will be used: $\hbar = c = 1, \quad \epsilon_0 = 1$.

[7] In general, the lepton can also be a neutrino. In the most general case the exchanged boson is either a photon or a Z^0 for neutral currents, and a $W^{\pm}$ boson for charged currents. However, for energies much below the Z^0 and $W^{\pm}$ threshold this possibility is strongly suppressed. From now on we shall consider just photon exchange.

$$Q^2 = -q^2 > 0, \tag{5}$$

the virtuality of the exchanged photon; and

$$W^2 = M_X^2 = (P+q)^2, \tag{6}$$

the invariant mass of the hadronic system X. It is also useful to define scaling variables

$$x = \frac{Q^2}{2P\cdot q} = \frac{Q^2}{W^2+Q^2-M^2}, \tag{7}$$

$$y = \frac{P\cdot q}{P\cdot k} = \frac{W^2+Q^2-M^2}{s-M^2}, \tag{8}$$

where the mass of the leptons has been neglected. x is the Bjorken variable, measuring the inelasticity of the process, and y is a measure of the amount of energy transfered between the lepton and the hadron.

The inclusive double differential cross section for the process in Figure 1 is

$$\frac{d^2\sigma}{dxdQ^2} = \frac{2\pi\alpha^2}{Q^4 x}\left[1+(1-y)^2F_2(x,Q^2) - y^2F_2(x,Q^2) - 2xF_1(x,Q^2)\right], \tag{9}$$

where all the information about the structure of the hadron is encoded in the structure functions F_1 and F_2. In eq. (9) the recoil of the hadron has been neglected. A full description of the hadron structure amounts, therefore, to the knowledge of the structure functions for all x and Q^2.

The investigation of the deep structure of hadrons began with the SLAC-MIT experiments of the late 1960s (for a review of these experiments, see [5–7]), where 20 GeV electrons were scattered off proton and deuterium targets.

The picture of nucleons prevalent at that moment was that of extended objects – seen in elastic electron-nucleon scattering – with a diffuse internal structure consistent with the results from pion and proton scattering. By resolving smaller distances than ever before, the SLAC-MIT experiment revealed a new, and conceptually very different, layer on the structure of hadrons. The rate of electrons scattered at large angles was much larger than what could be expected from the diffuse picture, strongly suggesting

that the scattering happened off hard point-like constituents inside the nucleon [8]. Furthermore, scaling of the structure functions was observed [9,10]. Scaling is the fact that the structure functions depend only on one single variable, x, rather than on two as allowed by kinematics. Scaling had been predicted by Bjorken [11] as a result of studies in the framework of current algebras.

2.3 The parton model and parton distribution functions

The parton model, introduced by Feynman, provides an intuitive physical picture of DIS, and a transparent understanding of scaling. Historically it preceded QCD and, by establishing the crucial link between DIS and the quark model of Gell-Mann and Zweig [12,13], was one of the key developments leading to the formulation of QCD as the theory of strong interactions.

Motivated by the SLAC-MIT results, Feynman assumed the existence of point-like constituents – partons – within the hadron. In a reference frame in which the hadron moves at high velocity, the time scale characteristic of interactions between the partons is far larger, due to Lorentz time-dilation, than that characteristic of the interaction with the virtual photon ($\Delta t \sim 1/Q$). A key point in the parton model is that the scattering of the hadron is due entirely to the incoherent elastic scattering of its constituents, which behave as free during the interaction. This is the impulse approximation and is one of the crucial assumptions in the quark parton model. Thus, the DIS cross section can be written as

$$\frac{d^2\sigma}{dxdQ^2} = \sum_f \int_0^1 d\xi \, \phi_{f|p}(\xi) \, \frac{d^2\hat{\sigma}}{dxdQ^2}(l, f), \tag{10}$$

where $\phi_{f|p}$ are the parton distribution functions (p.d.f.'s) i. e. the probability of finding a parton of type f (quark, anti-quark or gluon) in the hadron (p) carrying a fraction ξ of the hadron total longitudinal momentum. Note that the probabilistic character of the p.d.f. is due to the incoherent character of the process and, therefore, to the absence of interference terms. Finally, $\hat{\sigma}$ is the elastic lepton-parton cross section.

In the Born approximation, only quarks couple to the virtual photon. The structure functions can then be written as

$$F_2(x) = \sum_q e_q^2 x \left[q(x) + \bar{q}(x)\right], \tag{11}$$

where e_q is the electric charge of the quark q[8]. $q(x)$ ($\bar{q}(x)$) is the quark (anti-quark) distribution function.

Bjorken scaling is the manifestation of the fact that the scattering occurs off point-like non-interacting constituents. If this were not true, the structure functions would not be independent of Q^2, but rather depend on the ratio Q/Q_0, with $1/Q_0$ being some length scale characteristic of the partons.

Another important feature of the parton model is the Callan-Gross relation [14]

$$F_2(x) = 2xF_1(x), \tag{12}$$

which implies the vanishing of the longitudinal structure function $F_L(x) = F_2(x) - 2xF_1(x)$. This result is a direct consequence of the spin-1/2 nature of the partons (quarks) with which the probe interacts. In fact, the vanishing of the longitudinal cross section in the SLAC-MIT data permitted the identification of partons with quarks.

Gluons do not have electromagnetic charge, so they do not couple directly to photons and are not directly measured in DIS experiments.

The parton model is not a field theory. Although it provides a clear and successful picture of DIS, the proper theoretical description rests with QCD. The parton model is, indeed, the zeroth order approximation of a QCD description of the hadron structure (in the perturbative domain).

In eq. (10) the parton distribution functions have been factorized from the elementary cross section. In other words, long-distance and small-distance physics have been factorized. This factorization has been proven exactly in QCD in the framework of the Operator Product Expansion [15], and together with the concept of evolution constitutes the basis of perturbative QCD (pQCD). While the calculation of parton distribution functions from first principles is intrinsically non-perturbative, their rate of change with the relevant physical scales in the process i.e. energy and momentum transfer,

[8] $e_q = +2/3$ for q=u,c,t and $e_q = -1/3$ for q=d,s,b. The electric charge of an anti-quark $\bar{f}$ is the opposite to that of the quark f.

can be computed perturbatively. Thus, a complete description of the hadronic structure amounts to knowing the parton distribution functions at a certain scale and their evolution laws.

The analysis of the vast amount of experimental data collected in the last thirty years has provided sets of parton distribution functions which can be used reliably as input for any process involving strong interactions at high energy[9].

2.4 Deep Inelastic Scattering on nucleus

The use of nuclei instead of protons in high-energy scattering experiments, such as DIS, provides unique possibilities to study the space-time development of strongly interacting systems. In experiments with nucleon targets the products of the scattering processes can only be observed by a detector that is far away from the collision point, whereas a nuclear target can serve as a detector directly located at the place where the microscopic interaction takes place. Consequently, with nuclei one can study coherence effects in QCD which are not accessible in DIS off nucleons.

2.4.1 Coherence effects: Nuclear shadowing

When considering DIS on a nuclear target one may expect that the resulting nuclear structure functions were very similar to those measured off a nucleon target. This is so because the nucleons are very loosely tighted inside a nucleus, and the interaction between the external probe, the virtual photon, and the constituent nucleons could be expected to be incoherent.

However, the experimental data indicate that the ratio

$$R_{AN}(x,Q^2) = \frac{F_{2A}(x,Q^2)}{AF_{2N}(x,Q^2)}\,, \tag{13}$$

where F_{2A} (F_{2N}) is the nuclear (nucleon) structure function, and A is the mass number of the nucleus i.e. the number of nucleons inside the nucleus is, in general, different from one. The observed difference between the nuclear structure function and that

[9]For details on the background and results of these global fits, see e.g. [16].

corresponding to the simple addition of its constituent nucleons is commonly refered to as the EMC effect [17, 18].

Whether there is enhancement or suppression of the nuclear structure functions with respect to those of the nucleon depends on the kinematical region of interest. The general Bjorken-x dependence of such modification is as follows:

- $R_{AN} > 1$ for $x \to 1$.
- $R_{AN} < 1$ for $0.3 \lesssim x \lesssim 0.8$.
- $R_{AN} > 1$ for $0.1 \lesssim x \lesssim 0.25$.
- $R_{AN} < 1$ for $x \lesssim 0.05$

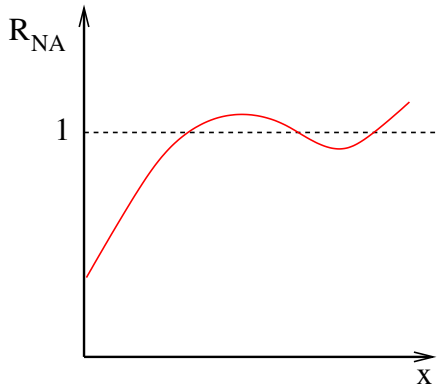

At high energies, small-x, nuclear structure functions are suppressed with respect to those in a nucleon. This phenomenon is known as nuclear shadowing, and its physical interpretation depends strongly on the choice of the reference frame. In a frame in which the nucleus is fast moving, the infinite momentum frame, the constituent nucleons necessarily overlap due to Lorentz contraction and partons associated to different nucleons can interact with each other, as shown in Figure 2, which can result in gluon recombination.

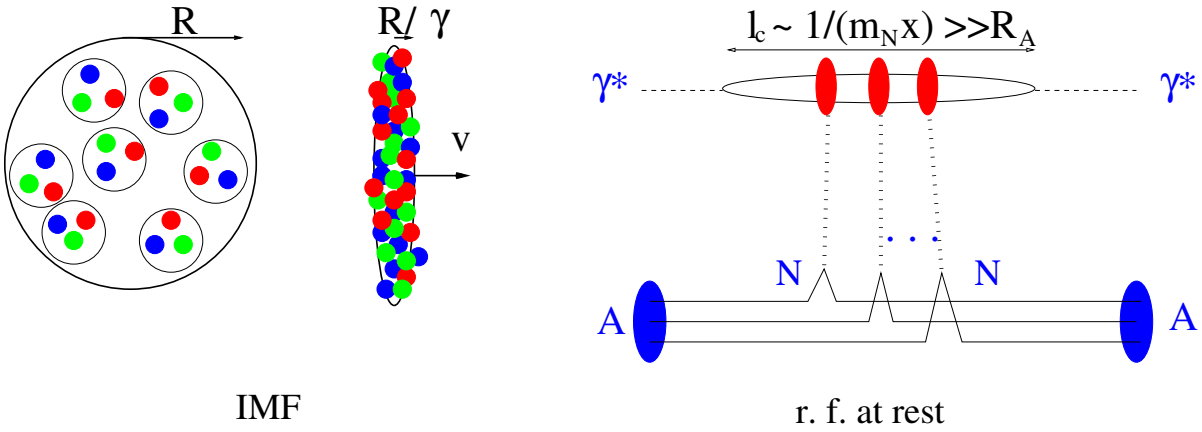

Figure 2: Picture of nuclear shadowing in the infinite momentum frame (left), and in a reference system at rest (right).

In a frame in which the nucleus is at rest, the dipole frame, the virtual photon fluctuates into a quark-antiquark pair long before reaching the nucleus and then multiply scatters with the constituent nucleons. The uncertainty principle lets us estimate the characteristic coherence length of this hadronic fluctuation, $l_c \sim 1/(x\, m_N)$, where $m_N \approx 1$ GeV is the nucleon mass. The amplitude for this process receives contributions from arbitrary number of rescatterings. When l_c happens to be much larger than the nuclear radius ($R_A \sim A^{1/3}$), individual nucleons are not resolved individually, and the interaction is strongly coherent, which leads to the appearance of interference terms that strongly suppress the total cross section, and, therefore, the nuclear structure function.

2.5 Multiple scattering and diffraction

Diffractive processes are those in which the colliding hadron survives to the collision i.e. those in which its internal quantum numbers remain unchanged after the collision. The existence of such processes is due to the internal structure of hadrons, and is difficult to conciliate with the simple partonic interpretation of standard DIS processes. In the latter a quark is struck by the virtual photon and expulsed outside the proton, a colour flux is produced and the proton loses its colour neutrality, which is restored by soft processes, transforming it in a different hadronic state. Thus, the exchanged object in diffractive processes cannot be a quark nor a gluon, because none of them have trivial quantum numbers, but an object with the same quantum numbers as the vacuum. Such an object is called the pomeron [19].

Though there are several theoretical realizations of the pomeron within QCD (the best known one identifies the pomeron with a gluon ladder [20,21]), it remains a mysterious, not very well understood object. Thus, diffractive processes can be defined as those mediated by the exchange of a pomeron. Analogously to standard DIS, diffractive DIS processes are characterized by the diffractive structure function, $F_2^{\mathcal{D}}$.

Nuclear shadowing is intimately related to diffraction by means of the Abramovsky-Gribov-Kancheli (AGK) cutting rules [22] (see also Appendix A), which relate a given amplitude with the cross section that can be obtained from it by cutting[10] the propaga-

[10]Here, the meaning of 'cut' is to put the exchanged particles on their mass-shell i.e. make them satisfy the relativistic dispersion relation for a free particle, $p^2 = m^2$.

tors. These rules, shown in particular cases and postulated in others, make it possible to sum up the contributions arising from different cuts through a simple combinatorial calculation.

In particular, the AGK rules relate the two-scattering amplitude with the cross section for diffractive processes in photon-nucleon scattering [23, 24]. This is very interesting, since this relation links two different physical phenomena.

A model for nuclear shadowing based on this relation is presented in article I. A good description of experimental data is obtained with no free parameters, the only ansatz being the unitarization of the total cross-section i.e. the n-order scattering terms in the expansion of the total scattering amplitude beyond the first and second terms. Two different ways have been considered: Unitarization 'à la Schwimmer' and eikonal unitarization. Within this same formalism we also obtain the factor for multiplicity reduction in nucleus-nucleus collisions, due to the inherent shadowing of their respective wave functions, as well as its dependence on energy, rapidity, impact parameter, atomic size and transverse mass of the produced particles.

3 QCD evolution I: Linear evolution equations

Bjorken scaling in the parton model is a consequence of the non-interacting character of hadron constituents assumed by this model, and is violated once quantum corrections are taken into account. This violation reflects the fact that the quark struck by the virtual photon may have a story prior to the interaction i.e. it may come from a radiation process or have radiated itself new gluons. The differential probability for the emission of a new parton is:

$$dP_i \sim \alpha_s \frac{dx_i}{x_i} \frac{d^2k_t}{k_t^2}\,, \tag{14}$$

where k_t and x_i are the transverse momentum and the fraction of longitudinal momentum of the newly created parton respectively. This probability, when integrated over the available phase space, leads to logarithmic singularities. However one must also include in the calculation quantum loop corrections which are of the same order in the perturbative expansion as those terms for real particle emission. Once it is done, it can

be shown that the singularities coming from the real and virtual quantum corrections exactly cancel each other.

The value of the quantum corrections depends on the energy scales of the DIS process, x and Q^2. Essentially, in spite of the smallness of the coupling, at high scales the phase space for additional emissions increases rapidly and makes the perturbative expansion ill-behaved. The solution to this problem is to resum the leading logarithms coming from quantum corrections to all orders, thus rearranging the perturbative expansion into a more rapidly convergent series. Equivalently, pQCD evolution equations provide the rate of change of parton distributions functions with the variation of the energy scales of the collision.

3.1 DGLAP

The Dokshitzer-Gribov-Lipatov-Altarelli-Parisi (DGLAP) evolution [25–27] is the most familiar resummation strategy. It provides the evolution of hadron structure to higher values of Q. Such processes are dominated by diagrams where the transverse momenta of the successive emitted partons are strongly ordered,

$$\frac{1}{R_h} \ll k_{t1} \ll k_{t2} \cdots \ll k_{tn} \ll Q \lesssim s, \tag{15}$$

where R_h is the length scale of the order of the hadron size, whereas the longitudinal momenta are less constrained:

$$x_B \leq x_n \cdots \leq x_2 \leq x_1. \tag{16}$$

The k_t-ordering gives rise to large logarithms $\ln Q^2$. DGLAP resums terms $\alpha_s \ln Q^2 \sim 1$ to all orders. Subleading terms are suppressed by extra factors of α_s. It relates the probability of finding a parton a in the hadron with a fraction of longitudinal momentum x to that of finding another parton b with fraction $y > x$, at a given scale Q^2, by means of the splitting function P_{ab}[11]:

$$\frac{\partial a(x,Q^2)}{\partial \ln Q^2} = \frac{\alpha(Q^2)}{2\pi} \int_x^1 \frac{dy}{y} P_{ab}(x/y) b(y,Q^2). \tag{17}$$

[11]Here, a and b denote a quark, an anti-quark or a gluon.

The splitting functions are calculated perturbatively as a power series in α_s. Their explicit expressions can be found in [1, 4].

The complete DGLAP evolution equations can be written in a compact matrix way that explicitly shows how different components are mixed through evolution:

$$\frac{\partial}{\partial \ln Q^2} \begin{bmatrix} \Sigma(x,Q^2) \\ g(x,Q^2) \end{bmatrix} = \frac{\alpha_s(Q^2)}{2\pi} \begin{bmatrix} P_{qq} & 2N_f P_{qg} \\ P_{gq} & P_{gg} \end{bmatrix} \otimes \begin{bmatrix} \Sigma(y,Q^2) \\ g(y,Q^2) \end{bmatrix}, \tag{18}$$

where $\Sigma(x,Q^2) = q(x,Q^2) + \bar{q}(x,Q^2)$.

3.2 BFKL

At asymptotically large energies, it is believed that the theoretically correct description of the structure function of DIS processes is given by the Balitsky-Fadin-Kuraev-Lipatov (BFKL) equation [20, 21]. It provides the evolution of hadron structure with increasing center of mass energy of the virtual photon-hadron system, W^2, for a fixed value of the photon virtuality, Q^2. The high-energy limit in which it is formally derived is defined by the conditions

$$\begin{aligned} &W^2 \to \infty \quad , \qquad Q^2 \quad \text{fixed}, \\ &x \simeq \tfrac{Q^2}{W^2} \to 0 \quad , \quad Y = \ln(1/x) \to \infty, \end{aligned} \tag{19}$$

where Y is the rapidity variable. In this limit of very small values of Bjorken-x, the relevant degrees of freedom are gluons, and gluon radiation is the leading mechanism for evolution. Contrary to DGLAP, the leading contribution for BFKL evolution comes from diagrams in which the longitudinal momenta of the successively radiated gluons are strongly ordered, so that each new gluon takes a very small fraction of the energy of the propagating gluon,

$$x_1 \gg x_2 \cdots \gg x_n. \tag{20}$$

The transverse momenta of the gluons in the radiative cascade are no longer ordered, contrary to the case for DGLAP evolution. Rather, they describe a random walk in k_t-space, which leads to a diffusion of the initial distribution to larger and smaller values of k_t.

Under these conditions BFKL resums leading terms $\alpha_s \ln 1/x$ to all orders.

At leading logarithmic accuracy, the BFKL equation reads [28]:

$$\frac{\partial\phi(k,Y)}{\partial \ln(1/x)} = \frac{\alpha_s N_c}{\pi} \int \frac{d^2q}{(k-q)^2} \left[\frac{\phi(q,Y)}{q^2} - \frac{\phi(k,Y)}{q^2+(k-q)^2} \right]. \tag{21}$$

The evolved object is the unintegrated gluon distribution function, $\phi(x,k)$. It gives the probability of finding a gluon in the parent hadron with fraction of longitudinal momentum x and a transverse momentum k. The unintegrated gluon density can be related to the usual integrated one $xG(x,Q^2)$ by

$$xG(x,Q^2) \simeq \int^{Q^2} d^2k \phi(x,k). \tag{22}$$

The sign $\simeq$ in the above equation indicates that there is not a strict equality between integrated and unintegrated distributions, as neither are observables. Indeed, a precise definition of them requires the use of light-front quantization [29].

3.3 Small-x solutions

In order to extract the small-x behaviour of the parton distributions from the DGLAP equations, one has to consider the case where both logarithms, $\ln Q^2$ and $\ln 1/x$, are large. This approximation, the double logarithm approximation of DGLAP (DLA), is valid in the kinematical region where both longitudinal and transverse momenta are strongly ordered:

$$k_{t1} \ll k_{t2} \cdots \ll k_{tn} \ll Q \lesssim s, \tag{23}$$

$$x_1 \gg x_2 \cdots \gg x_n. \tag{24}$$

The DLA solution for the gluon distribution for running coupling is [30, 31]

$$xG^{DLA}(x,Q^2) \sim \exp\left\{ \left(\frac{48}{11-\frac{2}{3}N_f} \ln \frac{\ln Q^2/\Lambda^2}{\ln Q_0^2/\Lambda^2} \ln 1/x \right)^{1/2} \right\}, \tag{25}$$

showing a fast increase with decreasing x.

In the case of BFKL with fixed coupling, for which the equation is derived, the gluon distribution behaves in an even more singular way

$$xG^{BFKL}(x,Q^2) \sim x^{-4N_c \ln 2 \frac{\alpha_s}{\pi}} \sim x^{-0.5}, \quad \text{for} \quad \alpha_s \sim 0.2. \tag{26}$$

3.4 The small-x problem

As discussed in the previous section, both linear evolution schemes, DGLAP and BFKL, predict a sharp rise of gluon densities at high energies (small-x). This singular behaviour for the distribution of soft gluons poses many theoretical problems. The most important one is that it leads to the violation of unitarity, an essential property of quantum field theories.

The energy dependence of total hadron-hadron cross sections is constrained by the Froissart bound [32], which establishes that they cannot grow faster than a logarithm squared of the center of mass energy of the collision, s,

$$\sigma^{hh}(s) \lesssim \frac{1}{m_\pi^2} \ln^2 s, \tag{27}$$

where m_π is the pion mass.

This bound is obtained from unitarity, analiticity properties of the scattering amplitude and from the short range nature of hadronic interactions. Despite the fact that the Froissart bound is not directly applicable to DIS processes, the small-x behaviour of the solutions of linear evolution equations indicate a stronger energy dependence than allowed by this bound, thus violating unitarity.

The strong growth of gluon distributions is rooted in the linearity of evolution equations. In them, only radiative processes that increase the number of partons in the hadron wave function are taken into account, and they implicitly assume that the virtual photon interacts with a single parton in the hadron. Such a picture is only valid if the average distance between partons is larger than the resolution power of the probe or, in other words, if the hadron is a dilute system and parton-parton interactions can be safely neglected. However, due to the radiative processes that drive the evolution to higher energies, more and more partons add to the hadron wave function and a

dense system with a large number of partons is created, see e.g. [33], and gluon fusion processes become important.

Equivalently, as the density grows the distance between partons gets smaller than the resolution length of the probe, which no longer resolves isolated partons. On the contrary, the interaction is now coherent, appearing destructive interference terms which account for gluon recombination processes. The packing factor i.e. the probability of gluon-gluon interaction, serves as an estimator of when saturation effects become sizable:

$$\kappa = \frac{\alpha_s(Q^2) x G(x, Q^2)}{Q^2 R_h^2}. \tag{28}$$

It is equal to the typical cross section for gluon interactions (α_s/Q^2) times the gluon density per unit of transverse area ($xG(x, Q^2)/R_h^2$, with R_h the radius of the hadron). Note that at very high energies, a hadron is essentially a two-dimensional system due to Lorentz contraction in the longitudinal direction. The packing factor becomes of order 1 when evaluated at the saturation momentum, Q_s:

$$Q_s^2(x) = \alpha_s N_c \frac{1}{\pi R_h^2} x G(x, Q_s^2). \tag{29}$$

Thus, the saturation scale has the meaning of the average colour charge squared of the gluons in the hadron wavefunction per unit of transverse area.

For nuclear collisions, assuming that the nuclear gluon distribution is A times that of a nucleon, which may have an anomalous dimension γ, and given the relation between radii $R_A = A^{1/3} R_p$, we get that the packing factor for a nucleus is

$$\kappa_A = \frac{\alpha_s(Q^2) A x G(x, Q^2)}{Q^2 A^{2/3} R_h^2} = A^{1/3(1-\gamma)} \kappa. \tag{30}$$

Thus, it is enhanced by a factor $A^{1/3(1-\gamma)}$ with respect to that of a nucleon. This is why saturation effects are expected to set in at lower energies in nuclear collisions. The saturation mechanism tame the endless growth of gluon occupation numbers and is expected to restore unitarity.

4 QCD evolution II: Non-linear evolution equations

As discussed in the previous sections, a right description of the evolution of hadron structure to high energies requires the inclusion of non-linear terms in the evolution equations. This aim has been pursued during the last 25 years by many groups.

Apart from its intrinsic interest as a theoretical problem, a deeper study of the small-x domain has also been triggered by experimental needs. A good knowledge of parton distribution functions at small-x is relevant in the analysis of data coming from several currently active experimental programs:

On one hand, saturation-based models successfully account for a wide range of data from DIS and Diffractive Deep Inelastic Scattering (DDIS) at small-x from the HERA experimental program.

On the other hand, small-x physics is important in determining the initial conditions for heavy ion collisions. In such collisions it is believed that the Quark Gluon Plasma is formed [34–36].

All these approaches share a common goal of attempting to improve, in one form or another, the standard linear evolution schemes to make them suitable for the description of the non-linearities characteristic of the high-energy domain, see Figure 3. In this section I will review some of these approaches.

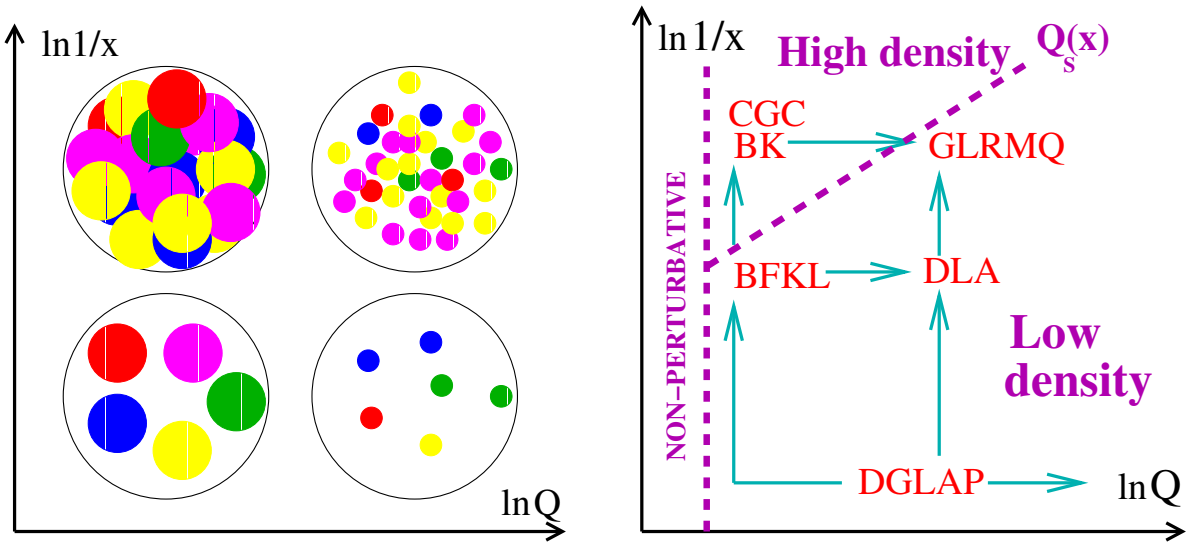

Figure 3: Scheme of evolution equations in the $\ln 1/x - \ln Q$ plane.

4.1 GLRMQ

Historically, the first step in that direction dates back to the early eighties. Gribov, Levin and Ryskin [37] developed a picture of parton recombination, introduced the concept of saturation and proposed the first non-linear evolution equation. This equation includes non-linear gluon fusion terms by resuming multiple pomeron exchange in the double logarithmic approximation and in the large-N_c limit. The resulting equation, with the coefficient of the non-linear term determined by Mueller and Qiu [38] for a low density picture of a spherical proton of radius R, reads

$$\frac{\partial^2 xG(x,Q^2)}{\partial \ln(1/x)\partial \ln Q^2} = \frac{\alpha_s N_c}{\pi} xG(x,Q^2) - \frac{4\alpha_s^2 N_c}{3C_F R^2}\frac{1}{Q^2}[xG(x,Q^2)]^2. \tag{31}$$

The more refined analysis by Muller and Qiu also includes non-linear modifications to the sea quark distributions. The linear limit of eq. (31) reproduces the DLA-DGLAP equation.

4.2 The Color Glass Condensate

Another approach for the study of systems with large gluon densities relies in the applicability of semi-classical methods. In such multiparticle systems, the occupation numbers of gluons with transverse momentum smaller than the saturation momentum, N_k with $k < Q_s$, are large, larger than the Heisenberg commutator for creation, $a(k)$, and annihilation, $a^\dagger(k)$, operators:

$$[a, a^\dagger] = 1; \quad aa^\dagger \sim N_k \gg 1. \tag{32}$$

These conditions define a classical system and allow to treat the small-x gluons as classical gauge fields. Besides, a dense gluon system is characterized by a large saturation momentum, so one may expect that it would also be the relevant scale for the running of the coupling. For large values of Q_s we are in a weak coupling regime, $\alpha_s(Q_s) \ll 1$, so pQCD methods can be applied.

4.2.1 The Classical Theory. The MV model

Such approach was pioneered by McLerran and Venugopalan [39–41] (MV) as an attempt to calculate, from first principles, the parton distribution functions at small-x for a large ultrarelativistic nucleus. The MV model makes a sharp distinction between fast and soft modes in the hadron wavefunction. The fast modes correspond to the energetic partons (valence quarks), those carrying a large fraction of momentum of the parent hadron, whereas the small-x gluons are the soft modes.

The separation between fast and soft modes is more precisely done in terms of their light cone (LC) momentum[12], p^+. Partons with $p^+ > \Lambda^+$ are considered fast and those with $q^+ < \Lambda^+$, soft. $\Lambda^+ = xP^+$ is an arbitrary scale at which the theory is defined and P^+ is the LC momentum of the parent hadron. This separation of modes is physically justified in a frame in which the hadron is fast moving, the infinite momentum frame (IMF). In this frame the hadron LC momentum is large $P^\mu = (P^+, 0^-, 0_\perp)$, with $P^+ \gg \Lambda_{QCD}$. The fast partons move in the z direction with large longitudinal momentum, p^+. As quantum fields they are delocalized within a distance $\lambda \sim 1/p^+$, much smaller than that corresponding to the soft gluons, $1/q^+$, so they appear to be sharply localized in the light-cone. The fast partons can either emit or absorb soft gluons, but in a first approximation they do not deviate from their light-cone trajectories $x^+ = 0$ (eikonal approximation), so that they are integrated out and no longer considered as dynamical modes. Thus they generate a colour current only in the + direction, $J^\mu_a = \delta^{\mu+}\rho_a(x^-, x_\perp)$.

In the MV model, one assumes that the soft gluons can be described as classical colour fields, A^a_μ, found after solving the Yang-Mills equations of motion with the static source:

$$D_\nu F^{\mu\nu} = \delta^{\mu+}\rho_a(x^-, x_\perp). \tag{33}$$

Fast partons are treated as a random variable. All the information about them is

[12]For an arbitrary 4-vector $a^\mu = (a_0, a_1, a_2, a_3)$ the LC coordinates $a^\mu = (a^+, a^-, a_\perp)$ are defined as follows:

$$a^+ = \frac{a_0 + a_3}{\sqrt{2}}, \qquad a^- = \frac{a_0 - a_3}{\sqrt{2}}, \qquad a_\perp = (a_1, a_2).$$

The scalar product reads $a \cdot b = a^+b^- + a^-b^+ - a_\perp \cdot b_\perp$. The p^- and p^+ component are commonly refered to as LC energy and longitudinal momentum respectively, and x^+ and x^- as the LC time and longitudinal coordinate.

encoded in a functional weight $W_\Lambda[\rho]$ that gives the probability of having a certain configuration of the source in the hadron at a scale Λ^+. In order to compute any physical observable involving the small-x gluons, $\mathcal{O}(A^a_\mu)$, one must first solve the equations (33) for the classical gluon fields and then average over all possible configurations of the sources:

$$\langle \mathcal{O}(A^a_\mu[\rho])\rangle_\Lambda = \int \mathcal{D}\rho W_\Lambda[\rho]\mathcal{O}(A[\rho]). \tag{34}$$

Even though the MV model is a leading order approximation in the strong coupling, it is intrinsically non-perturbative. A standard perturbative expansion is not only a expansion in powers of the coupling, but also in powers of the charge density. In the MV model, the charge density is not assumed to be small. On the contrary, interesting non-linear saturation effects are expected when the density is large, of order α_s^{-1}.

Noticeably, the unintegarated distribution functions found in the MV model with a gaussian ansatz for the statistical weight, W_Λ, saturate i.e. they show a power-like, perturbative behaviour for large values of the transverse momentum, while they show a much milder logarithmic behaviour for small transverse momentum (smaller than the saturation momentum):

$$\phi^{MV}(x,k_\perp) \sim \begin{cases} \ln(k_\perp^2/Q_s^2) & \text{for} \quad k_\perp \ll Q_s, \\ Q_s^2/k_\perp^2 & \text{for} \quad k_\perp \gg Q_s. \end{cases} \tag{35}$$

4.2.2 The Quantum Theory. The Renormalization Group Equation

The MV model is purely classic. It is well suited to describe gluon modes with a value of x close to that at which the classical action is defined, $x \lesssim \Lambda^+/P^+$. However, the quantum corrections to this classical approximation are large if one tries to describe modes with a much smaller value of x. For $x' = bx$, they are of order $\ln 1/b$ and, therefore, become large for $b \ll 1$. This is due to the fact that the separation scale between hard and soft modes is totally arbitrary, and the interactions do not disappear as we move away from this scale.

These corrections can, however, be resumed by means of a renormalization group procedure in which quantum fluctuations inside the momentum strip $\Lambda^+ > p^+ > b\Lambda^+$

are integrated out and incorporated in the effective theory by renormalizing the colour sources, ρ_a, and its correlations (that is, the statistical weight $W_\Lambda[\rho]$). In this way the classical + quantum calculation can be reproduced by a purely classical calculation, but with a modified statistical weight $W_{b\Lambda}$, whose variation with the scale is given by a Renormalization Group Equation (RGE). The resulting evolution equation is

$$\frac{\partial W_x[\rho]}{\partial \ln 1/x} = \alpha_s \left\{ \frac{1}{2} \frac{\delta^2}{\delta\rho_x^a(x_\perp)\delta\rho_x^b(y_\perp)}[W_x\chi_{xy}^{ab}] - \frac{\delta}{\delta\rho_x^a(x_\perp)}[W_x\sigma_x^a] \right\}. \tag{36}$$

The resummation is done at leading logarithmic accuracy, $\alpha_s \ln 1/x$, but to all orders in the strong background fields. The quantities $\chi[\rho]$ and $\sigma[\rho]$ in eq. (36) have the meaning of the mean fluctuation and the average value of the extra charge density induced by the high longitudinal momentum modes that have been integrated out.

Eq. (36) was first derived by Jalilian-Marian, Kovner, McLerran and Weigert in [42], and has been further analyzed and discussed in many works [43–48].

In the low density, or weak field, limit this equation linearizes and reduces to the BFKL equation, as shown in ref. [49].

4.2.3 The Balitsky hierarchy

In the Color Glass Condensate (CGC) approach, the evolution of the dense glue is obtained by boosting the target, which induces additional gluon radiation. An alternative formalism to the CGC approach to study unitarization at high energy was developed by Balitsky from the operator product expansion for high-energy scattering [50]. In this approach the target is not evolving, but is taken to be a high-density system represented by strong colour fields, and the evolution is achieved by boosting the projectile. The projectile is assumed to have quark and gluon components, whose propagation through the dense target is given, in the eikonal approximation, by Wilson lines:

$$V(x) = P \exp\left\{ ig \int dx^- A_a^-(x^-, x) t_a \right\}, \tag{37}$$

where t^a are in the fundamental (adjoint) representation for quarks (gluons), and A^- the target colour fields, in the light-cone gauge $A^+ = 0$.

More precisely, Balitsky's equations form an infinite hierarchy of coupled equations

for correlators of these Wilson lines. Weigert showed in [51] the complete equivalence between JIMWLK equations and the Balitsky hierarchy.

4.3 BK equation

The infinite set of coupled equations given by the JIMWLK-Balitsky hierarchy is very difficult to handle in practice. Their solutions are not known analytically nor easy to find numerically [52].

The mean-field version of JIMWLK-Balitsky hierarchy was derived by Kovchegov in the limit of large number of colours as a single closed non-linear evolution equation for the imaginary part of the dipole scattering amplitude off a hadronic target [53]. The resulting equation, known as the Balitsky-Kovchegov (BK) equation, has become, despite its approximate nature, the starting point for the study of unitarity effects in high energy evolution of hadron structure.

Kovchegov's derivation relies in the Mueller dipole picture for high energy evolution [54,55]. It exploits the equivalence betweens gluons and zero-size quark-antiquark pairs given by the large-N_c limit. This equivalence is straightforward from the Fierz identity

$$\sum_a t^a_{ij}\, t^a_{kl} = \frac{1}{2}\delta_{il}\,\delta_{jk} - \frac{1}{2N_c}\delta_{ij}\,\delta_{kl}, \tag{38}$$

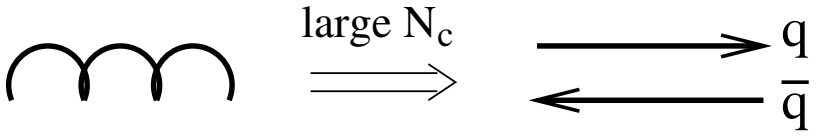

Figure 4: Equivalence between gluons and $q\bar{q}$ pairs in the large-N_c limit.

so that quark and gluons are replaced by dipoles as the effective degrees of freedom at small-x.

The relation between the dipole scattering amplitude and hadron structure becomes clear in the dipole picture of DIS [56], in which the process factorizes into two pieces: First the virtual photon fluctuates into a quark-antiquark pair long before reaching the nucleus. The quark and antiquark are located at transverse positions $\mathbf{x}$ and $\mathbf{y}$

respectively. The probability for such splitting is given by the virtual photon-dipole wavefunction squared. Then the dipole scatters off the hadron at fixed transverse positions (eikonal approximation) with a cross section $\sigma_{dip}(\mathbf{r}, x)$ given by the integral of the imaginary part[13] of the dipole scattering amplitude over the impact parameter b:

$$\sigma^{\gamma^* h}(x, Q^2) = \int_0^1 dz \int d^2\mathbf{r} |\Psi_{TL}^{\gamma^*}(z, \mathbf{r}, Q^2)|^2 \sigma_{dip}(\mathbf{r}, x), \tag{39}$$

$$\sigma_{dip}(\mathbf{r}, x) = 2 \int d^2\mathbf{b}\, \mathcal{N}(\mathbf{r}, \mathbf{b}, x). \tag{40}$$

Here, Ψ_{TL} are the perturbatively computed transverse and longitudinal wavefunctions for the $\gamma^* - q\bar{q}$ system, z is the fraction of the virtual photon's light-cone momentum carried by the quark, $\mathbf{r}$ the dipole size and $\mathbf{b}$ the impact parameter:

$$\mathbf{r} = \mathbf{x} - \mathbf{y}, \qquad \mathbf{b} = \frac{\mathbf{x} + \mathbf{y}}{2}\,. \tag{41}$$

The energy evolution of the collision is by achieved boosting the $q\bar{q}$-dipole to higher rapidity. After the boost gluon emission either by the quark or by the antiquark may take place with a probability

$$dP = \frac{\alpha_s N_c}{2\pi^2} \frac{(\mathbf{x} - \mathbf{y})^2}{(\mathbf{x} - \mathbf{z})^2 (\mathbf{y} - \mathbf{z})^2} dY d^2\mathbf{z}, \tag{42}$$

where z is the transverse position of the emitted gluon.

By means of the gluon-dipole equivalence provided by the large-N_c limit the system after the emission can be seen as an ensemble of dipoles: the pre-existing one and two new dipoles, the one formed by the parent quark and the antiquark line of the gluon $(\mathbf{x}, \mathbf{z})$, and other with the antiquark and the quark line of the gluon, $(\mathbf{y}, \mathbf{z})$. Within this picture further evolution can be interpreted as a dipole branching process.

Thus the scattering amplitude grows due to the contribution of the two newly created dipoles. The BK equation reads:

[13]The dipole scattering amplitude is assumed to be purely imaginary.

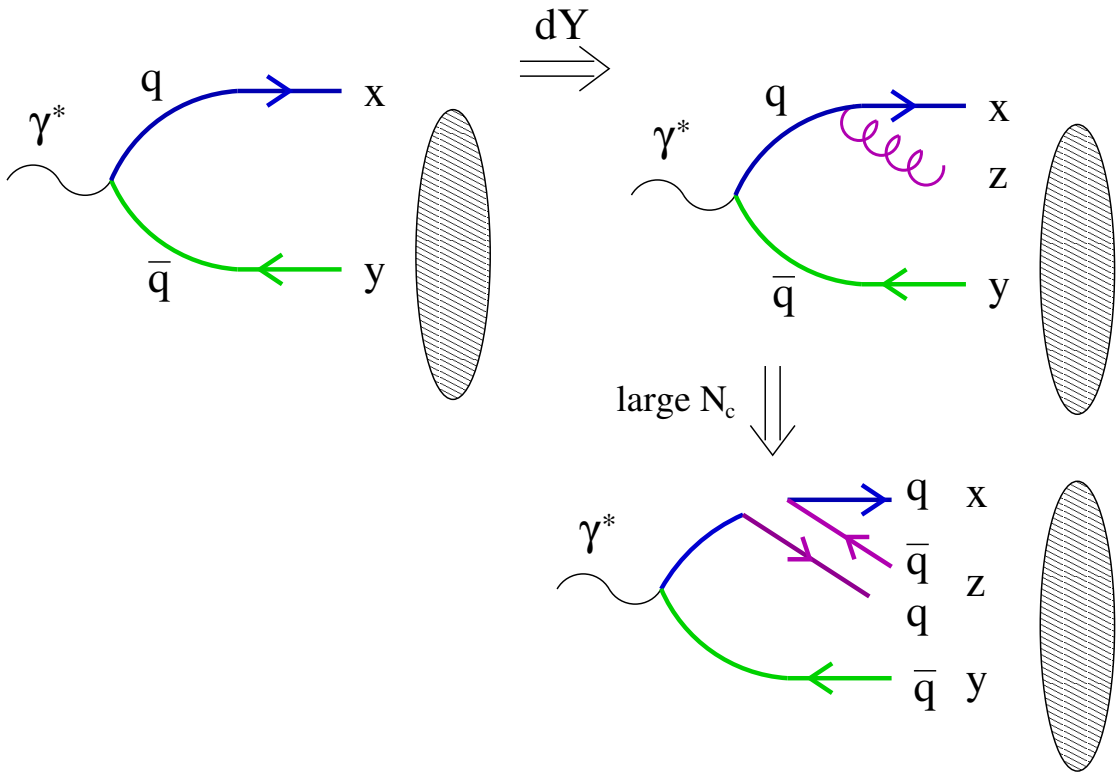

Figure 5: Picture of the evolution encoded in the BK equation.

$$\frac{\partial \mathcal{N}(\mathbf{x},\mathbf{y})}{\partial Y} = \frac{\alpha_s N_c}{\pi} \int \frac{d^2\mathbf{z}}{2\pi} \frac{(\mathbf{x}-\mathbf{y})^2}{(\mathbf{x}-\mathbf{z})^2(\mathbf{y}-\mathbf{z})^2} \left[\mathcal{N}(\mathbf{x},\mathbf{z}) + \mathcal{N}(\mathbf{y},\mathbf{z}) - \mathcal{N}(\mathbf{x},\mathbf{y}) - \mathcal{N}(\mathbf{x},\mathbf{z})\mathcal{N}(\mathbf{y},\mathbf{z})\right] \tag{43}$$

The meaning of this equation is straightforward: The two first terms in (43) account for the separate interaction of the two newly created dipoles. The third term corresponds to the probability of no gluon emission, whereas the non-linear term correspond to the simultaneous interaction of the two new dipoles. This term must be substracted in order to avoid double counting and prevents the amplitude to grow boundlessly with rapidity.

The mean field character of BK equation is understood as follows: In order to get the physical scattering amplitude one has to average the propagation of the quark and antiquark over all possible target configurations,

$$\mathcal{N}(\mathbf{x},\mathbf{y}) = \langle N(\mathbf{x},\mathbf{y})\rangle_{target} = \frac{1}{N_c}\langle 1 - V(\mathbf{x})V^\dagger(\mathbf{y})\rangle, \tag{44}$$

where a summation over colour indexes is understood. In the large-N_c limit the four-

point correlator factorizes into the product of two-point correlators:

$$\langle N(\mathbf{x},\mathbf{y})N(\mathbf{y},\mathbf{z})\rangle = \langle N(\mathbf{x},\mathbf{y})\rangle\langle N(\mathbf{y},\mathbf{z})\rangle + \mathcal{O}(1/N_c^2) = \mathcal{N}(\mathbf{x},\mathbf{z})\mathcal{N}(\mathbf{y},\mathbf{z}) + \mathcal{O}(1/N_c^2). \quad (45)$$

In this way the evolution equation for the two-point function decouples of the one for the four-point function and one gets a single, and relatively simple, closed non-linear evolution equation.

BK is an asymmetric equation in the sense that it does not account for high-density effects in the projectile wavefunction. Indeed, the evolution for the projectile only includes radiative terms and is, therefore, linear. The approximation that the projectile is a dilute object sets the validity of the BK equation and, obviously, breaks down at sufficiently high energy, when the dipole becomes crowded through successive gluon emission. Equivalently, pomeron loops are not included in the BK equation. The non-linearities in BK equation merge from simultaneous multiple scattering and just reflect the gluon recombination processes that occur in the high-density target. The inclusion of non-linear effects in the projectile evolution is a major topic of discussion nowadays [57–60].

The BK equation can also be written in transverse momentum space as an evolution equation for the unintegrated gluon distribution [61]:

$$\frac{\partial\phi(\mathbf{k},Y)}{\partial Y} = \frac{\alpha_s N_c}{\pi^2}k^2\int\frac{d^2\mathbf{q}}{(\mathbf{k}-\mathbf{q})^2}\left[\frac{\phi(\mathbf{q},Y)}{q^2} - \frac{\phi(\mathbf{k},Y)}{q^2+(\mathbf{k}-\mathbf{q})^2}\right] - \frac{\alpha_s N_c}{\pi}\phi^2(\mathbf{k},Y). \quad (46)$$

The dipole scattering amplitude and the unintegrated gluon distribution are related by a Fourier transform:

$$\phi(\mathbf{k}) = \int\frac{d^2\mathbf{r}}{2\pi r^2}e^{i\mathbf{k}\cdot\mathbf{r}}\mathcal{N}(\mathbf{r}). \quad (47)$$

The advantage of working in momentum space is that, assuming no azimuth dependence of the $\phi(x,\mathbf{k})$, the angular integral in eq. (46) can be done analytically, so that one is left with an equation with a single integral,

$$\frac{\partial\phi(k^2,Y)}{\partial Y} = \frac{\alpha_s N_c}{\pi}k^2\int\frac{dq^2}{q^2}\left[\frac{\phi(q^2,Y)-\phi(k^2,Y)}{|q^2-k^2|}+\frac{\phi(k^2,Y)}{\sqrt{4q^4+k^4}}\right]-\frac{\alpha_s N_c}{\pi}\phi^2(k^2,Y), \tag{48}$$

which is very advantageous for numerical purposes. The impact parameter dependence in equations (46), (47) and (48) is implicit.

4.3.1 Analytical Structure

The BK equation (43) has a rich symmetry structure. Introducing complex notation for the transverse vectors i.e. $x = x_1 + ix_2$, $\bar{x} = x_1 - ix_2$, for $\mathbf{x} = (x_1, x_2)$, it can be shown that the measure in eq. (43),

$$\frac{\alpha_s N_c}{2\pi^2}\frac{(\mathbf{x}-\mathbf{y})^2}{(\mathbf{x}-\mathbf{z})^2(\mathbf{y}-\mathbf{z})^2}d^2\mathbf{z}, \tag{49}$$

is invariant under Möbius transformations[14]:

$$x \longrightarrow \frac{ax+b}{cx+d}\,, \qquad \bar{x} \longrightarrow \frac{\bar{a}\bar{x}+\bar{b}}{\bar{c}\bar{x}+\bar{d}}\,, \tag{50}$$

where the parameters $a, b, c, d \in \mathbb{C}$ and $ad - bc \neq 0$. Identical transformations are also applied to $y(\bar{y})$ and $z(\bar{z})$. In particular, BK is invariant under the following elementary transformations:

- global two-dimensional translations by a vector b: $x \to x + b$;
- global two-dimensional rotations by an angle ϕ: $x \to O(\phi)x$;
- scale transformations with a real, positive parameter λ: $x \to \lambda x$;
- inversion (in complex notation): $x \to 1/x$.

Noticeably, if the initial condition, $\mathcal{N}^0(\mathbf{x}, \mathbf{y})$, is invariant under any of the previous transformations, the solutions of the BK equation preserve the corresponding symmetry. In particular, if the initial condition is invariant under translations and rotations,

[14]Provided that the strong coupling constant is fixed.

$\mathcal{N}^0(\mathbf{x},\mathbf{y}) = \mathcal{N}^0(|\mathbf{x}-\mathbf{y}|)$ i.e. it only depends on the dipole size $r = |\mathbf{x}-\mathbf{y}|$ and not on the impact parameter b, then the solution at an arbitrary rapidity Y possesses the same property. The problem of finding the solutions of BK equation simplifies enormously in this case, since only one degree of freedom is relevant, namely the dipole size r. Physically, this approximation, called the local approximation, implies assuming an infinitely large and homogeneous target. This is only meaningful for very small dipoles compared to the target size, sitting close to the center of the target. Moreover, it leads to infinite cross-sections. However, many of the studies both analytical and numerical of the BK equation rely on this approximation as a first approach to the problem.

The scale-invariance of the BK kernel also allows the existence of scaling solutions i.e. solutions that are no longer functions of $\mathbf{r}$, $\mathbf{b}$ and x separately, but of a single variable $\tau = rQ_s(x,b)$, the scaling variable. In them, all the energy and impact parameter dependence is absorbed in the saturation momentum. Under the local approximation the scaling variable is defined as $\tau = rQ_s(x)$.

The scaling property of dipole scattering amplitude can be traced back to scaling of the DIS cross section, $\sigma^{\gamma^* h}$, by means of eq. (39). This is so because the wavefunctions $\Psi_{T,L}$ are proportional to Q^2 times a function of r^2Q^2. Consequently, if scaling holds for the dipole scattering amplitude, $\sigma_{\gamma^* h}$ depends solely on $\tau = Q/Q_s$.

The non-linearities of the BK equation ensure unitarity at the level of the amplitude, i.e. provided that the initial condition does not violate the black-disk limit value, $\mathcal{N}^0(x,y) \leq 1$, this property will be preserved by evolution, $\partial\mathcal{N}/\partial Y \leq 0$ for $\mathcal{N} = 1$.

The BK kernel is divergent for zero-size emitted dipoles. These infrared singularities can be mapped to ultraviolet divergences through the inversion transformation, $x \longrightarrow 1/x$. However, BK and BFKL are divergence-free if the initial condition falls steep enough, $\mathcal{N}(r \to 0) \sim r^\delta$ with $\delta > 0$.

4.3.2 Next-to-leading-log corrections

As discussed in the previous sections, the BK equation includes non-linear corrections to BFKL dynamics. However, BK is derived at leading logarithmic accuracy, and next-to-leading order (NLO) corrections are expected to be large, as it is the case for the BFKL equation [62–66]. Importantly, unitarity effects are expected to become sizable

at lower values of rapidity,

$$Y_U \sim \frac{1}{\alpha_P} \ln \frac{1}{\alpha_s} \,, \tag{51}$$

where $\alpha_P = 1 + \frac{4\alpha_s N_c}{\pi} \ln 2$ is the LO pomeron intercept, than next-to-leading order corrections emerging from the running of the coupling which have been estimated to become important at larger rapidities

$$Y_{NLO} \sim \frac{1}{\alpha_s^{5/3}} \,. \tag{52}$$

Thus, $Y_U \ll Y_{NLO}$ for parametrically small α_s, and NLO effects can be considered subleading with respect to saturation effects in small-x dynamics.

Nowadays there is no a fundamental derivation of NLO BK equation, and NLO effects can only be considered in a phenomenological way. Two main sources for such corrections have been identified: The running of the coupling and kinematical constraints. Both effects are expected to decrease the energy dependence of the saturation momentum with respect to fixed coupling evolution.

Essentially, the running of the coupling suppresses the emission of large transverse momentum gluons (small size dipoles). This retards the growth of the non-saturated part of the gluon distribution, thus slowing down the evolution and taming the increase of the saturation momentum with energy. In the article III, NLO corrections arising from the running of the strong coupling have been included in an effective way through different modifications of the original BK kernel.

Kinematical constraints are addressed by the introduction of a physical rapidity separation parameter Δ, so that successive emitted gluons in the radiative cascade are enforced to have a minimum separation in rapidity, $Y_{i+i} - Y_i > \Delta$.

None of these effects modify the global picture of the evolution, but they are known to be numerically large and, therefore, must be taken into account for realistic phenomenological applications of the BK equation.

4.3.3 Properties of the solution

In spite of the relative simplicity of the BK equation, its exact analytical solutions are not known. In the last years general properties of its solutions have been extensively

studied through a combination of both analytical and numerical methods. Here I will summarize some of these properties.

From dimensional arguments, it is natural to expect scaling of the solution in the region of small momenta, $k_t \leq Q_s$, where the hadron is characterized by a single dimensionful scale, Q_s [67, 68]. However, analytical estimates [69] suggest that the scaling property extends to a larger kinematical region, where the system is dilute and evolution is governed by linear schemes. This region, known as the extended scaling window, is bounded as

$$Q_s \leq k_t \leq \frac{Q_s^2(Y)}{Q_0} \quad , \tag{53}$$

where Q_0 is the initial value of the saturation momentum.

Using non-trivial mathematical properties of a class of non-linear evolution equations, it is possible to obtain the universal terms in the asymptotic expansion in rapidity of the saturation scale and of the unintegrated gluon density (forward scattering amplitude). The meaning of 'universality' is twofold: They are independent of the details of both the non-linear terms in the nonlinear evolution equation and of the initial conditions.

These equations admit traveling wave solutions i.e. scaling solutions. Their existence is possible due to the damping non-linear terms, although most of their asymptotic properties are governed by the linearized equation, being relatively insensitive to the saturating terms. This is why these expansions are valid for a broad range of non-linear equations sharing the same linear limit.

In the case of the BK equation:

$$\partial_Y \mathcal{N} = \alpha\chi\left(-\partial_L\right)\mathcal{N} - \alpha\mathcal{N}^2, \tag{54}$$

where $L = \ln(k^2/\Lambda_{QCD})$, and the function χ is the Mellin transform[15] of the BFKL

[15]The Mellin transform of a function $f(x)$ is defined as:

$$\tilde{f}(\omega) = \int dx e^{-\omega x} f(x),$$

and the inverse transformation as

$$f(x) = \int_{-i\infty}^{+i\infty} \frac{d\omega}{2\pi i} e^{\omega x} \tilde{f}(\omega).$$

kernel:

$$\chi(\gamma) = 2\psi(1) - \psi(\gamma) - \psi(1-\gamma), \tag{55}$$

where $\psi(\gamma) = d\ln\Gamma(\gamma)/d\gamma$ and $\Gamma(\gamma)$ is the Euler gamma function.

The function $\chi\left(-\partial_L\right)$ is an integro-differential operator which can be expanded:

$$\chi\left(-\partial_L\right) = \chi\left(\gamma_0\right) + \chi'\left(\gamma_0\right)\left(-\partial_L - \gamma_0\right) + \frac{1}{2}\chi''\left(\gamma_0\right)\left(-\partial_L - \gamma_0\right)^2 + \ldots \tag{56}$$

for some value γ_0 between 0 and 1 i.e. for the principal branch of the function χ. Retaining only up to the quadratic term in the expansion for $\chi(-\partial_L)$ (this is known as the 'diffusive' approximation), introducing the notation $\omega = \chi\left(\frac{1}{2}\right)$, $D = \chi'''\left(\frac{1}{2}\right)$, and defining $\bar{\gamma} = 1 - \frac{1}{2}\sqrt{1 + 8\omega/D}$, the change of variables

$$t = \frac{\bar{\alpha}D}{2}\left(1-\bar{\gamma}\right)^2 Y \quad , \quad x = \left(1-\bar{\gamma}\right)\left(L + \frac{\bar{\alpha}D}{2}\right), \tag{57}$$

$$u(t,x) = \frac{2}{D(1-\bar{\gamma})^2}\mathcal{N}\left(\frac{2t}{\bar{\alpha}D(1-\bar{\gamma})^2}, \frac{x}{1-\bar{\gamma}} - \frac{t}{(1-\bar{\gamma})^2}\right), \tag{58}$$

brings BK equation into the Fisher-Kolmogorov-Petrovsky-Piscounov (FKPP) equation [70, 71] for u:

$$\partial_t u(t,x) = \partial_x^2 u(t,x) + u(t,x)\left[1 - u(t,x)\right]. \tag{59}$$

It has been proven that FKPP equation, and therefore BK under the diffusive approximation, admits traveling wave solutions at large rapidities. That means that asymptotic solutions are a function w of a single variable such that

$$\mathcal{N}(Y \to \infty) = w\left[\ln k^2 - \ln Q_s^2(Y)\right]. \tag{60}$$

Universal expansions, in the sense defined above, both for the dipole scattering amplitude in the transition region and for the rapidity dependence of the saturation momentum have been determined [72]:

$$\mathcal{N}(k,Y) = C\left(\frac{k^2}{Q_s^2(Y)}\right)^{-\gamma_c}\left[\gamma_c \ln\left(\frac{k^2}{Q_s^2(Y)}\right) + f(z,\gamma_c,\chi,\chi'',\chi^{(3)}) + \mathcal{O}(1/\sqrt{Y})\right]e^{-z^2}, \tag{61}$$

with z being a small parameter that controls the pattern of scaling violations,

$$z = \frac{\ln\left(k^2/Q_s^2(Y)\right)}{\sqrt{2\bar{\alpha}_s\chi''(\gamma_c)Y}}\,, \tag{62}$$

and the leading exponent $\gamma_c = 0.627\ldots$ is the solution of the implicit equation

$$\chi(\gamma_c) = \gamma_c\chi'(\gamma_c). \tag{63}$$

This expansion is valid for the transition between the 'front interior', defined by the condition $z \ll 1$, and the 'leading edge', $z \sim 1$. The behaviour of the saturation scale is

$$\ln Q_s^2(Y) = \bar{\alpha}\frac{\chi(\gamma_c)}{\gamma_c}Y - \frac{3}{2\gamma_c}\ln Y - \frac{3}{\gamma_c^2}\sqrt{\frac{2\pi}{\bar{\alpha}\chi''(\gamma_c)}}\frac{1}{\sqrt{Y}}\,. \tag{64}$$

Theoretical estimations have also been made for running coupling evolution. It has been argued that the extended scaling also holds for running coupling. The proposed asymptotic expansions for the dipole solutions of BK equation and for the rapidity dependence of the saturation momentum are [69, 73]:

$$\mathcal{N}(k,Y) = C\left(\frac{k^2}{Q_s^2(Y)}\right)^{-\gamma_c}\left[\ln\left(\frac{k^2}{Q_s^2(Y)}\right) + \frac{1}{\gamma_c}\right], \tag{65}$$

$$\ln Q_s^2(Y) = aY^{1/2} + bY^{1/6} + c. \tag{66}$$

Noticeably, the leading behaviour of the solution estimated for running and fixed coupling evolution coincide. It is equal to a power, with the same value of the exponent, times a logarithmic correction.

The nuclear size dependence of the saturation momentum has also been object of research. It is encoded in the initial condition

$$Q_{sA}^2(Y=0) = h(A)Q_{sp}^2(Y=0), \tag{67}$$

where $Q_{sA(p)}$ stands for the saturation momentum of a nucleus (proton), and $h(A)$ is some function of its mass number, A.

This dependence is strictly preserved by fixed coupling evolution, provided scale invariance of the initial condition, whereas for running coupling, it has been proposed [74] that, at asymptotically large energies, it would be completely wiped out by running coupling evolution:

$$\ln\left(\frac{Q_{sA}^2(Y)}{Q_{sp}^2(Y)}\right) = \frac{\ln^2\left[\frac{hQ_s^2(Y=0)}{\Lambda^2}\right]}{2\sqrt{\Delta' {}^2 Y}} \longrightarrow 0. \tag{68}$$

This is a very attractive result which would imply universality oh high-energy hadronic processes i.e. independence of the particular class of hadrons involved in the collision.

All the analytical estimations exposed in this section are only valid for the asymptotic and do not keep track of the dependence on the initial conditions, whose influence is extremely important in the early stages of the evolution and, therefore, for phenomenological applications[16].

Most of them have been rederived and checked numerically in the article III, where numerical solutions both for fixed and running coupling evolution up to ultra-high rapidities are provided, as well as a detailed study of their asymptotic properties. In this work, traveling 'soliton-like' wave solutions at asymptotically large energies have been found both for fixed and running coupling evolution. Remarkably, the asymptotic shape of the solutions is different in both cases. This result is contrary to the analytical estimates and needs to be better understood. The energy and atomic mass dependence of the saturation scale derived from our results is in agreement with the expectations shown above.

5 Phenomenology of Saturation

There are two main sources of experimental data with which confront our present knowledge about the saturation phenomenon: Deep Inelastic Scattering experiments at HERA and heavy ion collisions experiments at RHIC. Both situations involve a large number of participating gluons, generated by small-x evolution. In the nuclear

[16]The highest value of rapidity studied at RHIC is $Y \sim 3$, while at HERA it is $Y \sim 9$. At the LHC a maximum measurable value $Y \sim 5 \div 6$ is expected.

case, this evolution is enhanced since the nuclear wavefunction contains many gluons already at moderate values of energy.

It was expected that non-linear corrections should already be considerable at HERA. Indeed, saturation models [75,76] are very successful describing many observables measured at HERA. Nevertheless, present HERA data can also be described rather well both by the simple linear evolution and by models that explicitly exclude saturation [77]. Consequently, no definite statement about the presence of saturation effects in present HERA data can be done.

This can be explained by the fact that HERA data is not extensive in the region of interest. The smallest values of x measured at HERA are $\sim 10^{-5}$ for $Q^2 = 1$ GeV^2. A similar situation happens in current heavy ion collision experiments. Estimations indicate that the relevant value of x in gold-gold collisions at a center of mass energy $\sqrt{s_{NN}} = 200$ GeV per nucleon at RHIC is $x \sim 10^{-2}$. These values are not small enough for the eikonal approximation, underlying in all the formalisms developed for saturation physics, to be plenty reliable, and there may be some ground for finite energy corrections in present data. Moreover, it is questionable whether the saturation momentum associated to these values of x is large enough for perturbative techniques to be safely applied.

With the advent in the next years of the LHC heavy ion program the full coherence domain will be reached and the saturation-based formalisms could be better checked. Besides, the ideal experimental ground to study saturation physics would be in an electron-nucleus collider, where nuclear parton distributions could be directly measured [78–81].

In this section I will discuss the accumulated evidence for the presence of saturation effects in currently available experimental data.

5.1 Saturation in DIS

The dipole formalism has established as a useful tool for the study of deep inelastic and related diffractive cross sections in $\gamma^* p$ scattering. In it, the photon wavefunction constitutes the calculable part of the process whereas the reminder, the dipole cross section, encodes all the information about the hadronic interactions, including unita-

rization effects. The latter is substantially influenced by nonperturbative contributions and needs to be modeled. The most successful model for the dipole cross section is the one proposed by Golec-Biernat and Wüstoff (GBW) [75]. The GBW model includes saturation effects and is very economical in the number of parameters which are used.

5.1.1 GBW model

Golec-Biernat and Wüsthoff proposed the following ansatz for the dipole cross section

$$\sigma_{dip}(r,x) = \sigma_0 \left(1 - \exp\left\{-\frac{r^2 Q_s^2(x)}{4}\right\}\right), \tag{69}$$

where $Q_s(x)$ plays the role of the saturation momentum parametrized as $Q_s^2(x) = (x_0/x)^\lambda$ GeV^2. σ_0 is a global normalization factor that accounts for the lack of impact parameter dependence on the model. The three free parameters of the model are determined from a global fit to small-x DIS data from HERA ($x \leq 0.01$ and $Q^2 \leq 45$ GeV^2). Their values are:

$$\sigma_0 = 23.03\,\text{mb}, \qquad \lambda = 0.288, \qquad x_0 = 3.04 \times 10^{-4}, \tag{70}$$

if only three lights quarks are assumed for the virtual photon wavefunction. These parameters vary slightly if one also considers the charm quark.

This model includes the main features expected for σ_{dip}. Saturation is visible in the fact that the dipole scattering amplitude

$$\mathcal{N}(r,x) = 1 - \exp\left\{-\frac{r^2 Q_s^2(x)}{4}\right\} \tag{71}$$

approaches the unitarity bound $\mathcal{N} = 1$ for dipoles sizes larger than a characteristic size $1/Q_s(x)$. Oppositely, small dipoles are very little interacting and the dipole cross section vanishes as r^2 for small r, leading to Bjorken scaling. This is the well-known property of colour transparency.

The GBW model gives a rather good description of HERA data, both for the inclusive and diffractive structure functions.

More recently a new CGC-inspired saturation model for the dipole cross section was proposed in [76]. It includes gluon saturation effects via an approximate solution of

the BK equation. The resulting dipole cross section is very similar to the GBW one and it has been shown that it leads to similar, successful predictions for DIS and DDIS data.

5.1.2 Geometric scaling

Geometric scaling is the observation that DIS cross section no longer depends on two separate variables, Q^2 and x. Rather it becomes a function on a single variable, $\tau = Q^2/Q_s^2(x)$. Thus, the energy dependence is completely absorbed by the saturation momentum,

$$\sigma^{\gamma^* p}(x, Q^2) \longrightarrow \sigma^{\gamma^* p}\left[\tau = Q^2/Q_s^2(x)\right]. \tag{72}$$

This scaling has been identified in deep inelastic scattering both on proton [82] and nuclear [83] targets at small-x, Figure 6, and reflects in the fact that all data lie within a same universal curve when plotted versus the scaling variable. The atomic size dependence of the saturation momentum extracted from fits to nuclear data is $Q_{sA}^2 \simeq A^{4/9} Q_{sp}^2$.

As was discussed in section 3.3, the BK equation allows for the existence of scaling solutions, so geometric scaling is one of the most compelling indications of the existence of saturation effects in present DIS data. However it remains an open question to elucidate whether this scaling is indeed dynamically generated by non-linear evolution.

5.1.3 Structure functions

Using the dipole picture, the structure function F_2 can be well described by saturation models. The results for the description of the data are remarkably good for $x \leq 10^{-2}$ and $Q^2 \leq 450$ GeV^2. One should note that this description includes both the low and high Q^2 data. Descriptions based on DGLAP evolution can account only for data within its applicability domain, $Q^2 > 1$ GeV^2.

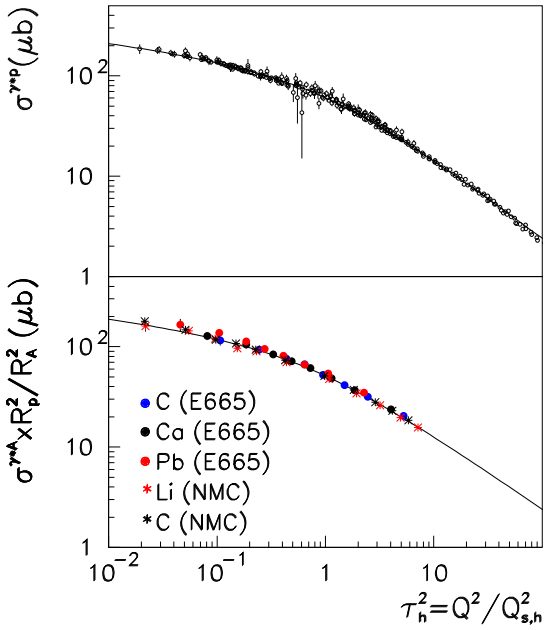

Figure 6: Geometric scaling found in DIS on proton (top) and nuclear (bottom) data.

5.1.4 Diffractive and quasi-elastic processes

The dipole model can also be applied to describe diffractive DIS processes,

$$\gamma^* + p \longrightarrow p + X \tag{73}$$

and diffractive exclusive processes[17], including Deeply Virtual Compton Scattering (DVCS),

$$\gamma^* + p \longrightarrow \gamma + p \tag{74}$$

and vector meson (V_μ) production,

$$\gamma^* + p \longrightarrow V_\mu + p. \tag{75}$$

To compute the DVCS cross-section within the dipole model one must evaluate the light-cone wavefunction of the outgoing real photon at $Q^2 = 0$. This means that the contribution due to longitudinally polarized photons vanishes and the process is purely transverse. Similarly, to compute the cross section for vector meson production one needs the meson light-cone wavefunction, which is usually modeled upon that of the photon.

[17]For a general reference on exclusive processes see e.g. [84].

5.2 Relativistic Heavy Ion Collisions

The experimental programs in relativistic ions started in the mid-seventies using the Bevalac[18] and SIS[19] facilities at LBL[20], and then continued over the years at the Alternating Gradient Synchrotron (AGS) at BNL and the Super Proton Synchrotron (SPS) at CERN. Presently, such collisions are performed at much higher energies at RHIC, which is designed for gold-gold collisions at a center of mass energy per nucleon $\sqrt{s_{NN}} = 200$ GeV.

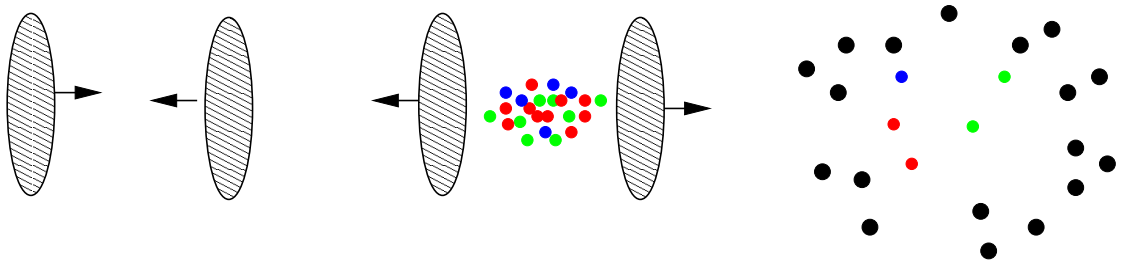

Figure 7: Pictorical representation of heavy ion collisions.

The general picture of heavy ion scattering consists of three stages: First, two energetic nuclei collide, depositing a large ammount of energy in a very small volume. Thus, the initial energy density is very large, eventually larger than the critical energy density[21] required for a phase transition between hadronized matter and deconfined quarks and gluons to take place. It is believed that this system of free quarks and gluons thermalizes, giving rise to a new state of matter, the Quark-Gluon Plasma (QGP). Afterwards the system expands, cools down, the energy density diminishes and, finally, the system hadronizes into the experimentally measured particles.

Deuteron-gold collisions are also performed at RHIC. In them, the initial energy density is not high enough for the QGP formation. Therefore, final state effects are strongly reduced with respect to gold-gold collisions and initial state effects can be more easily isolated.

[18]The Bevalac resulted from the coupling of the synchrotron Bevatron to the Super Heavy Ion Linear Accelerator, Super-HILAC.

[19]Heavy Ion Synchrotron.

[20]Lawrence Berkeley Laboratory at Berkeley, USA.

[21]Lattice QCD calculations estimate that the deconfined phase transitions occurs at energy density $\epsilon_c > 1$ GeV/fm^3.

A significant effort has been done to analyze RHIC data in terms of saturated initial conditions. Two of the experimentally measured signals where saturation can be identified are the intermediate transverse momentum spectrum and the total particle multiplicity.

5.2.1 The Cronin effect

The observed enhancement of particle yields at intermediate transverse momenta in proton-nucleus collisions with respect to proton-proton collisions is commonly refered to as the Cronin effect [85]. It is usually attributed to multiple scattering of the projectile partons propagating through the nucleus before the hard collision that will give rise to the detected particles takes place, which results in a k_t-broadening. The average transverse momentum gained by the projectile is expected to be of the order of the characteristic momentum scale of nucleus, that is, of the order of the saturation momentum.

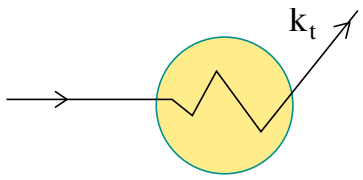

Figure 8: Cronin effect.

The Cronin peak has been observed in deuteron-gold collisions at central rapidity ($Y = 0$) at RHIC. It is usually quantified by means of the nuclear modification factor, R_{pA}:

$$R_{pA} = \frac{\frac{dN_{pA}}{dyd^2pd^2b}}{N_{coll}\frac{dN_{pp}}{dyd^2p\,d^2b}}, \tag{76}$$

where N_{coll} is the number of nucleon-nucleon collisions. R_{pA} is equal to one in the absence of collective nuclear effects.

However, when measured at higher rapidities, the Cronin enhancement tends to disappear and turn into a relative suppression of the produced particle yield [86]. Calculations based on multiple scattering cannot account for this suppression at forward

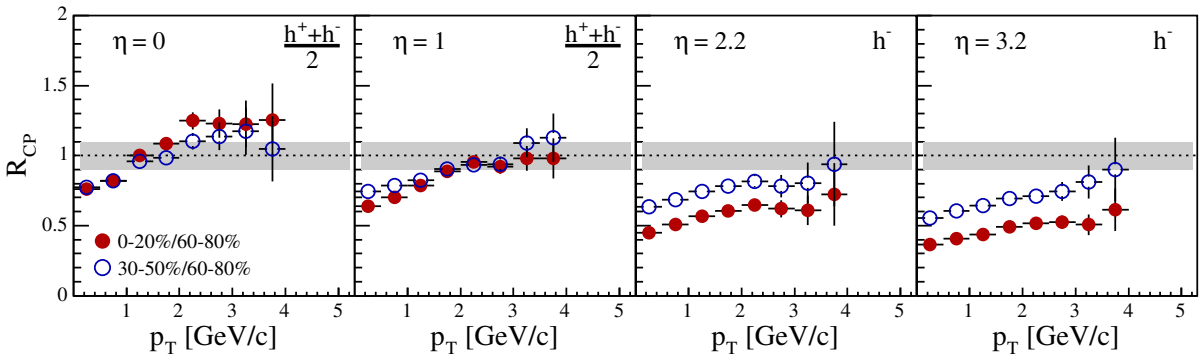

Figure 9: Evolution of the Cronin effect at RHIC measured by the Brahms collaboration.

rapidities. It is the result of the article II that this is a consequence of quantum non-linear evolution.

Oppositely to deuteron-gold collisions, the intermediate p_t hadron spectra at central rapidity is strongly suppressed in gold-gold collisions. The determination of the Cronin effect as an initial state effect was of the uttermost importance to identify the strong suppression of particles with large transverse momentum in Au-Au collisions as a final state effect [87].

5.2.2 Multiplicities

Most of the produced particles at RHIC have a low transverse momentum, below 1 GeV, which is close to the saturation momentum estimated for RHIC, $Q_s^2 \sim 1 \div 2$ GeV^2. Therefore, it is tempting trying to understand the rapidity spectrum $dN/d\eta$ as a manifestation of the saturated gluon distributions in the colliding nuclei. The gross features of the multiplicity distribution are reproduced by saturation based calculations [88, 89]. They rely on the transverse momentum factorization ansatz for the inclusive production of gluons [90]:

$$\frac{dN_g}{dyd^2p_td^2b} = \frac{4\pi N_c}{N_c^2-1}\frac{\alpha_s}{p_t^2} \times \int d^2k_t \phi_A(y,k^2,b)\phi_B(y,(k-p_t^2),b), \qquad (77)$$

where $\phi_{A,B}$ are the unintegrated gluon distributions of the colliding hadrons. It is also assumed local hadron-parton duality. Remarkably, calculations based just in the geometrical scaling found in DIS data and in the factorized expression (77) reproduce

very well the yield of particle produced at RHIC [83]. In all these calculations the energy dependence of the multiplicity is directly given by the energy dependence of the saturation scale, so predictions for the LHC are straightforward[22].

Ideally, the parton multiplicity computed within saturation-based formalisms could serve as initial condition for subsequent evolution of the system towards a thermalized medium, as it is done in hydrodynamical calculations. These consist in a dynamical mapping of a given initial condition to a final spectra through the equation of state.

[22]This is not the only framework in which multiplicity in heavy ion collisions can be understood, see e.g. [91, 92].

6 Conclusions

One main conclusion can be drawn from this thesis: Coherence effects are of the uttermost importance in the high-energy domain of QCD, both for a proper, self-consistent theoretical description of such processes and for phenomenological applications.

These effects play an important role in systems characterized by large gluon densities, in which gluon self-interactions must be taken into account. Special attention has been paid to the nuclear case, in which the coherence effects are already present at not very high energies, due to the large gluon numbers existing in the nucleus wavefunction at moderate energies.

In this work, the following aspects of small-x physics have been analyzed:

- Article I: A phenomenological model for shadowing of nuclear structure functions based on its relation to diffractive processes in proton targets has been presented. Within this formalism we predict a substantial reduction of the particle yield produced in nucleus-nucleus collisions due to the inherent shadowing of their respective wavefunctions. The agreement between the parameter-free results of the model and the experimental data verifies the validity of the approach and greatly constraints future developements.

- Article II: A semiquantitative study of the behaviour of the Cronin enhancement under small-x evolution has been performed. It is the result of this work that the disappearance of the Cronin effect observed at RHIC is mainly due to small-x dynamics.

- Article III: Non-linear small-x dynamics has been further analyzed, providing analytical estimates and numerical solutions of the Balitsky-Kovchegov equation, the simplest perturbative evolution equation that includes non-linear recombination effects. A detailed characterization of its asymptotic properties and comparison with analytical estimates is performed. Their main features exhibit a clear departure from those of the linear dynamics. We also see that the approach to the asymptotics is very slow.

In spite of the recent progress done in this field, as new experimental data from RHIC [93–96] and the LHC become available, the need for a better understanding

of the small-x domain will increase in importance. It is therefore essential for the undergoing theoretical effort to result in a framework capable of yielding phenomenological predictions. To this concern, there are two major problems to be faced in the near future:

On one hand, the current formalism must be extended beyond the leading approximations at which it is derived. This amounts to the symmetrization of evolution equations by including high-density effects in the projectile i.e. pomeron fusion terms, and to a better theoretical control on the role of fluctuations and on next-to-leading order corrections, whose importance has been shown in this thesis. Finite energy corrections due to breakdown of the eikonal approximation should also be taken into account for a realistic comparison with experimental data at present energies.

On the other hand, it is necessary a better determination of the initial conditions, which are presently very badly constrained and that determine the initial steps of the evolution up to a large extent, as has been pointed out in this thesis.

The non-linear nature of the small-x problem makes extremely difficult to obtain exact analytical solutions. Thus, numerical methods have played and will continue to play a crucial role to obtain explicit solutions of the evolution equations. Most of the progress done in the understanding of the high-density regime and some major breakthroughs, as the discovery of scaling solutions, have been managed numerically.

A AGK Rules

The AGK rules [22] provide a precise relation between a given amplitude and all the cross-sections that can be derived from it by cutting, putting on-shell, the propagators in all possible ways: between the exchanged objects and the exchanged objects themselves.

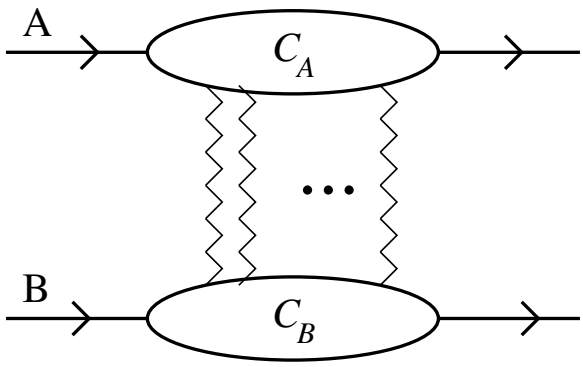

Figure 10: Multiple pomeron exchange in hadron-hadron collisions.

The original AGK work is centered in the analysis of multiple pomeron exchange in high-energy hadron-hadron scattering, Figure (10). It makes use of the Sommerfeld-Watson, or complex angular momentum, representation for the scattering amplitude

$$T_{AB}(s,t) = \int \frac{d\omega}{2i}\, \xi(\omega) s^{1+\omega} \mathcal{F}(\omega,t), \tag{78}$$

with

$$\xi(\omega) = \frac{\tau - \exp\{-i\pi\omega\}}{\sin \pi\omega}, \tag{79}$$

where $\tau = \pm 1$ is the signature factor. The partial wave $\mathcal{F}(\omega,t)$ has singularities in the complex ω-plane. In the frame of Regge theory each singularity corresponds to a reggeon exchange. In particular, pomerons are reggeons with $\tau = +1$ and intercept, see below, close to one. The central goal of the AGK analysis is the decomposition of the n-pomeron exchange contribution in terms of s-channel intermediate states. More precisely, one is interested in the total cross-section i.e. in the discontinuity with respect to energy of the scattering amplitude. It is quite obvious that the absorptive part of the

amplitude will consist of several different contributions: each one corresponding to a particular cuttting of a line in Figure 10, and that there are several ways of performing such cut.

The general formula for the discontinuity accross this cut is

$$\mathrm{disc}_\omega^n\big[\mathcal{F}(\omega,t)\big] = 2\pi i \int \frac{d\Omega_n}{n!}\,\gamma_{\{\beta_j\}}\,\mathcal{C}_n^A(\{k_j\};\omega)\,\mathcal{C}_n^B(\{k_j\};\omega)\,\delta(\omega-\sum_j \beta_j), \tag{80}$$

with

$$d\Omega_n = (2\pi)^2\delta^2(q-\sum_j k_j)\prod_{j=1}^n \frac{d^2k_j}{(2\pi)^2}, \tag{81}$$

where $\mathcal{C}_n^{A(B)}(\{k_j\};\omega)$ is the n-pomeron coupling to the external particle $A(B)$. $k_j(j=1,\ldots,n)$ denotes the transverse momentum of the j-th Regge pole, q is the sum over all transverse momentum with $q^2=-t$, and $\alpha(-k_j^2)=\alpha_j=1+\beta_j$ is the Regge pole trajectory function. The factor which determines the overall sign has the form

$$\gamma_{\{\beta_j\}} = (-1)^{n-1}\frac{\cos\big[\frac{\pi}{2}\sum_j\big(\beta_j+\frac{1-\tau_j}{2}\big)\big]}{\prod_j\cos\big[\frac{\pi}{2}\sum_j\big(\beta_j+\frac{1-\tau_j}{2}\big)\big]}. \tag{82}$$

Thus, the contribution of the contribution of the n-pomeron cut to the scattering amplitude reads

$$T_{AB}^{n-\mathrm{cut}}(s,t) = \int \frac{d\omega}{2i}\xi(\omega)s^{1+\omega}\mathrm{disc}_\omega^{(n)}\big[\mathcal{F}(\omega,t)\big]. \tag{83}$$

Doing the ω-integral we arrive at

$$T_{AB}^{n-\mathrm{cut}}(s,t) = \int \frac{d\Omega_n}{n!}\gamma_{\{\beta_j\}}\xi(\beta)s^{1+\beta}\mathcal{C}_n^A\mathcal{C}_n^B, \tag{84}$$

where $\beta\equiv\beta(\{k_j\})=\sum_{j=1}^n\beta_j$ and $\mathcal{C}_n^{A,B}\equiv\mathcal{C}_n^{A,B}(\{k_j\};\beta)$.

When relating an isolated contribution to the to the full diagram one requires a cut version of the reggeon particle coupling, $\mathcal{C}_n$. The basis of the AGK analysis is the observation that, under very general assumptions for the underlying dynamical theory,

the couplings $\mathcal{C}_n$ are fully symmetric under the exchange of reggeons, and all their cuts versions are identical. This property then allows to find simple relations between the different cut contributions, and to derive a set of counting rules.

One of the main results of AGK states that the s-discontinuity of the n-cut contribution to the amplitude, $\mathrm{disc}\big[T_{AB}^{n-\mathrm{cut}}(s,t)\big]$, can be written as a sum over the number k of cut pomerons ($k = 1, \ldots, n$),

$$\sigma^n(s,t) = \mathrm{disc}_s\big[T_{AB}^{n-\mathrm{cut}}(s,t)\big] = \sum_{k=0}^{n} \sigma_k^n(s,t), \tag{85}$$

and the terms in the sum are

$$\sigma_k^n(s,t) = 2\pi i \int \frac{d\Omega_n}{n!} \mathcal{P}_k^n s^{1+\beta} \mathcal{C}_n^A \mathcal{C}_n^B, \tag{86}$$

where we have introduced the AGK factors:

$$\mathcal{P}_k^n = \begin{cases} (-1)^n\, 2^{n-1} + \gamma_{\{\beta_j\}} & \text{if } k = 0, \\ (-1)^{n-k}\, 2^{n-1} \binom{n}{k} & \text{if } k > 0. \end{cases} \tag{87}$$

This way the total cross section reads

$$\sigma_{tot} = \sum_n \sigma^n(s,t). \tag{88}$$

The simplest case corresponds to the two-pomeron exchange. This process has three contributions, illustrated in Figure 11: The diffractive cut (left), in which all the pomerons are left uncut, the single multiplicity cut (center), in which a single pomeron has been cut and, finally, two pomerons cuts (right). Neglecting the real part of the pomeron signature factor, eq. (79), it reduces to the imaginary unit i, and the γ factor, eq. (82), is just $(-1)^{n-1}$. From eq. (87) we obtain the following AGK weight factors:

$$\begin{array}{rcl} 1: & \text{diffractive} & (k=0) \\ -4: & \text{single multiplicity} & (k=1) \\ 2: & \text{double multiplicity} & (k=2) \end{array} \tag{89}$$

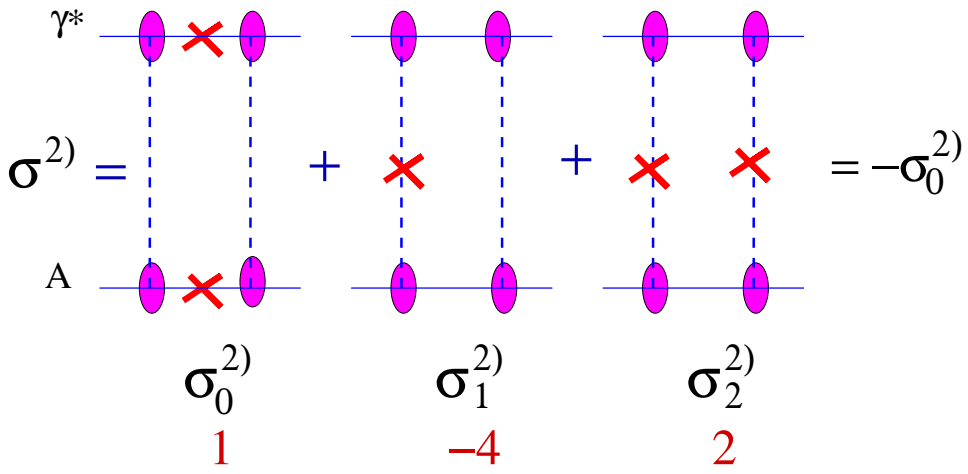

Figure 11: Contributions to the two-scattering $\gamma^* A$ cross-section and their relative AGK weights: Diffractive cut (left), one pomeron cut (center) and two pomeron cut (right).

From this result it is strightforward to derive the relation used in article I:

$$\sigma^{2)}_{\gamma^* A} = -\sigma^{diff}_{\gamma^* p} \tag{90}$$

B Articles published in journals:

B.1 **"Nuclear structure functions at small-x from inelastic shadowing and diffraction", by N. Armesto, A. Capella, A.B. Kaidalov, J. López-Albacete and C. A. Salgado. Published in the European Physical Journal C 29, 531 (2003).**

B.2 **"Energy dependence of the Cronin effect from non-linear QCD evolution", by J.L. Albacete, N. Armesto, A. Kovner, C.A. Salgado and U.A. Wiedemann. Published in Physical Review Letters 92, 082001 (2004).**

B.3 **"Numerical analysis of the Balitsky-Kovchegov equation with running coupling: Dependence of the saturation scale on nuclear size and rapidity", by J.L. Albacete, N. Armesto, J.G. Milhano, C.A. Salgado and U.A. Wiedemann. Published in Physical Review D 71, 014003 (2005).**

References

[1] F. J. Yndurain. *Quantum Chromodynamics: The Theory of Quark and Gluon Interactions*, Springer-Verlag (1999).

[2] D. J. Gross and F. Wilczek, *Ultraviolet behaviour of non-abelian gauge theories*, Phys. Rev. Lett. **30**, 1343 (1973).

[3] H. D. Politzer, *Reliable perturbative results for strong interactions*, Phys. Rev. Lett. **30**, 1346 (1973).

[4] R. G. Roberts, *The Structure of the Proton*, Cambridge University Press (1994).

[5] R. E. Taylor, *Deep inelastic scattering: The early years*, Rev. Mod. Phys. **63**, 573 (1991).

[6] H. W. Kendall, *Deep inelastic scattering: Experiments on the proton and the observation*, Rev. Mod. Phys. **63**, 597 (1991).

[7] J. I. Friedman, *Deep inelastic scattering: Comparisons with the quark model*, Rev. Mod. Phys. **63**, 615 (1991).

[8] W. K. H. Panofsky, *Electromagnetic interactions: Low Q^2 electrodynamics: Elastic and inelastic electron (and muon) scattering*, presented at 14th Int. Conf on High Energy Physics, Vienna, Aug. 1968.

[9] E. D. Bloom et al., *High energy ep scattering at 6-degrees and 10-degrees*, Phys. Rev. Lett. **23**, 930 (1969).

[10] M. Breidenbach et al., *Observed behaviour of highly inelastic electron-proton scattering*, Phys. Rev. Lett. **23**, 935 (1969).

[11] J. D. Bjorken, *Asymptotic sum rules at infinite momentum*, Phys. Rev. **179**, 1547 (1969).

[12] M. Gell-Mann, *A schematic model of baryons and mesons*, Phys. Lett. **8**, 214 (1964).

[13] G. Zweig, *A $SU(3)$ model for strong interaction symmetry and its breaking, 2.* CERN-TH-412.

[14] C. G. Callan and D. J. Gross *High-energy electroproduction and the constitution of the electric current*, Phys. Rev. Lett. **22**, 156 (1969).

[15] J. C. Collins, D. E. Sopper, and G. Sterman, *Factorization of hard processes in QCD*. In *Perturbative QCD*, A. H. Mueller ed., World Scientific (1989).

[16] A. D. Martin, R. G. Roberts, W. J. Stirling, and R. S. Thorne, *Parton distributions: A new global analysis*, Eur. Phys. J. **C4**, 463 (1998).

[17] M. Arneodo, *Nuclear effects in structure functions,* Phys. Rept. **240**, 301 (1994).

[18] D. F. Geesaman, K. Saito and A. W. Thomas, *The nuclear EMC effect*, Ann. Rev. Nucl. Part. Sci. **45**, 337 (1995).

[19] P. D. B. Collins, *An introduction to Regge theory and high-energy physics,* Cambridge University Press (1977).

[20] E. A. Kuraev, L. N. Lipatov and V. S. Fadin, *The Pomeranchuk Singularity In Nonabelian Gauge Theories*, Sov. Phys. JETP **45**, 199 (1977) [Zh. Eksp. Teor. Fiz. **72**, 377 (1977)].

[21] I. I. Balitsky and L. N. Lipatov, *The Pomeranchuk Singularity In Quantum Chromodynamics*, Sov. J. Nucl. Phys. **28**, 822 (1978) [Yad. Fiz. **28**, 1597 (1978)].

[22] V. A. Abramovsky, V. N. Gribov and O. V. Kancheli, *Character Of Inclusive Spectra And Fluctuations Produced In Inelastic Processes By Multi-Pomeron Exchange*, Yad. Fiz. **18**, 595 (1973) [Sov. J. Nucl. Phys. **18**, 308 (1974)].

[23] V. N. Gribov, *Interaction Of Gamma Quanta And Electrons With Nuclei At High-Energies,* Sov. Phys. JETP **30**, 709 (1970) [Zh. Eksp. Teor. Fiz. **57**, 1306 (1969)].

[24] V. N. Gribov, *A Reggeon Diagram Technique,* Sov. Phys. JETP **26**, 414 (1968) [Zh. Eksp. Teor. Fiz. **53**, 654 (1967)].

[25] V. N. Gribov and L. N. Lipatov, *Deep Inelastic E P Scattering In Perturbation Theory*, Sov. J. Nucl. Phys. **15**, 438 (1972) [Yad. Fiz. **15**, 781 (1972)].

[26] Y. L. Dokshitzer, *Calculation Of The Structure Functions For Deep Inelastic Scattering And E+E- Annihilation By Perturbation Theory In Quantum Chromodynamics*, Sov. Phys. JETP **46**, 641 (1977) [Zh. Eksp. Teor. Fiz. **73**, 1216 (1977)].

[27] G. Altarelli and G. Parisi, *Asymptotic Freedom In Parton Language*, Nucl. Phys. B **126**, 298 (1977).

[28] J. R. Forshaw, D .A . Ross, *QCD and the Pomeron*, Cambridge University Press (1997).

[29] J. C. Collins, *'What exactly is a parton density?*, Acta Phys. Polon. B **34**, 3103 (2003).

[30] A. de Rújula et al., *Possible nonregge behaviour of electroproduction structure functions*, Phys. Rev. D **10**, 1071 (1974).

[31] D. J. Gross, *How to test scaling in asymptotically free theories,* Phys. Rev. Lett. **32**, 935 (1974).

[32] M. Froissart, *Asymptotic Behaviour And Subtractions In The Mandelstam Representation*, Phys. Rev. **123**, 1053 (1961).

[33] *QCD Perspectives on Hot and Dense Matter (NATO Science Series II: Mathematics, Physics and Chemistry, Vol. 87)*, J.-P. Blaizot and E. Iancu eds. Kluwer (2002).

[34] *Quark-Gluon Plasma*, R. C. Hwa ed. (1990).

[35] *Quark-Gluon Plasma 2*, R. C. Hwa ed. (1995).

[36] *Quark-Gluon Plasma 3*, R. C. Hwa. and X. N. Wang ed. (2004).

[37] L. V. Gribov, E. M. Levin and M. G. Ryskin, *Singlet Structure Function At Small X: Unitarization Of Gluon Ladders*, Nucl. Phys. B **188**, 555 (1981).

[38] A. H. Mueller and J. Qiu, *Gluon recombination and shadowing at small values of* x, Nucl. Phys. B **268**, 427 (1986).

[39] L. D. McLerran and R. Venugopalan, *Computing quark and gluon distribution functions for very large nuclei*, Phys. Rev. D **49**, 2233 (1994).

[40] L. D. McLerran and R. Venugopalan, *Gluon distribution functions for very large nuclei at small transverse momentum*, Phys. Rev. D **49**, 3352 (1994).

[41] L. D. McLerran and R. Venugopalan, *Green's functions in the colour field of a large nucleus*, Phys. Rev. D **50**, 2225 (1994).

[42] J. Jalilian-Marian, A. Kovner, L. D. McLerran and H. Weigert, *The intrinsic glue distribution at very small x*, Phys. Rev. D **55**, 5414 (1997).

[43] J. Jalilian-Marian, A. Kovner, A. Leonidov and H. Weigert, *The Wilson renormalization group for low x physics: Towards the high density regime*, Phys. Rev. D **59**, 014014 (1999).

[44] J. Jalilian-Marian, A. Kovner, A. Leonidov and H. Weigert, *Unitarization of gluon distribution in the doubly logarithmic regime at high density*, Phys. Rev. D **59**, 034007 (1999) [Erratum-ibid. D **59**, 099903 (1999)].

[45] A. Kovner and J. G. Milhano, *Vector potential versus colour charge density in low-x evolution*, Phys. Rev. D **61**, 014012 (2000).

[46] E. Iancu, A. Leonidov and L. D. McLerran, *Nonlinear gluon evolution in the color glass condensate. I*, Nucl. Phys. A **692**, 583 (2001).

[47] E. Iancu, A. Leonidov and L. D. McLerran, *The renormalization group equation for the color glass condensate*, Phys. Lett. B **510**, 133 (2001).

[48] E. Ferreiro, E. Iancu, A. Leonidov and L. McLerran, *Nonlinear gluon evolution in the color glass condensate. II*, Nucl. Phys. A **703**, 489 (2002).

[49] J. Jalilian-Marian, A. Kovner, A. Leonidov and H. Weigert, *The BFKL equation from the Wilson renormalization group*, Nucl. Phys. B **504**, 415 (1997).

[50] I. Balitsky, *Operator expansion for high-energy scattering*, Nucl. Phys. B **463**, 99 (1996).

[51] H. Weigert, *Unitarity at small Bjorken-x*, Nucl. Phys. A **703**, 823 (2002).

[52] K. Rummukainen and H. Weigert, *Universal features of JIMWLK and BK evolution at small x*, Nucl. Phys. A **739**, 183 (2004).

[53] Y. V. Kovchegov, *Small-x F2 structure function of a nucleus including multiple pomeron exchanges,* Phys. Rev. D **60**, 034008 (1999).

[54] A. H. Mueller, *Soft gluons in the infinite momentum wave function and the BFKL pomeron,* Nucl. Phys. B **415**, 373 (1994).

[55] A. H. Mueller and B. Patel, *Single and double BFKL pomeron exchange and a dipole picture of high-energy hard processes,* Nucl. Phys. B **425**, 471 (1994).

[56] N. N. Nikolaev and B. G. Zakharov, *Colour Transparency And Scaling Properties Of Nuclear Shadowing In Deep Inelastic Scattering,* Z. Phys. C **49**, 607 (1991).

[57] A. H. Mueller and A. I. Shosi, *Small x Physics beyond the Kovchegov equation*, Nucl. Phys. B **692**, 175 (2004).

[58] E. Iancu and D. N. Triantafyllopoulos, *A Langevin equation for high energy evolution with pomeron loops,* [arXiv:hep-ph/0411405].

[59] A. H. Mueller, A. I. Shosi and S. M. H. Wong, *Extension of the JIMWLK equation in the low gluon density region*, Nucl. Phys. B **715**, 440 (2005).

[60] A. Kovner and M. Lublinsky, *Remarks on high energy evolution*, JHEP **0503**, 001 (2005).

[61] M. Braun, *Structure functions of the nucleus in the perturbative QCD with $N_c \to$ infinity (BFKL Pomeron fan diagrams),* Eur. Phys. J. **C16**, 337 (2000).

[62] V. S. Fadin and L. N. Lipatov, *BFKL Pomeron in the next-to-leading approximation*, Phys. Lett. B **429**, 127 (1998).

[63] G: C. Camici and M. Ciafaloni, *Energy scale(s) and next-to-leading BFKL equation*, Phys. Lett. B **430**, 349 (1998)

[64] D. A. Ross, *The effect of higher order corrections to the BFKL equation on the perturbative pomeron,* Phys. Lett. B **431**, 161 (1998).

[65] Y. V. Kovchegov and A. H. Mueller, *Running coupling effects in BFKL evolution*, Phys. Lett. B **439**, 428 (1998).

[66] N. Armesto, J. Bartels and M. A. Braun, *On the 2nd order corrections to the hard pomeron and the running coupling,* Phys. Lett. B **442**, 459 (1998).

[67] N. Armesto and M. A. Braun, *Parton densities and dipole cross-sections at small x in large nuclei*, Eur. Phys. J. **C20**, 517 (2001).

[68] M. Lublinsky, *Scaling phenomena from nonlinear evolution in high-energy DIS*, Eur. Phys. J. **C21**, 513 (2001).

[69] E. Iancu, K. Itakura and L. McLerran, *Geometric scaling above the saturation scale,* Nucl. Phys. A **708**, 327 (2002).

[70] R. A. Fischer, Ann. Eugenics **7**, 355 (1937).

[71] A. Kolmogorov, I. Petrovsky and N. Piscounov, Moscow Univ. Bull. Math A **1**, 1 (1937).

[72] S. Munier and R. Peschanski, *Universality and tree structure of high energy QCD,* Phys. Rev. D **70**, 077503 (2004).

[73] A. H. Mueller and D. N. Triantafyllopoulos, *The energy dependence of the saturation momentum,* Nucl. Phys. B **640**, 331 (2002).

[74] A. H. Mueller, *Nuclear A dependence near the saturation boundary,* Nucl. Phys. A **724**, 223 (2003).

[75] K. Golec-Biernat and M. Wusthoff, *Saturation effects in deep inelastic scattering at low Q**2 and its implications on diffraction,* Phys. Rev. D **59**, 014017 (1999).

[76] E. Iancu, K. Itakura and S. Munier, *Saturation and BFKL dynamics in the HERA data at small x*, Phys. Lett. B **590**, 199 (2004).

[77] J. R. Forshaw, G. Kerley and G. Shaw, *Extracting the dipole cross-section from photo- and electro-production total cross-section data,* Phys. Rev. D **60**, 074012 (1999).

[78] T. Hallman, T. Kirk, T. Roser and R. G. Milner, *RHIC II/eRHIC White Paper*,

[79] M. Arneodo et al., in *Proceedings of the Workshop of Future Physics at HERA* (Hamburg, Germany, September 1995).

[80] H. Abramowicz et al., *Tesla Technical Design Report, Part VI, Chapter 2*, R. Klanner, U. Katz, M. Klein and A. Levy eds.

[81] *EIC White Paper*, preprint BNL-68933, A. Desphande, R. Milner and R. Venugopalan eds.

[82] A. M. Stasto, K. Golec-Biernat and J. Kwiecinski, *Geometric scaling for the total gamma* p cross-section in the low x region,* Phys. Rev. Lett. **86**, 596 (2001).

[83] N. Armesto, C. A. Salgado and U. A. Wiedemann, *Relating high-energy lepton-hadron, proton-nucleus and nucleus-nucleus collisions through geometric scaling*, Phys. Rev. Lett. **94**, 022002 (2005).

[84] M. Diehl, *Generalized parton distributions*, Phys. Rept. **388**, 41 (2003).

[85] J. W. Cronin, H. J. Frisch, M. J. Shochet, J. P. Boymond, R. Mermod, P. A. Piroue and R. L. Sumner, *Production Of Hadrons With Large Transverse Momentum At 200-Gev, 300-Gev, And 400-Gev,* Phys. Rev. D **11**, 3105 (1975).

[86] I. Arsene et. al , *Evolution of the nuclear modification factors with rapidity and centrality in d+Au collisions at* $\sqrt{s_{NN}} = 200$ *GeV*, Phys. Rev. Lett. **93**, 242303 (2004).

[87] S. S. Adler *et al.* [PHENIX Collaboration], *Absence of suppression in particle production at large transverse momentum in s(NN)**(1/2) = 200-GeV d + Au collisions,* Phys. Rev. Lett. **91**, 072303 (2003).

[88] D. Kharzeev and M. Nardi, *Hadron production in nuclear collisions at RHIC and high density QCD,* Phys. Lett. B **507**, 121 (2001).

[89] D. Kharzeev and E. Levin, *Manifestations of high density QCD in the first RHIC data,* Phys. Lett. B **523**, 79 (2001).

[90] L. V. Gribov, E. M. Levin and M. G. Ryskin, *Semihard Processes In QCD,* Phys. Rept. **100**, 1 (1983).

[91] N. Armesto and C. Pajares, *Central rapidity densities of charged particles at RHIC and the LHC*, Int. J. Mod. Phys. A **15**, 2019 (2000).

[92] C. Pajares, *String and parton percolation*, [arXiv:hep-ph/0501125].

[93] K. Adcox et al., *Formation of dense matter in relativistic nucleus-nucleus collisions at RHIC: Experimental evaluation by the Phenix collaboration*, [arXiv:nucl-ex/0410003].

[94] I. Arsene et al., *Quark Gluon Plasma and Color Glass Condensate at RHIC? The perspective from the Brahms experiment*, [arXiv:nucl-ex/0410020].

[95] B. B. Back et al., *The Phobos perspective on discoveries at RHIC*, [arXiv:nucl-ex/0410022].

[96] J. Adams et al., *Experimental and theoretical challenges in the search for the Quark Gluon Plasma: The Star collaboration's critical assesment of the evidence from RHIC collisions,* [arXiv:nucl-ex/0501009].

Eur. Phys. J. C 29, 531–540 (2003)
Digital Object Identifier (DOI) 10.1140/epjc/s2003-01243-0

THE EUROPEAN PHYSICAL JOURNAL C

Nuclear structure functions at small x from inelastic shadowing and diffraction

N. Armesto[1,a], A. Capella[2,b], A.B. Kaidalov[3,c], J. López-Albacete[1,4,d], C.A. Salgado[1,e]

[1] Theory Division, CERN, 1211 Genève 23, Switzerland
[2] Laboratoire de Physique Théorique, Université de Paris XI, Bâtiment 210, 91405 Orsay Cedex, France
[3] Institute of Theoretical and Experimental Physics, B. Cheremushkinskaya 25, Moscow 117259, Russia
[4] Departamento de Física, Módulo C2, Planta baja, Campus de Rabanales, Universidad de Córdoba, 14071 Córdoba, Spain

Received: 17 April 2003 /
Published online: 23 June 2003 –

Abstract. Nuclear structure functions at small x and small or moderate Q^2 are studied using the relation with diffraction on nucleons which arises from Gribov's reggeon calculus. A reasonable description of the experimental data is obtained with no fitted parameters. A comparison with other models and predictions for future lepton–ion colliders are provided. Consequences for the reduction of multiplicities in nucleus–nucleus collisions at energies of RHIC and LHC are examined.

1 Introduction

The study of nuclear structure functions has become a fashionable subject. Apart from its intrinsic interest, such analysis has a great impact on the interpretation of results from heavy ion experiments. At small values of the Bjorken variable x ($\lesssim 0.01$, shadowing region), the structure function F_2 per nucleon turns out to be smaller in nuclei than in a free nucleon [1,2]. Several explanations to this shadowing have been proposed.

On the one hand, some models use the fact that in the rest frame of the nucleus the incoming photon splits into a $q\bar{q}$ pair long before reaching the nucleus, and this $q\bar{q}$ pair interacts with it with typical hadronic cross sections, which results in absorption [3–9]. Thus nuclear shadowing is a consequence of multiple scattering which in turn is related to diffraction [6,10,11]. This relationship will be developed in this paper. Equivalently, in a frame in which the nucleus is moving fast, gluon recombination due to the overlap of the gluon clouds from different nucleons reduces the gluon density in the nucleus [12,13]. These studies have received a great theoretical impulse with the development of semiclassical ideas in QCD and the appearance of non-linear equations for evolution in x in this framework (see [14–17] and references therein; also [18] for a simple geometrical approach in this framework).

On the other hand, other approaches [19–21] do not address the origin of shadowing but only its evolution with $\ln Q^2$: parton densities inside the nucleus are parameterized at some scale Q_0^2 and then evolved using the DGLAP [22] evolution equations.

The results from different models usually depend on phenomenological assumptions and their predictions (notably for small values of x which are of the utmost importance to compute particle production at RHIC and LHC) turn out to be very different. For example, concerning the Q^2-dependence of shadowing, it can be either constant [4–9], or die out logarithmically [19–21] or behave as a higher-twist [12,13].

In this paper we will use the relation of diffraction to nuclear shadowing which arises from Gribov theory [23], reggeon calculus [24] and the AGK rules [25]. In this way we obtain a parameter-free description of nuclear structure functions in the shadowing region valid for $x < 0.01$ and $Q^2 < 10\,\mathrm{GeV}^2$, using a model for F_2 and $F_{2\mathcal{D}}$ [26, 27]. The same strategy has been used in [10,11], but our extrapolation to smaller x or higher W^2 is more reliable than that of [10] due to the model employed for the nucleon; besides, our description is valid for small Q^2 while that of [11] applies to $Q^2 \geq 4\,\mathrm{GeV}^2$. In Sect. 2 the model will be described. In Sect. 3 numerical results will be presented together with comparisons with experimental data and with other models. In Sect. 4 the model will be applied to calculate the multiplicity reduction factors [28, 29] relevant to compute particle production in heavy ion collisions at RHIC and LHC. Finally, the last section will contain our conclusions.

2 Description of the model

We assume that nuclei are made of nucleons in the spirit of the Glauber model. In order to relate diffraction on

[a] e-mail: Nestor.Armesto.Perez@cern.ch
[b] e-mail: Alphonse.Capella@th.u-psud.fr
[c] e-mail: kaidalov@heron.itep.ru
[d] e-mail: Javier.Lopez.Albacete@cern.ch
[e] e-mail: Carlos.Salgado@cern.ch

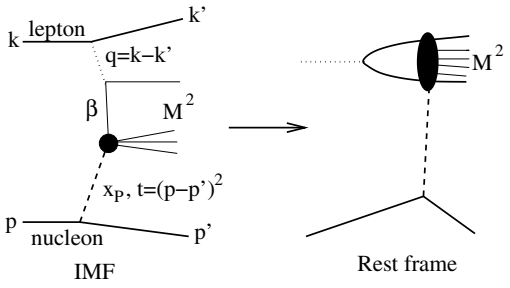

Fig. 1. Diagram showing diffractive DIS with the corresponding kinematical variables in the infinite momentum frame (left) and its equivalence in the rest frame of the nucleon (right)

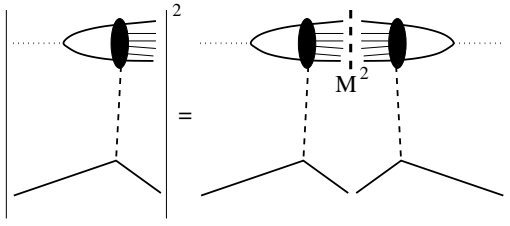

Fig. 2. Diagram showing the equivalence between diffractive DIS and two exchanged amplitudes with a cut between the amplitudes

nucleons with nuclear shadowing, we will follow the procedure explained in [10]. The γ^*–nucleus cross section can be expanded in a multiple scattering series containing the contribution from $1, 2, \ldots$ scatterings:

$$\sigma_A = \sigma_A^{(1)} + \sigma_A^{(2)} + \cdots . \tag{1}$$

$\sigma_A^{(1)}$ is simply equal to $A\sigma_{\rm nucleon}$. Let us consider now the first correction to the non-additivity of cross sections which comes from the second-order rescattering $\sigma_A^{(2)}$. In Fig. 1 diffractive DIS is shown in both the infinite momentum frame and in the rest frame of the nucleon. In Fig. 2 it becomes clear that the square of such a contribution is equivalent to a double exchange with a cut between the exchanged amplitudes, a so-called diffractive cut. To compute the first contribution to nuclear shadowing $\sigma_A^{(2)}$, which comes from these two exchanges, we need its total contribution to the γ^*–nucleon cross section, which arises from cutting the two-exchange amplitude in all possible ways (between the amplitudes and the amplitudes themselves in all possible manners). For purely imaginary amplitudes, it can be shown [24,25] that this total contribution is identical to minus the contribution from the diffractive cut. Thus diffractive DIS is directly related to the first contribution to nuclear shadowing. The final expression reads

$$\sigma_A^{(2)} = -4\pi A(A-1) \times \int {\rm d}^2b\, T_A^2(b) \int_{M^2_{\rm min}}^{M^2_{\rm max}} {\rm d}M^2 \left.\frac{{\rm d}\sigma^{\mathcal{D}}_{\gamma^* {\rm p}}}{{\rm d}M^2 {\rm d}t}\right|_{t=0} F_A^2(t_{\rm min}), \tag{2}$$

with $T_A(b) = \int_{-\infty}^{+\infty} {\rm d}z \rho_A(\mathbf{b}, z)$ the nuclear profile function normalized to 1, $\int {\rm d}^2b\, T_A(\mathbf{b}) = 1$, and M^2 the mass of the diffractively produced system. The usual variables for diffractive DIS: Q^2, x, M^2 and t, or $x_{\rm P} = x/\beta$, $\beta = \frac{Q^2}{Q^2+M^2}$, are shown in Fig. 1.

Coherence effects, i.e. the coherence length of the $q\bar{q}$ fluctuation of the incoming virtual photon, is taken into account through

$$F_A(t_{\rm min}) = \int {\rm d}^2b\; J_0(b\sqrt{-t_{\rm min}}) T_A(b), \tag{3}$$

with $t_{\rm min} = -m_N^2 x_{\rm P}^2$ and m_N the nucleon mass. This function is equal to 1 at $x \to 0$ and decreases with increasing x due to the loss of coherence for $x > x_{\rm crit} \sim (m_N R_A)^{-1}$.

Let us briefly examine (2). Here the real part of the pomeron amplitude, which is small for the value of the intercept which will be used [27], $\Delta = \alpha_{\rm P}(t=0) - 1 = 0.2$, has not been taken into account. Also it has been deduced under the approximation $R_A^2 \gg R_N^2$, so the t-dependence of the γ^*–nucleon cross section has been neglected.

For $A > 20$ a nuclear density in the form of a 3-parameter Fermi distribution with parameters taken from [30] will be employed to compute both $T_A(b)$ and (3). For $2 < A \leq 20$ a Gaussian profile function is used [31]:

$$T_A(b) = \frac{3}{2\pi R_A^2}\; \exp\left(-\frac{3b^2}{2R_A^2}\right), \quad R_A = 0.82A^{1/3} + 0.58\,{\rm fm}, \tag{4}$$

but, in order to take into account the t-dependence for these light nuclei, we make in the computation of the form factors (3) the substitution

$$R_A^2 \longrightarrow R_A^2 + R_N^2, \quad R_N = 0.8\,{\rm fm}. \tag{5}$$

Finally, for the deuteron the double rescattering contribution has the form

$$\sigma_A^{(2)} = -2 \int_{-\infty}^{t_{\rm min}} {\rm d}t \times \int_{M^2_{\rm min}}^{M^2_{\rm max}} {\rm d}M^2\; \left.\frac{{\rm d}\sigma^{\mathcal{D}}_{\gamma^* {\rm nucleon}}}{{\rm d}M^2 {\rm d}t}\right|_{t=0} F_D(t), \tag{6}$$

where $F_D(t) = {\rm e}^{at}$, $a = 40\,{\rm GeV}^{-2}$.

The lower integration limit in (2) and (6) is $M^2_{\rm min} = 4m_\pi^2 = 0.08\,{\rm GeV}^2$, while the upper one is taken from the condition

$$x_{\rm P} = x\left(\frac{M^2+Q^2}{Q^2}\right) \leq x_{\rm Pmax} \Longrightarrow M^2_{\rm max} = Q^2\left(\frac{x_{\rm Pmax}}{x} - 1\right), \tag{7}$$

with $x_{\rm Pmax} = 0.1$; this value was used in [27] motivated by the fact that the model is only valid for $M^2 \ll W^2$ or $x_{\rm P} \ll 1$, i.e. a large rapidity gap is required. In our case, variations of $x_{\rm Pmax}$ by a factor 2 do not affect the description of nuclear shadowing at $x < 0.01$, but the choice $x_{\rm Pmax} = 0.1$ is convenient as it guarantees the disappearance of nuclear shadowing at $x \sim 0.1$ (see below) as in the experimental data.

The relation between $\left.\frac{\mathrm{d}\sigma^{\mathcal{D}}_{\gamma^*\mathrm{p}}}{\mathrm{d}M^2\mathrm{d}t}\right|_{t=0}$ and $x_{\mathrm{P}}F^{(3)}_{2\mathcal{D}}(Q^2,x_{\mathrm{P}},\beta)$ is provided by the model [27]

$$\begin{aligned} & x_{\mathrm{P}}F^{(3)}_{2\mathcal{D}}(Q^2,x_{\mathrm{P}},\beta) \\ & = x_{\mathrm{P}}\frac{Q^2}{4\pi^2\alpha_{\mathrm{em}}}\int_{-\infty}^{0}\mathrm{d}t\frac{\mathrm{d}\sigma^{\mathcal{D}}_{\gamma^*\mathrm{p}}(Q^2,x_{\mathrm{P}},\beta,t)}{\mathrm{d}x_{\mathrm{P}}\mathrm{d}t} \\ & \Longrightarrow \\ & \left.\frac{\mathrm{d}\sigma^{\mathcal{D}}_{\gamma^*\mathrm{p}}(Q^2,x_{\mathrm{P}},\beta)}{\mathrm{d}M^2\mathrm{d}t}\right|_{t=0} \\ & = \frac{4\pi^2\alpha_{\mathrm{em}}B}{Q^2(Q^2+M^2)}x_{\mathrm{P}}F^{(3)}_{2\mathcal{D}}(Q^2,x_{\mathrm{P}},\beta), \end{aligned} \tag{8}$$

where the usual factorization has been assumed:

$$\frac{\mathrm{d}\sigma^{\mathcal{D}}_{\gamma^*\mathrm{p}}(x,Q^2,M^2,t)}{\mathrm{d}M^2\mathrm{d}t} = \left.\frac{\mathrm{d}\sigma^{\mathcal{D}}_{\gamma^*\mathrm{p}}(x,Q^2,M^2)}{\mathrm{d}M^2\mathrm{d}t}\right|_{t=0}\mathrm{e}^{Bt}, \tag{9}$$

with $B = 6\,\mathrm{GeV}^{-2}$ (as in [32], see the discussion there; this value is slightly smaller than the experimental values $7.2 \pm 1.1(\mathrm{stat.})^{+0.7}_{-0.9}(\mathrm{syst.})\,\mathrm{GeV}^{-2}$ [33] at $\langle Q^2\rangle = 8\,\mathrm{GeV}^2$ and $6.8 \pm 0.9(\mathrm{stat.})^{+1.2}_{-1.1}(\mathrm{syst.})\,\mathrm{GeV}^{-2}$ [34] for photoproduction). Note that $\left.\frac{\mathrm{d}\sigma^{\mathcal{D}}_{\gamma^*\mathrm{p}}(x,Q^2,M^2)}{\mathrm{d}M^2\mathrm{d}t}\right|_{t=0}$ can be obtained directly from σ_{tot}. However, the model for diffraction we are using [27] has mainly been tested after integration in t (most available data are integrated in t). For this reason, we use the integrated expression together with the experimental value of B. While this is legitimate at present values of x, it can lead to an underestimation of shadowing at very small x, due to the increase of B with energy[1].

The model in [27] is based on the dipole picture of the photon and contains two components. The small-distance (S) component corresponds to transverse distances r between the q and the $\bar{q}$ of the dipole such that $r < r_0$, and the large-distance (L) component to $r > r_0$, with $r_0 = 0.2\,\mathrm{fm}$. In each component a quasi-eikonal iteration is introduced in order to enforce unitarity. Reggeon and pomeron exchanges are allowed. For diffraction, a third component is used, namely a contribution from the triple interaction of reggeons and pomerons. This model has been designed to describe the small $x < 10^{-2}$, small or moderate $Q^2 < 10\,\mathrm{GeV}^2$ region, and it contains the basic ingredients which allow one to make a safe extrapolation[2] to very small x or high W^2.

[1] Nevertheless, the effect is not too large: we have checked that an increase of B from 6 to $7.2\,\mathrm{GeV}^{-2}$ produces an increase of shadowing for Pb of at most 10% at $x = 10^{-7}$. As estimates indicate an increase $\lesssim$50% in B for the smallest x we have studied, $x = 10^{-7}$, the increase of shadowing due to this effect would be at most $\sim 25\%$ for these values of x

[2] In order to use the model for larger x, $0.01 < x < 0.1$, we have made some modifications in [27]: there, in (26) β_{min} in the normalization denominators has been set to 0, and in (25) the reggeon–reggeon contribution has been ignored. These two changes slightly modify the description of diffraction but we have checked that the agreement with experimental data is as good as in the original version of the model

Equation (2) corresponds to the case with only two scatterings. Its extension to include higher-order rescatterings is model-dependent. We will use two models: a Schwimmer unitarization [35] which is obtained from a summation of fan diagrams with triple pomeron interactions,

$$\begin{aligned} \sigma^{\mathrm{Sch}}_{\gamma^*A} &= \sigma_{\gamma^*\mathrm{nucleon}} \\ &\times \int \mathrm{d}^2b\,\frac{AT_A(b)}{1+(A-1)f(x,Q^2)T_A(b)}\,, \end{aligned} \tag{10}$$

and an eikonal unitarization,

$$\begin{aligned} \sigma^{\mathrm{eik}}_{\gamma^*A} &= \sigma_{\gamma^*\mathrm{nucleon}}\int \mathrm{d}^2b\,\frac{A}{2(A-1)f(x,Q^2)} \\ &\times \left\{1-\exp\left[-2(A-1)T_A(b)f(x,Q^2)\right]\right\}, \end{aligned} \tag{11}$$

where we use the relation $\sigma_{\gamma^*\mathrm{nucleon}} = \frac{4\pi^2\alpha_{\mathrm{em}}}{Q^2}F_2(x,Q^2)$, valid at small x. Here, $F_2(x,Q^2)$ is the nucleon structure function, taken from [27]. Both expressions (10) and (11), expanded to the first non-trivial order, reproduce the second rescattering result (2). Eikonal unitarization will produce larger shadowing than Schwimmer, as can be expected by comparing the second non-trivial order in the expansion of both expressions. Finally,

$$\begin{aligned} f(x,Q^2) &= \frac{4\pi}{\sigma_{\gamma^*\mathrm{nucleon}}} \\ &\times \int_{M^2_{\mathrm{min}}}^{M^2_{\mathrm{max}}}\mathrm{d}M^2\,\left.\frac{\mathrm{d}\sigma^{\mathcal{D}}_{\gamma^*\mathrm{p}}}{\mathrm{d}M^2\mathrm{d}t}\right|_{t=0}F^2_A(t_{\mathrm{min}}), \end{aligned} \tag{12}$$

as required by consistency with (2).

The shadowing in nuclei is usually studied through the ratios of cross sections per nucleon for different nuclei, defined as

$$R(A/B) = \frac{B}{A}\frac{\sigma_{\gamma^*A}}{\sigma_{\gamma^*B}}\,. \tag{13}$$

In the simplest case of the ratio over the nucleon (equivalent to the proton at small x where the valence contribution can be neglected), we get

$$\begin{aligned} & R^{\mathrm{Sch}}(A/\mathrm{nucleon}) \\ & = \int \mathrm{d}^2b\,\frac{T_A(b)}{1+(A-1)f(x,Q^2)T_A(b)}\,, \end{aligned} \tag{14}$$

$$\begin{aligned} R^{\mathrm{eik}}(A/\mathrm{nucleon}) &= \int \mathrm{d}^2b\,\frac{1}{2(A-1)f(x,Q^2)} \\ &\times \left\{1-\exp\left[-2(A-1)T_A(b)f(x,Q^2)\right]\right\}. \end{aligned} \tag{15}$$

To calculate shadowing in photoproduction, x is no longer a relevant kinematical variable. Instead we use the γ^*–nucleon center of mass energy W^2.

In our framework shadowing can also be studied as a function of the impact parameter b:

$$R(A/\mathrm{nucleon})^{\mathrm{Sch}}(b) = \frac{1}{1+(A-1)f(x,Q^2)T_A(b)}\,, \tag{16}$$

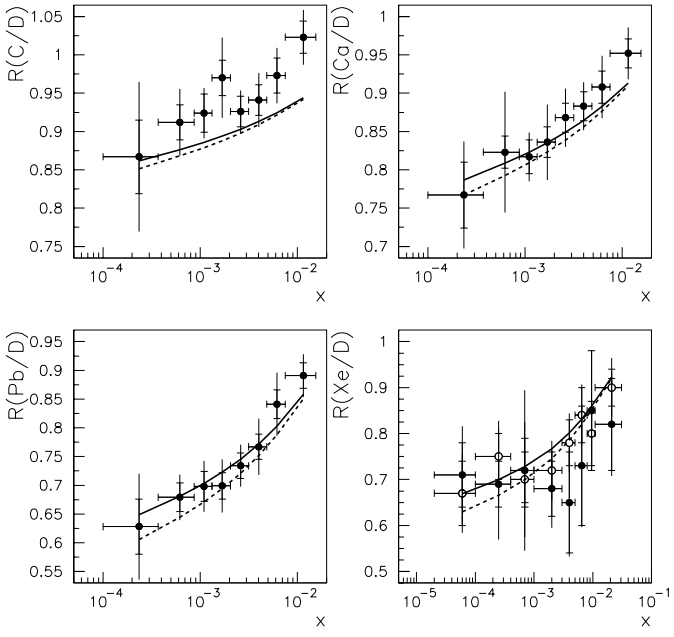

Fig. 3. Results of the model using Schwimmer (solid lines) and eikonal (dashed lines) unitarization compared with experimental data versus x, for the ratios C/D, Ca/D, Pb/D [36] and Xe/D [37] (filled circles correspond to the analysis with hadron requirement and open circles to that with electromagnetic cuts; see the experimental paper for more details)

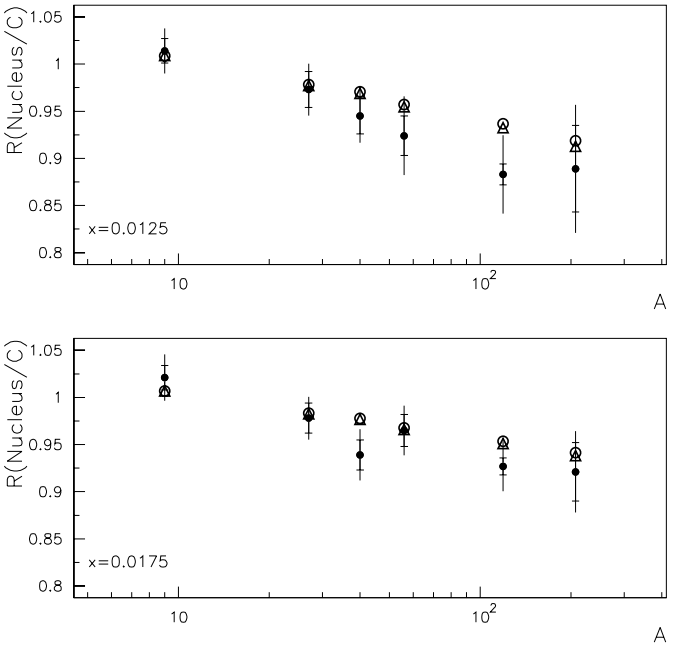

Fig. 4. Results of the model using Schwimmer (open circles) and eikonal (open triangles) unitarization compared with experimental data versus A, for the ratios Be/C, Al/C, Ca/C, Fe/C, Sn/C and Pb/C [38] at two fixed values of x

$$R(A/\text{nucleon})^{\text{eik}}(b) = \frac{1}{2(A-1)T_A(b)f(x,Q^2)} \times \left\{1 - \exp\left[-2(A-1)T_A(b)f(x,Q^2)\right]\right\}. \quad (17)$$

Finally, the region of applicability of our model is the same as that of the model for diffraction on the nucleon [27], i.e. small $x \lesssim 0.01$ and small or moderate $Q^2 \lesssim 10\,\text{GeV}^2$, including photoproduction.

3 Numerical results

In our model and in [27] we work in the small x region and thus no distinction is made between protons and neutrons. Although usually joined with straight lines, our results are computed at the same $\langle x \rangle$ and $\langle Q^2 \rangle$ as the experimental data. For the latter, inner error bars show statistical errors, and outer error bars correspond to statistical and systematical errors added in quadrature.

In Figs. 3–6 a comparison with the experimental data at small x from E665 [36,37] and NMC [38–40] is presented. As expected, eikonal unitarization produces larger shadowing than Schwimmer. The agreement with the experimental data is quite reasonable taking into account that no parameters have been fitted to reproduce the data. Two comments are in order: First, for C/D and Ca/D in Fig. 3 which shows the comparison with the E665 data, shadowing looks overestimated for $x \sim 0.01$, while in Fig. 5 which shows the comparison with the NMC data, it looks underestimated. This corresponds to the known difference between the results of both experiments for ratios over D, while the compatibility is restored [38] when ratios are computed over C. Second, from Fig. 6 it becomes clear that the evolution with Q^2 in the model is too slow at $x \sim 0.01$, a problem related with the lack of DGLAP evolution in the model [27] (see [10,11,41] for an application of DGLAP evolution to initial conditions).

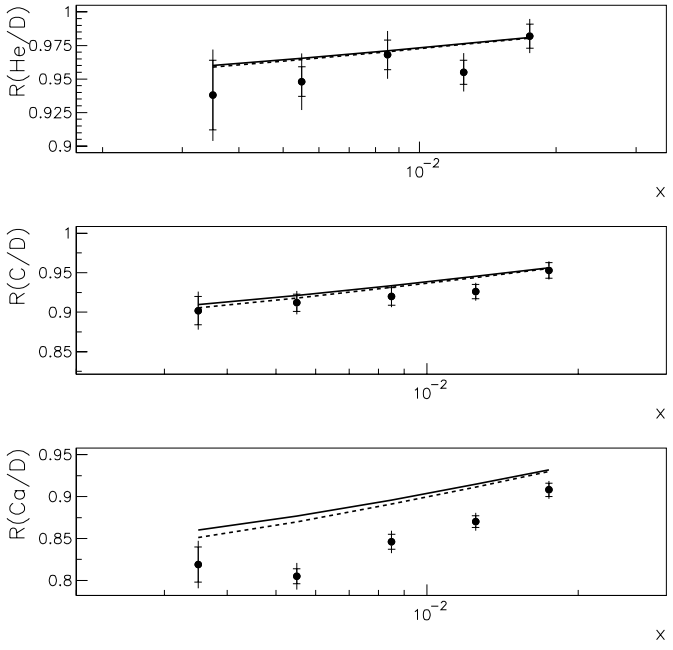

Fig. 5. Id. to Fig. 3 but for the ratios He/D, C/D and Ca/D [39]

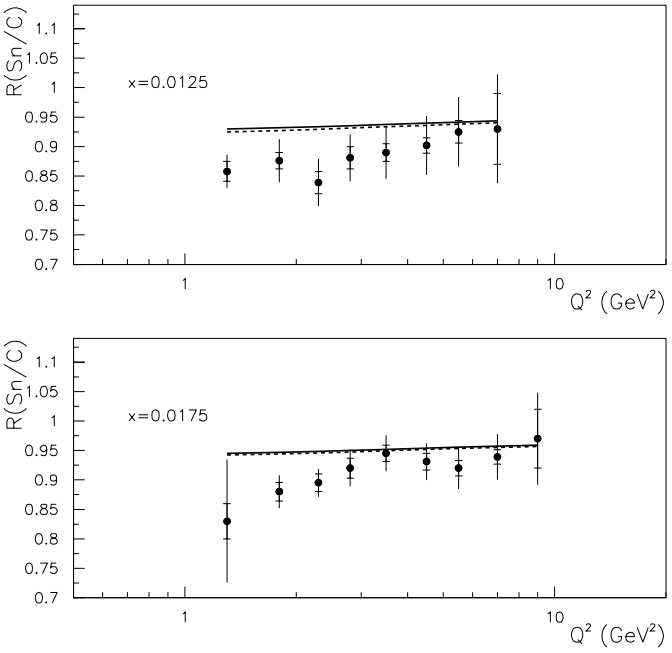

Fig. 6. Results of the model using Schwimmer (solid lines) and eikonal (dashed lines) unitarization compared with experimental data versus Q^2, for the ratio Sn/C [40] at two fixed values of x

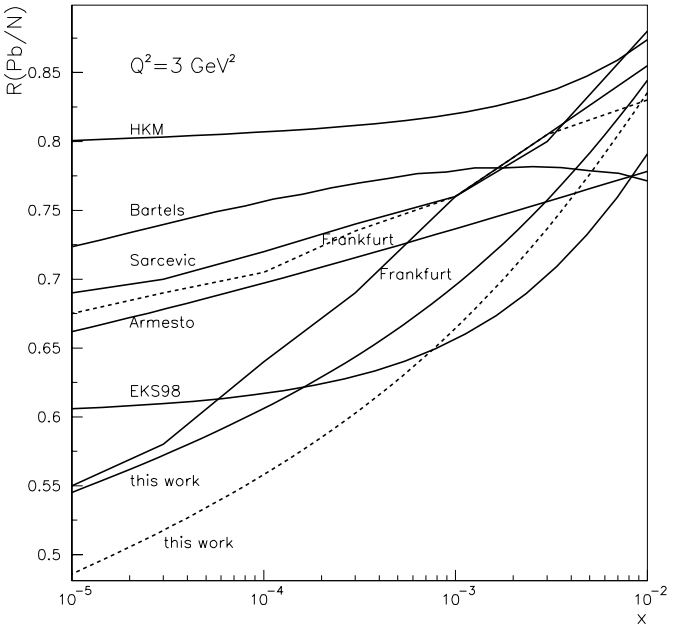

Fig. 7. Comparison of the results of our model using Schwimmer (solid lines) and eikonal (dashed lines) unitarization for the ratio Pb/nucleon with other models, versus x at fixed $Q^2 = 3\,\mathrm{GeV}^2$. HKM are the results from [21], Sarcevic from [42], Bartels from [43], Frankfurt from [11] (at $Q^2 = 4\,\mathrm{GeV}^2$), Armesto from [8] and EKS98 from [19]

In Fig. 7 a comparison of the results of our model with those of others is shown, for $Q^2 = 3\,\mathrm{GeV}^2$ (except the results of [11] which are at $Q^2 = 4\,\mathrm{GeV}^2$). It can be seen that the results of different models agree within 15% at $x \sim 0.01$ where experimental data exist, while they differ up to a factor 0.6 at $x = 10^{-5}$. At this x, our results are the lowest ones but roughly agree with those of [19] and with one set of [11], while the results from [21] are the highest ones, and those of [8,42,43] and the second set of [11] lie in between. Let us briefly comment on these models: In [19,21] an initial condition is parameterized at some Q_0^2 and then evolved using DGLAP; the initial condition is fitted from the comparison of the evolved results with experimental data (see [44] for a comparison between these two models). Reference [8] is a model which uses a saturating ansatz for the total γ^*–nucleon cross section in the proton, which is introduced in a Glauber expression for its extension to the nuclear case. In [11] some parameterization of hard diffraction at Q_0^2, which as in the present work gives nuclear shadowing through Gribov's reggeon calculus, is employed; this nuclear shadowing computed at Q_0^2 is used as initial condition for DGLAP evolution. In [42] a Glauber ansatz provides with the initial condition for DGLAP evolution. Finally, in [43] a non-linear equation for small x evolution is numerically solved [45] and used in the nuclear case. In view of the differences at small x among different models, a measurement of F_2 in nuclei with $\sim 10\%$ precision would be a sensitive test to discriminate among them. Lepton–ion colliders [46] could provide us with such data.

In Fig. 8 our predictions for the ratios D, He, Li, C, Ca, Sn and Pb over the nucleon for $Q^2 = 0.5$, 2 and $5\,\mathrm{GeV}^2$ are given for $x > 10^{-8}$. Let us notice that our model is designed for the small x region and that no antishadowing or any other effects relevant for $x \gtrsim 0.1$ have been introduced. The disappearance of shadowing at $x \sim 0.1$ is a

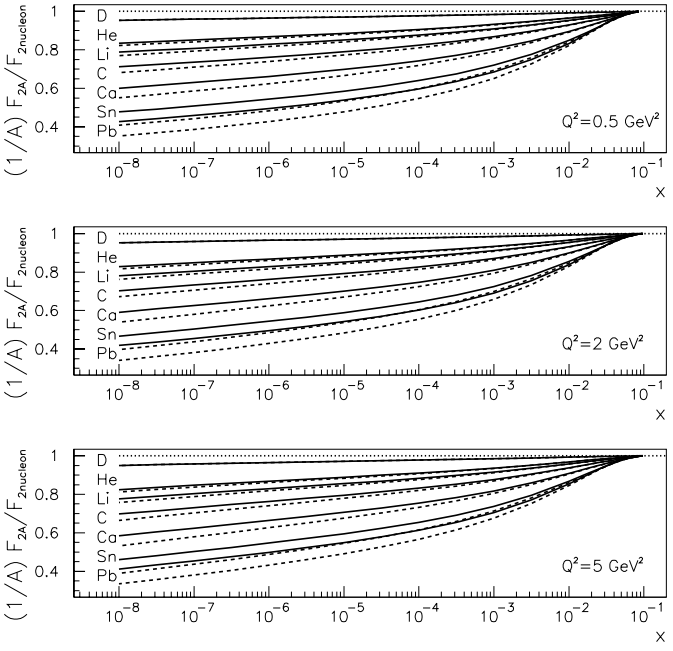

Fig. 8. Results of the model using Schwimmer (solid lines) and eikonal (dashed lines) unitarization for the ratios D/nucleon, He/nucleon, Li/nucleon, C/nucleon, Ca/nucleon, Sn/nucleon and Pb/nucleon versus x at $Q^2 = 0.5$, 2 and $5\,\mathrm{GeV}^2$

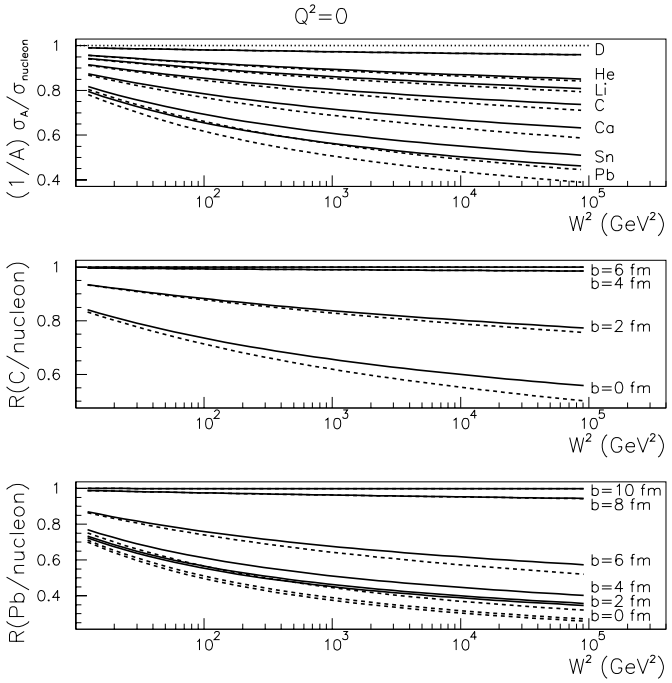

Fig. 9. Results of the model for $Q^2 = 0$ using Schwimmer (solid lines) and eikonal (dashed lines) unitarization for the ratios D/nucleon, He/nucleon, Li/nucleon, C/nucleon, Ca/nucleon, Sn/nucleon and Pb/nucleon (upper plot), and for different impact parameters b for the ratios C/nucleon (plot in the middle) and Pb/nucleon (lower plot), versus W^2

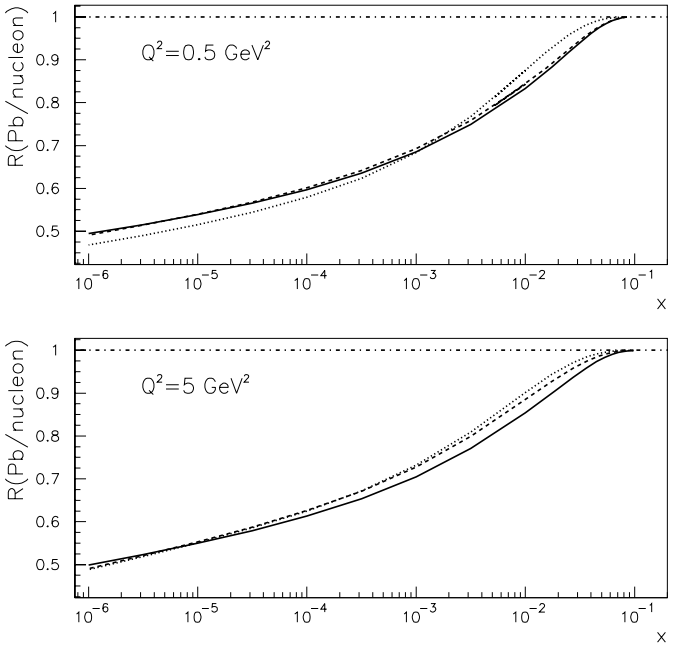

Fig. 10. Results for $Q^2 = 0.5$ (upper plot) and 5 (lower plot) GeV^2 using Schwimmer unitarization for the ratio Pb/nucleon versus x of the model without modifications (solid lines), without the higher-twist contribution in the short-distance component (dashed lines), and without the higher-twist contribution in the short-distance component plus some modification in parameters (dotted lines) to check the sensibility of the results; see text

consequence of both the coherence effects in (3) and the vanishing integration domain in (2); see (7). In Fig. 9 results in photoproduction for the same ratios as in Fig. 8 are given for $W^2 < 10^5\,\mathrm{GeV}^2$, together with predictions for the evolution of the ratios C and Pb over nucleon with impact parameter b. Values as low as 0.3 are reached for central Pb/nucleon. This evolution with centrality is very important to compute the corresponding evolution of particle production in nuclear collisions, and could also be measured in lepton–ion colliders [46].

As a last comment in this section, let us discuss the twist structure of the model (i.e. its structure in powers of $1/Q^2$). In the model of [27] the unitarity corrections to the L component are all of order $1/Q^2$. On the contrary, in the S component the unitarity corrections are higher-twist (they can be expanded as a sum of terms, each one containing an additional factor $1/Q^2$ as compared to the previous one). The fact that diffraction is related to the unitarity corrections allows one to study the $1/Q^2$ behavior of shadowing in this model. In order to keep only the leading-twist contribution (terms $\propto 1/Q^2$ in the cross section) we ignore the higher-twist contribution of the S component to the diffractive cross section[3]. The results are given in Fig. 10. One can see that neglecting these terms introduces only a small difference. The fact that nuclear shadowing corrections are predominantly leading-twist is not unexpected, as the diffractive cross section is also leading-twist for the relevant kinematical region (indeed, in the model of [27] the S component diffraction is almost negligible for small Q^2 and/or large M^2). This is also seen in the fact that the ratio of diffractive to inclusive cross sections does not show any strong Q^2-dependence for large M^2 [47]. Here a comment is in order: in [27] a parameter s_0 is introduced in x and β to control the limit $Q^2 \to 0$, so that all the equations are written for $\bar{x} = x + s_0/(W^2+Q^2)$, $\bar{\beta} = \beta + s_0/(M^2+Q^2)$. These terms could mimic higher-twist corrections. In Fig. 10 we check that the effect of varying this parameter[4] from the original $s_0 = 0.79\,\mathrm{GeV}^2$ to $s_0 = 0.2\,\mathrm{GeV}^2$ is also very small. So, we can conclude that the contribution from higher-twist terms to the shadowing of F_2 is small. In contrast, in [11] a large higher-twist correction for the shadowing is claimed. The approach in this reference is very similar to ours: the authors also compute shadowing from the diffractive cross section, but using the H1 parameterization [48]. The shadowing obtained in this way for $Q_0^2 = 4\,\mathrm{GeV}^2$ is then employed as initial condition for DGLAP evolution, taking the shadowing for valence quarks from [19]. When evolved downwards to $Q^2 = 3\,\mathrm{GeV}^2$ a disagreement is found with experimental data on the ratio Ca over D. This disagreement is attributed to higher-twist contributions.

[3] Concretely, we ignore the S component in (17) of [27], and in (20) of [27] we set the exponential containing χ_S to 1

[4] And setting $c = 0$ in (27) of [27]

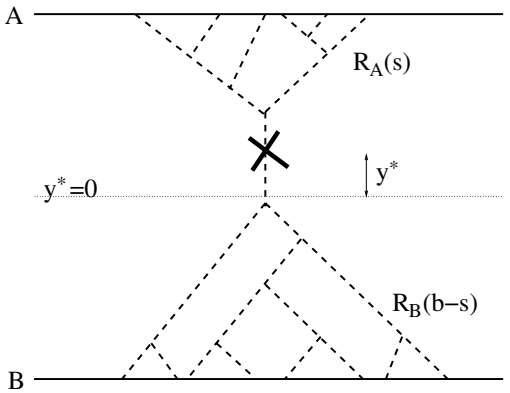

Fig. 11. Diagram showing the contribution to particle production in the central region in AB collisions

4 Multiplicity reduction in nucleus–nucleus collisions

In this framework it is also possible to study the reduction of multiplicities in nucleus–nucleus collisions [49,28,29]. We will denote the rapidity of the produced system in the center of mass frame by y^*. Shadowing as a function of the rapidity of the produced particle can be computed taking into account the general relation with the diffractive variables:

$$y = \ln\left(\frac{1}{x_{\mathrm{P}}}\right) = \ln\left(\frac{s}{M^2}\right). \tag{18}$$

Then the factor for reduction of multiplicities at fixed impact parameter b is [49,28,29]

$$R_{AB}(b) = \frac{\int \mathrm{d}^2 s\; R_A(\mathbf{s}) R_B(\mathbf{b}-\mathbf{s})}{T_{AB}(b)}\ . \tag{19}$$

$R_{A(B)}(b)$ is given by the r.h.s. of (16) multiplied by $T_{A(B)}(b)$ and with $f(x,Q^2)$ substituted by $F(s,y^*)$ (see below), and

$$T_{AB}(b) = \int \mathrm{d}^2 s\; T_A(\mathbf{s}) T_B(\mathbf{b}-\mathbf{s}). \tag{20}$$

Equation (19) takes into account the summation of Schwimmer's fan-like diagrams for the projectile and target, which are joined by a single pomeron whose cut gives rise to the produced particle (Fig. 11). It follows from AGK cancellation [25] that this is the only contribution of this type (more complicated diagrams with lines joining upper and lower parts of the diagram cancel). This provides the justification for the factorized expression (19), which is true even if more general rescattering diagrams are taken into account.

The reduction factor as a function of the rapidity of the produced particles $F(s,y^*)$, can be calculated in several ways. The first one is using (12), but with the integration limits inspired by the parton model for hard processes: for projectile A (target B),

$$x_{A(B)} = \frac{m_{\mathrm{T}}}{\sqrt{s}} \mathrm{e}^{\pm y^*}, \tag{21}$$

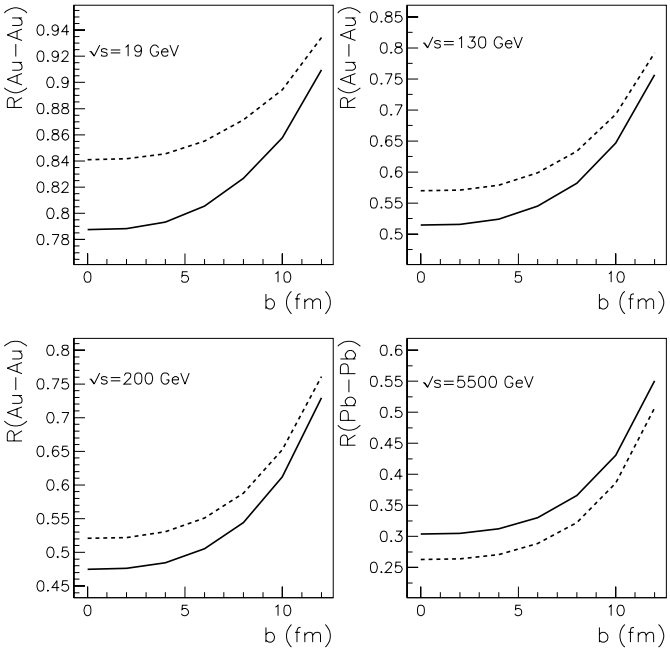

Fig. 12. Results of the model for the multiplicity reduction factor versus impact parameter b at $y^* = 0$, for AuAu collisions at $\sqrt{s} = 19$, 130 and 200 GeV per nucleon, and for PbPb collisions at $\sqrt{s} = 5500$ GeV per nucleon, in the parton model-like realization (solid lines) and for [$C = 0.31\,\mathrm{fm}^2$, $\Delta = 0.13$] (dashed lines)

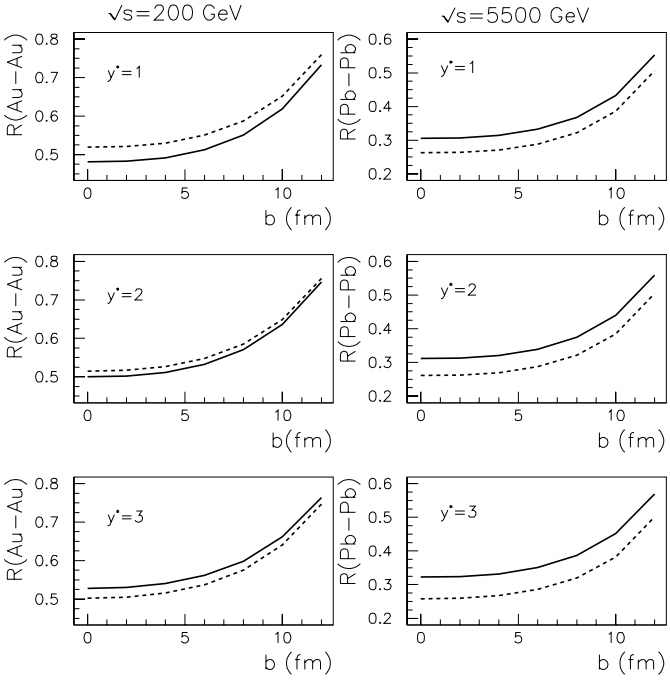

Fig. 13. Id. to Fig. 12 but for AuAu collisions at $\sqrt{s} = 200$ GeV per nucleon and for PbPb collisions at $\sqrt{s} = 5500$ GeV per nucleon, for $y^* = 1$, 2 and 3

with $y^* > 0$ for the projectile hemisphere and $y^* < 0$ for the target one, and $m_{\mathrm{T}} = \sqrt{m^2 + p_{\mathrm{T}}^2}$ the transverse mass of the produced particle. Substituting in the general relation for $M^2_{\max}$, (7), we get

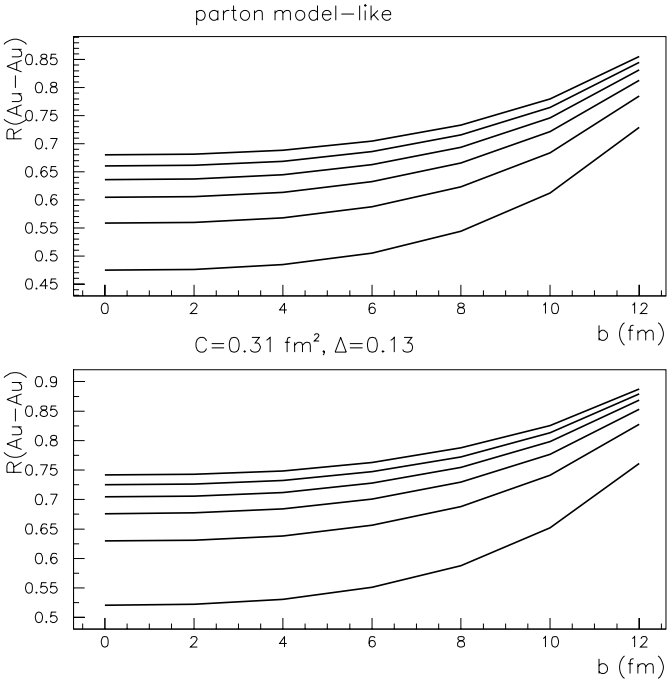

Fig. 14. Results of the model for the multiplicity reduction factor versus impact parameter b at $y^* = 0$, for AuAu collisions at $\sqrt{s} = 200\,\mathrm{GeV}$ per nucleon, in the parton model-like realization (upper plot) and for [$C = 0.31\,\mathrm{fm}^2$, $\Delta = 0.13$] (lower plot). In each plot, lines from bottom to top correspond to $m_\mathrm{T}^2 = 0.16$, 1, 2, 3, 4 and $5\,\mathrm{GeV}^2$

$$M_{\max}^{2(A(B))} = Q^2 \left(\frac{x_{\mathrm{P}\max}}{x_{A(B)}} - 1 \right) = Q^2 \left(\frac{x_{\mathrm{P}\max}\sqrt{s}}{m_\mathrm{T}} \mathrm{e}^{\mp y^*} - 1 \right), \quad (22)$$

while $M_{\min}^2$ remains fixed and equal to $0.08\,\mathrm{GeV}^2$, and $Q^2 = m_\mathrm{T}^2$.

On the other hand, we can also compute the reduction factor from the formulas [28,29]

$$F(s, y^*) = 4\pi \int_{y_{\min}}^{y_{\max}} \mathrm{d}y \, \frac{1}{\sigma_{\mathrm{P}}(s)} \left. \frac{\mathrm{d}\sigma^{\mathrm{PPP}}}{\mathrm{d}y\mathrm{d}t} \right|_{t=0} F_A^2(t_{\min}), \quad (23)$$

where $\sigma_{\mathrm{P}}(s)$ is the single pomeron exchange cross section and $\frac{\mathrm{d}\sigma^{\mathrm{PPP}}}{\mathrm{d}y\mathrm{d}t}$ the triple pomeron cross section. Using the standard triple pomeron formula for the latter, we get

$$\frac{1}{\sigma_{\mathrm{P}}(s)} \left. \frac{\mathrm{d}\sigma^{\mathrm{PPP}}}{\mathrm{d}y\mathrm{d}t} \right|_{t=0} = C\Delta \exp(\Delta y), \quad (24)$$

with $C = \frac{g_{pp}^{\mathrm{P}}(0) r_{\mathrm{PPP}}(0)}{4\Delta}$, $g_{pp}^{\mathrm{P}}(0)$ the pomeron–proton coupling and $r_{\mathrm{PPP}}(0)$ the triple pomeron coupling, both evaluated at $t = 0$. In this case, the same integration limits used above correspond to

$$y_{\min}^{(A(B))} = \ln \left(\frac{s}{M_{\max}^{2(A(B))}} \right), \quad (25)$$

with $M_{\max}^{2(A(B))}$ given by (22), and

$$y_{\max}^{(A(B))} = \frac{1}{2} \ln \left(\frac{s}{m_\mathrm{T}^2} \right) \mp y^*. \quad (26)$$

In the calculations we have used [$C = 0.31\,\mathrm{fm}^2$, $\Delta = 0.13$] taken from [50] (used in [28,29]). A value $m_\mathrm{T} = 0.4\,\mathrm{GeV}$ is employed by default (in [28,29] the nucleon mass m_N was used). The sensibility of our results to variations in m_T will be examined.

In Fig. 12 our results at $y^* = 0$ are presented for AuAu at RHIC energies and for PbPb collisions at the LHC, versus impact parameter. Reductions of multiplicities at $b = 0$ by factors $\sim 1/2$ for RHIC and $\sim 1/3$ for LHC are found, with a clear increase of the suppression with increasing energy. In Fig. 13 results are presented for AuAu at RHIC and PbPb at LHC for different y^*. Finally, in Fig. 14 the variation with m_T of the results at $y^* = 0$ for AuAu at RHIC is studied. A reduction of the suppression with increasing m_T is seen, as expected. Let us make two comments: First, our results for the reduction factors are very similar to the ones estimated in [28,29]. It has been shown in [28,29] that when these reduction factors are used to correct the results of the dual parton model, one obtains a good description of the RHIC data on multiplicities and their evolution with centrality. Thus, our results provide a detailed calculation of these reduction factors, which confirms the estimations in [28,29].

Second, our results are important in studying particle production in heavy ion collisions. In particular, the dependence of the reduction factors on m_T gives the variation of shadowing corrections with the p_T of the produced particle[5].

5 Conclusions

In this paper, we have used the relation which arises from reggeon calculus and the AGK rules, between the diffractive cross section measured in DIS on nucleons and the first contribution (i.e. double scattering) to nuclear shadowing. The next contributions have been estimated using two different methods for unitarization. In this way we have obtained a description of nuclear shadowing, based on the model of [27] for diffraction, which agrees with the existing experimental data without any fitted parameter. The model is designed for the region of $x < 0.01$ and $Q^2 < 10\,\mathrm{GeV}^2$, i.e. small x and small or moderate Q^2.

The same method has been applied in [10,11]. In [10], a model for diffraction [50] has been used that takes into account unitarization effects in an effective manner, so the extrapolation to smaller x or larger W^2 is not so reliable as in the full unitarization program followed in [27]; furthermore, the description of diffraction in the model we use is substantially better due to the inclusion in the fits of new, more precise experimental data. In [11], a model for diffraction is used in order to obtain an initial condition for DGLAP evolution at $Q_0^2 = 4\,\mathrm{GeV}^2$, so their leading-twist description for nuclear shadowing is not valid at small Q^2.

[5] For reduction factors based on other mechanisms, see [51,52]

On the contrary, we develop a model valid for the full low Q^2 region which does not correspond to any definite twist but contains contributions from all twist orders.

Nevertheless, it turns out that, as discussed at the end of Sect. 3, the leading-twist contribution is the dominant one in our model, which is in reasonable agreement with the existing experimental data. Precise data on the Q^2-dependence of nuclear structure functions should disentangle these two possibilities. The existing data from NMC [40] can be well reproduced within the leading-twist DGLAP evolution [19] with an appropriate set of initial conditions.

An extension of our results using DGLAP evolution for large values of Q^2 is thus a natural continuation of our work [41].

In this framework we have also obtained the factor for multiplicity reduction in nucleus–nucleus collisions. This factor reaches values $\sim 1/2$ and $\sim 1/3$ for central AuAu and PbPb collisions at RHIC and LHC respectively. It is therefore a very important ingredient for the computation of particle production at these energies which should be taken into account together with other possible effects.

Comparison among models shows differences of a factor 0.6 for the ratio of structure functions Pb/nucleon at $x = 10^{-5}$ and $Q^2 = 3\,\mathrm{GeV}^2$. These differences have a large impact on the computation of particle production in nuclear collisions at the energies of RHIC and LHC. They should be testable in future lepton–ion colliders [46].

To conclude, the method which we have followed offers a natural link between the measurements of nucleon diffractive structure functions and nuclear shadowing, and between the latter and the suppression of particle production in nuclear collisions. In this way the study of low x physics at HERA is linked to that of nuclear structure functions at future lepton–ion colliders and with heavy ion physics at RHIC and LHC [15].

Acknowledgements. The authors express their gratitude to B. Badelek, E. G. Ferreiro, B. Z. Kopeliovich, J. Raufeisen and M. Strikman for useful comments and discussions. They also thank M. Lublinsky for discussions and for providing the results [43], and C. Pajares for a reading of the manuscript. A.C., A.B.K. and C.A.S. acknowledge financial support by grant INTAS 00-00366, and A.B.K. by grants RFBR 00-15-96786, RFBR 01-02-17383 and DFG 436 RUS 113/721/0-1. N.A. thanks the Institute for Nuclear Theory at the University of Washington for its hospitality and the US Department of Energy for partial support during the completion of this work. J.L.-A. thanks CERN Theory Division for kind hospitality, and Universidad de Córdoba and Ministerio de Educación, Cultura y Deporte of Spain (grant AP2001-3333) for financial support. C.A.S. is supported by a Marie Curie Fellowship of the European Community programme TMR (Training and Mobility of Researchers), under the contract number HPMF-CT-2000-01025.

References

1. M. Arneodo, Phys. Rept. **240**, 301 (1994)
2. D.F. Geesaman, K. Saito, A.W. Thomas, Ann. Rev. Nucl. Part. Sci. **45**, 337 (1995)
3. S.J. Brodsky, T.E. Close, J.F. Gunion, Phys. Rev. D **6**, 177 (1972); S.J. Brodsky, H.J. Liu, Phys. Rev. Lett. **64**, 1342 (1990)
4. N.N. Nikolaev, B.G. Zakharov, Z. Phys. C **49**, 607 (1991)
5. V. Barone, M. Genovese, N.N. Nikolaev, E. Predazzi, B.G. Zakharov, Z. Phys. C **58**, 541 (1993)
6. B.Z. Kopeliovich, B. Povh, Phys. Lett. B **367**, 329 (1996)
7. N. Armesto, M.A. Braun, Z. Phys. C **76**, 81 (1997)
8. N. Armesto, Eur. Phys. J. C **26**, 35 (2002)
9. B.Z. Kopeliovich, J. Raufeisen, A.V. Tarasov, Phys. Rev. C **62**, 035204 (2000); J. Nemchik, hep-ph/0301043
10. A. Capella, A.B. Kaidalov, C. Merino, D. Pertermann, J. Tran Thanh Van, Eur. Phys. J. C **5**, 111 (1998)
11. L. Frankfurt, V. Guzey, M. McDermott, M. Strikman, JHEP **0202**, 027 (2002); L. Frankfurt, V. Guzey, M. Strikman, hep-ph/0303022
12. L.V. Gribov, E.M. Levin, M.G. Ryskin, Phys. Rept. **100**, 1 (1983)
13. A.H. Mueller, J.-W. Qiu, Nucl. Phys. B **268**, 427 (1986); J.-W. Qiu, Nucl. Phys. B **291**, 746 (1987); E.L. Berger, J.-W. Qiu, Phys. Lett. B **206**, 42 (1988)
14. L.D. McLerran, R. Venugopalan, Phys. Rev. D **49**, 2233, 3352 (1994); D **50**, 2225 (1994)
15. A.H. Mueller, hep-ph/0208278
16. R. Venugopalan, Acta Phys. Polon. B **30**, 3731 (1999)
17. QCD Perspectives on Hot and Dense Matter, edited by J.-P. Blaizot, E. Iancu, NATO Science Series (Kluwer Academic Publishers 2002)
18. N. Armesto, C.A. Salgado, Phys. Lett. B **520**, 124 (2001)
19. K.J. Eskola, V.J. Kolhinen, P.V. Ruuskanen, Nucl. Phys. B **535**, 351 (1998); K.J. Eskola, V.J. Kolhinen, C.A. Salgado, Eur. Phys. J. C **9**, 61 (1999)
20. D. Indumathi, W. Zhu, Z. Phys. C **74**, 119 (1997)
21. M. Hirai, S. Kumano, M. Miyama, Phys. Rev. D **64**, 034003 (2001)
22. Yu.L. Dokshitzer, Sov. Phys. JETP **46**, 641 (1977) [Zh. Eksp. Teor. Fiz. **73**, 1216 (1977)]; V.N. Gribov, L.N. Lipatov, Yad. Fiz. **15**, 781 (1972) [Sov. J. Nucl. Phys. **15**, 438 (1972)]; G. Altarelli, G. Parisi, Nucl. Phys. B **126**, 298 (1977)
23. V.N. Gribov, Sov. Phys. JETP **29**, 483 (1969) [Zh. Eksp. Teor. Fiz. **56**, 892 (1969)]; Sov. Phys. JETP **30**, 709 (1970) [Zh. Eksp. Teor. Fiz. **57**, 1306 (1969)]
24. V.N. Gribov, Sov. Phys. JETP **26**, 414 (1968) [Zh. Eksp. Teor. Fiz. **53**, 654 (1967)]
25. V.A. Abramovsky, V.N. Gribov, O.V. Kancheli, Yad. Fiz. **18**, 595 (1973) [Sov. J. Nucl. Phys. **18**, 308 (1974)]
26. A. Capella, E.G. Ferreiro, A.B. Kaidalov, C.A. Salgado, Nucl. Phys. B **593**, 336 (2001)
27. A. Capella, E.G. Ferreiro, A.B. Kaidalov, C.A. Salgado, Phys. Rev. D **63**, 054010 (2001)
28. A. Capella, A.B. Kaidalov, J. Tran Thanh Van, Heavy Ion Phys. **9**, 169 (1999)
29. A. Capella, D. Sousa, Phys. Lett. B **511**, 185 (2001)
30. C.W. De Jager, H. De Vries, C. De Vries, Atom. Data Nucl. Data Table **14**, 479 (1974)
31. M.A. Preston, R.K. Bhoduri, Structure of the nucleus (Addison-Wesley, New York 1975)
32. K. Golec-Biernat, M. Wüsthoff, Phys. Rev. D **60**, 114023 (1999)
33. J. Breitweg et al. [ZEUS Collaboration], Eur. Phys. J. C **1**, 81 (1998)

34. J. Breitweg et al. [ZEUS Collaboration], Eur. Phys. J. C **2**, 237 (1998)
35. A. Schwimmer, Nucl. Phys. B **94**, 445 (1975)
36. M.R. Adams et al. [E665 Collaboration], Z. Phys. C **67**, 403 (1995)
37. M.R. Adams et al. [E665 Collaboration], Phys. Rev. Lett. **68**, 3266 (1992)
38. M. Arneodo et al. [NMC Collaboration], Nucl. Phys. B **481**, 3 (1996)
39. P. Amaudruz et al. [NMC Collaboration], Nucl. Phys. B **441**, 3 (1995)
40. M. Arneodo et al. [NMC Collaboration], Nucl. Phys. B **481**, 23 (1996)
41. N. Armesto, A. Capella, A.B. Kaidalov, J. López-Albacete, C.A. Salgado, in preparation
42. Z. Huang, H.J. Lu, I. Sarcevic, Nucl. Phys. A **637**, 79 (1998)
43. J. Bartels, E. Gotsman, E.M. Levin, M. Lublinsky, U. Maor, hep-ph/0304166
44. K.J. Eskola, H. Honkanen, V.J. Kolhinen, C.A. Salgado, hep-ph/0302170
45. E. Gotsman, E.M. Levin, M. Lublinsky, U. Maor, Eur. Phys. J. C **27**, 411 (2003)
46. M. Arneodo et al., in Proceedings of the Workshop on Future Physics at HERA (Hamburg, Germany, September 1995); H. Abramowicz et al., in TESLA Technical Design Report, Part VI, Chapter 2, edited by R. Klanner, U. Katz, M. Klein, A. Levy; EIC White Paper, preprint BNL-68933, edited by A. Deshpande, R. Milner, R. Venugopalan
47. F.P. Schilling [H1 Collaboration], hep-ex/0210027
48. C. Adloff et al. [H1 Collaboration], Z. Phys. C **76**, 613 (1997)
49. L. Caneschi, A. Schwimmer, R. Jengo, Nucl. Phys. B **108**, 82 (1976); S. Bondarenko, E. Gotsman, E. M. Levin, U. Maor, Nucl. Phys. A **683**, 649 (2001)
50. A. Capella, A.B. Kaidalov, C. Merino, J. Tran Thanh Van, Phys. Lett. B **343**, 403 (1995); A. Capella, A.B. Kaidalov, C. Merino, D. Pertermann, J. Tran Thanh Van, Phys. Rev. D **53**, 2309 (1996)
51. Proceedings of the XVIth International Conference On Ultrarelativistic Nucleus–Nucleus Collisions: Quark Matter 2002 (QM 2002) (Nantes, France, 18–24 July 2002), to appear in Nucl. Phys. A
52. N. Armesto, C. Pajares, Int. J. Mod. Phys. A **15**, 2019 (2000)

Energy Dependence of the Cronin Effect from Nonlinear QCD Evolution

Javier L. Albacete,[1,2] Néstor Armesto,[2] Alex Kovner,[2,3] Carlos A. Salgado,[2] and Urs Achim Wiedemann[2]

[1]*Departamento de Física, Universidad de Córdoba, 14071 Córdoba, Spain*

[2]*Theory Division, CERN, CH-1211 Geneva 23, Switzerland*

[3]*Department of Mathematics and Statistics, University of Plymouth, Drake Circus, Plymouth PL4 8AA, United Kingdom*

(Received 14 July 2003; published 24 February 2004)

The nonlinear evolution of dense partonic systems has been suggested as a novel physics mechanism relevant for the dynamics of *p*-*A* and *A*-*A* collisions at collider energies. Here we study to what extent the description of Cronin enhancement in the framework of this nonlinear evolution is consistent with the recent observation in $\sqrt{s} = 200$ GeV *d*-Au collisions at the Relativistic Heavy Ion Collider. We solve the Balitsky-Kovchegov evolution equation numerically for several initial conditions encoding Cronin enhancement. We find that the properly normalized nuclear gluon distribution is suppressed at all momenta relative to that of a single nucleon. For the resulting spectrum of produced gluons in *p*-*A* and *A*-*A* collisions, the nonlinear QCD evolution is unable to generate a Cronin-type enhancement, and it quickly erases any such enhancement which may be present at lower energies.

DOI: 10.1103/PhysRevLett.92.082001 PACS numbers: 12.38.Bx

The observation that the ratio of particle yields in *p*-*A* and *A*-*A*, scaled by the number of collisions, exceeds unity in an intermediate transverse momentum range of a few GeV is commonly referred to as Cronin effect. The effect was first seen at lower fixed target energies [1] and has recently been confirmed in $\sqrt{s} = 200$ GeV *d*-Au collisions at Relativistic Heavy Ion Collider (RHIC) [2]. The current interest focuses mainly on comparing this Cronin *enhancement* in *d*-Au to the relative *suppression* of produced hadrons in Au-Au collisions at the same center of mass energy and in the same transverse momentum range [3]. The opposite trend of the two effects and their centrality dependence suggests that *d*-Au data may serve as an efficient benchmark measurement to distinguish between the two different physical mechanisms suggested for the relative suppression of hadron spectra in Au-Au collisions: initial state parton saturation [4] and final state jet quenching [5].

In particular, it has been suggested that, due to quantum evolution, saturation effects can account for the suppression of the high-p_T hadronic spectra in Au-Au collisions at RHIC above the saturation scale [4]. On the other hand, it is known that saturation models based on multiple scattering (the so-called Glauber-Mueller [6] or McLerran-Venugopalan [7] models) exhibit Cronin enhancement in *p*-*A* [8–10] and *A*-*A* [9,11]. In these models, quantum evolution is not implemented, and the saturation of low p_T gluons is the result of a redistribution of gluons in transverse phase space [12,13] which does not change the total number of gluons, thus resulting in a compensating enhancement at momenta just above the saturation momentum Q_s. These models are now being used to understand bulk properties of ultrarelativistic heavy ion collisions such as the multiplicity, rapidity distribution, and centrality dependence of particle production [14]. What is not fully understood is (i) whether such Cronin enhancement encoded in the initial condition of a nuclear wave function persists in the nonlinear perturbative QCD evolution to higher energy and (ii) whether such Cronin enhancement can be generated by the nonlinear evolution itself. This Letter goes beyond earlier discussions [9–11] by providing the first complete (numerical) answer to these questions. We do not address other approaches to Cronin enhancement [15].

We start from the Balitsky-Kovchegov (BK) evolution equation [16,17], which describes the evolution of the forward scattering amplitude $N(\mathbf{r}, y)$ of a QCD dipole of transverse size $|\mathbf{r}|$ with rapidity Y and $y = (\alpha_s N_c/\pi) Y$,

$$\frac{dN(|\mathbf{r}|, y)}{dy} = \frac{1}{2\pi}\int d^2z \frac{\mathbf{r}^2}{(\mathbf{r}-\mathbf{z})^2\,\mathbf{z}^2} \times [N(|\mathbf{r}-\mathbf{z}|) + N(|\mathbf{z}|) - N(|\mathbf{r}|) - N(|\mathbf{r}-\mathbf{z}|)N(|\mathbf{z}|)]. \quad (1)$$

The unintegrated gluon distribution is related to the inclusive gluon distribution $\phi(k) \propto \{d[xG(x, k^2)]\}/(d^2k d^2b)$ and is given in terms of the dipole amplitude

$$\phi(k) = \int \frac{d^2r}{2\pi r^2} \exp\{i\mathbf{r}\cdot\mathbf{k}\} N(r). \quad (2)$$

In the following, we also use the modified gluon distribution

$$h(k) = k^2 \nabla_k^2 \phi(k). \quad (3)$$

The two definitions coincide for the leading order perturbative distribution $\phi(k) \propto 1/k^2$, but are different in general, and especially at low momenta.

Using the second order Runge-Kutta algorithm [18], we solve the BK Eq. (1) numerically with 8000 equally spaced intervals in $\ln k$ space between -15 and 35 and a step $\Delta y = 0.0025$. The accuracy of this algorithm is better than 2% in the entire range of k discussed below.

We evolve two initial conditions given by the McLerran-Venugopalan [7] (MV) and Golec-Biernat–Wüsthoff [19] (GBW) model, respectively:

$$N_{\mathrm{MV}}^{Q_s} = 1 - \exp\left[-\frac{Q_s^2 r^2}{4}\ln\left(\frac{1}{r^2\Lambda_{\mathrm{QCD}}^2} + e\right)\right], \quad (4)$$

$$N_{\mathrm{GBW}}^{Q_s} = 1 - \exp\left[-\frac{Q_s^2 r^2}{4}\right], \quad (5)$$

where $\Lambda_{\mathrm{QCD}} = 0.2$ GeV. For momenta $k \geq O(1\ \mathrm{GeV})$, the sensitivity on the infrared cutoff e is negligible. The amplitudes N_{MV} and N_{GBW} are similar for momenta of order Q_s, but differ strongly in their high k behavior; $\phi_{\mathrm{GBW}}(k)$ decays exponentially while ϕ_{MV} has a power-like tail $1/k^2$.

Figure 1 shows the evolution of $h(k, y)$ and $\phi(k, y)$ for different initial conditions. The solutions for $h(k, y)$ quickly approach a universal solitonlike shape and do not change further except uniformly moving in k on the logarithmic plot. The position of the maximum is the evolved value of the saturation momentum $Q_s(y)$. The solutions for different initial conditions and different rapidities scale as a function of the scaling variable $\rho = k/Q_s(y)$. The shape of the initial condition affects only the value of the saturation momentum $Q_s(y)$, but not the shape of the evolved function $h(\rho, y)$. The y dependence of $h(\rho, y)$ is very weak: The function evolves fast towards a scaling form $h(\rho)$. As the rapidity changes between $y = 4$ and $y = 10$, the ratio $h(\rho, y_1)/h(\rho, y_2)$ varies by at most 40% over 3 orders of magnitude of the scaling variable ρ. Similar behavior was found for ϕ (results not shown). This is consistent with previous numerical works [20,21].

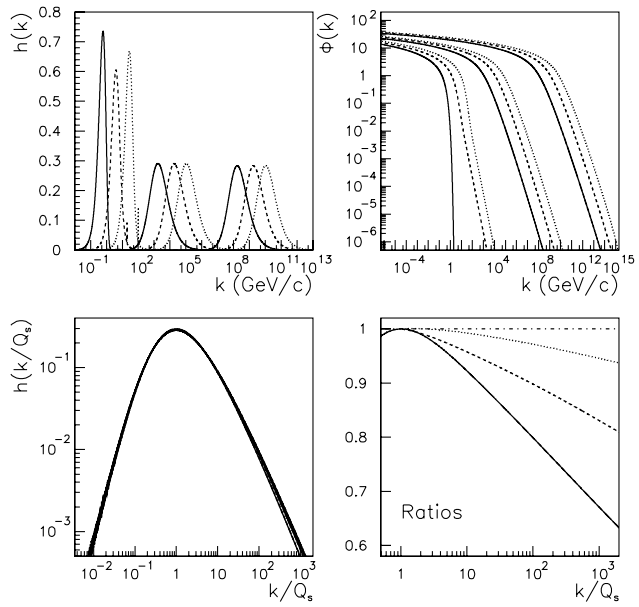

FIG. 1. Solutions of the BK equation. Upper left: $h(k)$ evolved (left to right) from $y = 0$ to 5 and 10 for different initial conditions: GBW with $Q_s^2 = 0.36\,\mathrm{GeV}^2$ (solid lines), MV with $Q_s^2 = 4\ \mathrm{GeV}^2$ (dashed lines), and MV with $Q_s^2 = 100\ \mathrm{GeV}^2$ (dotted lines). Upper right: The same as upper left for $\phi(k)$. Lower left: The scaled function $h(\rho)$ versus $\rho = k/Q_s$ for $y = 4$, 6, 8, and 10, and the same initial conditions and conventions (lines cannot be distinguished). Lower right: Ratio of $h(y, \rho)/h(y, \rho = 1)$ over $h(y = 10, \rho)/h(y = 10, \rho = 1)$ for $y = 4$ (solid line), 6 (dashed line), 8 (dotted line), and 10 (dash-dotted line), and initial condition MV with $Q_s^2 = 4\ \mathrm{GeV}^2$.

To get a quantitative idea of the behavior of the scaling solution, we fitted the numerical solution of $\phi(\rho)$ to two analytical expressions: $s_1(\rho) = a\rho^{2(1-\lambda)}$ and $s_2(\rho) = a\ln(b\rho)\rho^{2(1-\lambda)}$ for $\rho > 5$. The functional form s_1 with $\lambda = 0.37$ and $\ln Q_s \propto y$ describes the scaling behavior of solutions of the linear Balitsky-Fadin-Kuraev-Lipatov (BFKL) equation [22]. It was argued in Ref. [23] that s_2 with the same value of λ and $\ln Q_s \propto \{[2\chi(\lambda)]/(1-\lambda)\}y - \{3/[2(1-\lambda)]\}\ln y$ accounts for the effects of nonlinearities in (1). We find that s_1 does not give an acceptable fit to $\phi(\rho)$ in any extended range of ρ. For values of ρ between 1 and 10^3, the value of λ varies between 0.39 and 0.46. This is in contrast to the BFKL equation, where we find numerically that s_1 with $\lambda = 0.37$ does indeed approximate the solution over several orders of magnitude with very good accuracy (results not shown). On the other hand, for $5 < \rho < 1000$, s_2 gives a good fit with $\lambda = 0.32$. If, following [23], we fix $\lambda = 0.37$, the fit is still good.

To study the effect of the evolution on the Cronin enhancement, we consider two initial conditions, $N_{\mathrm{MV}}^q(r)$ and $N_{\mathrm{MV}}^Q(r)$ with $q^2 = 0.1\ \mathrm{GeV}^2$ and $Q^2 = 2\ \mathrm{GeV}^2$. Since $q \sim \Lambda_{\mathrm{QCD}}$ and Q is of the order of the estimated saturation momentum for a gold nucleus [14], this choice mimics the gluon distributions of a proton and of a nucleus, respectively. At large transverse momenta, the ratio of the corresponding Fourier transforms is given by the ratio of the saturation momenta,

$$\frac{h^Q(k, y = 0)}{h^q(k, y = 0)} = \frac{Q^2}{q^2} = A^{1/3}. \quad (6)$$

This relation also holds for ϕ. As discussed in [9,10], these initial conditions exhibit Cronin enhancement, namely, $[h^Q(k, y = 0)]/[A^{1/3}h^q(k, y = 0)] > 1$ for $k \sim Q$. We solve the BK equation with these two initial conditions and construct the ratio $R(k, y) = h^Q(k, y)/A^{1/3}h^q(k, y)$ and the corresponding ratio for ϕ (see Fig. 2). The initial Cronin enhancement at rapidity $y = 0$ is seen to be wiped out very quickly by the evolution. Within less than half a unit of rapidity y, the ratios show uniform suppression for all values of transverse momentum. The observed behavior persists if different amounts of Cronin enhancement are included in the initial condition.

As seen in the lower panel of Fig. 2, the Cronin enhancement also disappears rapidly with rapidity when gluon distributions are evolved according to the linear BFKL equation. Qualitative differences between the BFKL and BK dynamics are only visible at momenta $k < Q_s$, where saturation effects are important. For larger

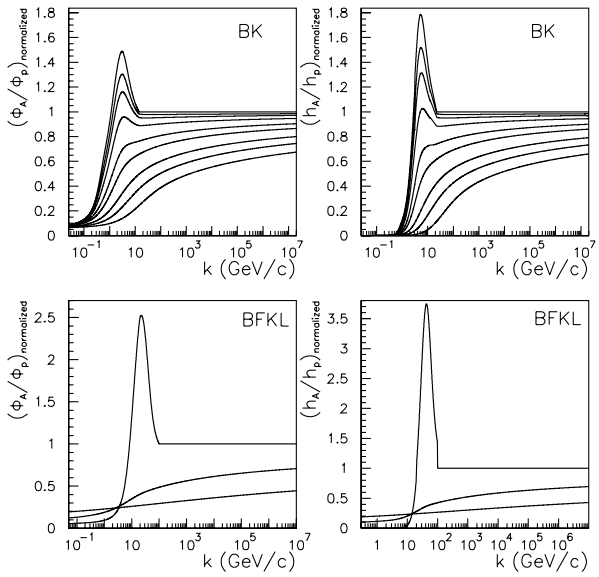

FIG. 2. Ratio of distributions ϕ and h in nucleus and proton, normalized to 1 at $k \to \infty$. Upper plots: BK evolution, with MV as initial condition with $Q_s^2 = 0.1$ GeV^2 for p and 2 GeV^2 for A. Lines from top to bottom correspond to $y = 0$, 0.05, 0.1, 0.2, 0.4, 0.6, 1, 1.4, and 2. Lower plots: BFKL evolution, with MV as initial condition with $Q_s^2 = 4$ GeV^2 for p and 100 GeV^2 for A. Lines from top to bottom correspond to $y = 0$, 1, and 4.

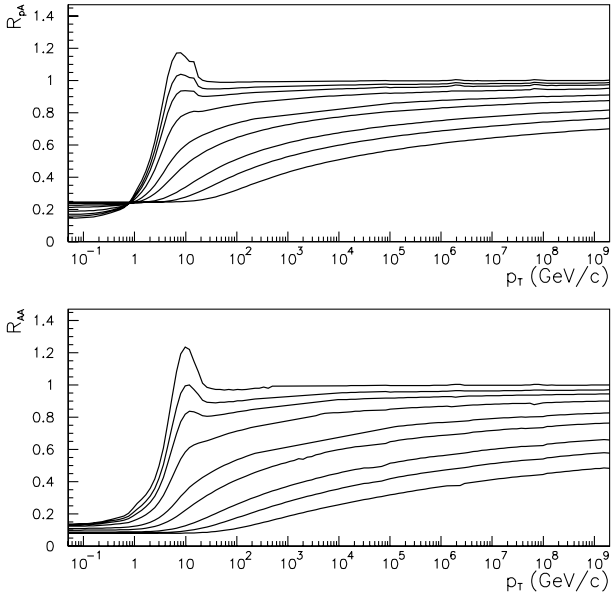

FIG. 3. Ratios R_{pA} and R_{AA} of gluon yields in p-A (upper plot) and A-A (lower plot) for BK evolution, with MV as initial condition with $Q_s^2 = 0.1$ GeV^2 for p and 2 GeV^2 for A. Lines from top to bottom correspond to $y = 0$, 0.05, 0.1, 0.2, 0.4, 0.6, 1, 1.4, and 2.

momenta k, the ratios are very similar for linear and nonlinear QCD evolution. We, thus, conclude that the wiping out of the initial enhancement is primarily driven by the linear BFKL dynamics which is contained in the BK equation as well.

For the evolved gluon distributions determined above, we have calculated the yield of produced gluons in p-A and A-A collisions at central rapidity according to the factorized expressions [24]

$$\frac{dN_{pA}}{dyd^2pd^2b} \propto \frac{1}{p^2}\int d^2k\, h^q(y,k)h^Q(y,\mathbf{p}-\mathbf{k}), \qquad (7)$$

$$\frac{dN_{AA}}{dy\,d^2p\,d^2b} \propto \frac{A^{2/3}}{p^2}\int d^2k\, h^Q(y,k)h^Q(y,\mathbf{p}-\mathbf{k}). \qquad (8)$$

From these spectra we compute the p- and y-dependent ratios

$$R_{pA} = \frac{\frac{dN_{pA}}{dyd^2pd^2b}}{A^{1/3}\frac{dN_{pp}}{dyd^2pd^2b}}, \qquad R_{AA} = \frac{\frac{dN_{AA}}{dyd^2pd^2b}}{A^{4/3}\frac{dN_{pp}}{dyd^2pd^2b}}.$$

As seen in Fig. 3, the nonlinear BK evolution quickly wipes out any initial Cronin enhancement not only on the level of single parton distribution functions but also on the level of particle spectra. We performed several checks to establish that this behavior is generic. First, we checked the disappearance of Cronin enhancement by evolving different initial conditions corresponding to different initial amounts of enhancement. Second, we note that, in some calculations of gluon production in p-A, the gluon distribution ϕ [25] rather than h [24,26,27] enters the right-hand side of (7). Results using ϕ were found to be close to those shown in Fig. 3. Third, different calculations of (7) employ h defined in terms of the scattering amplitude either of the fundamental [24] dipole used here, or of the adjoint [10,26,27] one. By expressing the adjoint dipole amplitude in terms of the fundamental one, $N_{\rm adj} = 2N - N^2$, we checked that our results remain qualitatively the same for the adjoint case. To summarize, the expressions (7) and (8) are subject to uncertainties as discussed in more detail in [9]. However, our conclusion about the disappearance of Cronin enhancement during QCD evolution is likely to persist in more refined ways of calculating particle spectra, since it is rooted directly in the rapidity dependence of gluon distributions [9].

We now comment on a recent formal argument which — in contrast to our numerical findings — suggests enhancement survives the nonlinear evolution. It is based on the observation that at very short distances $r \to 0$, $N(r)$ is not affected by evolution. Thus, the integral of ϕ over the transverse momentum is expected to be rapidity independent,

$$\int d^2k\, \phi(k) = \frac{1}{r^2}N(r)|_{r=0}. \qquad (9)$$

One thus obtains the sum rule

$$\int d^2k\, \phi_A(k,y) = A^{1/3}\int d^2k\, \phi_p(k,y), \qquad (10)$$

valid for any rapidity, since it is satisfied by the initial condition $\phi_{\rm MV}$. Since the nonlinear evolution leads to the

depletion of the gluon distribution $\phi_A(k)$ relative to $A^{1/3}\phi_p(k)$ at low momenta, it must follow that in some range of momenta this effect is compensated by enhancement of ϕ_A. However, this argument breaks down since the quantity defined in (9) is infinite. As such, (10) relates only the (UV) divergent parts of the integrals, and carries no information about possible behavior at finite momentum. To be more specific, we use the scaling property $\phi(k, y) = \phi[k/Q_s(y)]$ of the solution of the BK equation established above. It is known that the ratio of the saturation momenta for any two solutions is preserved by the BK evolution [20–22]. For our two solutions representing a nucleus and a nucleon, this implies $[Q_s^A(y)]/[Q_s^p(y)] = A^{1/6}$. We now rewrite the sum rule (10) by regulating the divergent integrals with a large but finite UV cutoff $aQ_s^A(y)$,

$$\int_0^{a^2(Q_s^A)^2} d^2k\, \phi_A(k, y) = (Q_s^A)^2 \int_0^{a^2} d^2\rho\, \phi(\rho) = A^{1/3}(Q_s^p)^2 \int_0^{a^2} d^2\rho\, \phi(\rho) = A^{1/3} \int_0^{a^2(Q_s^p)^2} d^2k\, \phi_p(k, y). \quad (11)$$

The formal limit $a \to \infty$ recovers Eq. (10). However, since $Q_s^A \gg Q_s^p$, the regularized sum rule (11) is satisfied even if the nuclear distribution is suppressed relative to that of a single nucleon uniformly at all momenta. Thus, the sum rule (10) carries no information about either presence or absence of Cronin enhancement.

In summary, we have found that the nonlinear QCD evolution to high energy is very efficient in erasing any Cronin-type enhancement which may be present in the initial conditions. For "realistic" initial conditions, this disappearance occurs within half a unit of rapidity. We note that in our units the evolution from 130 to 200 GeV corresponds to $\delta y \simeq 0.1$ for $\alpha_s = 0.2$, and thus is not sufficient to completely eliminate an initial enhancement at central rapidity. For forward rapidity, δy is greater. The evolution to the LHC energy corresponds to $\delta y \sim 1$. Thus, the BK evolution suggests the reduction of the Cronin effect in d-Au for forward rapidities at RHIC and predicts its disappearance for p-A collisions at LHC.

We thank the CERN TH Division (J. L. A. and A. K.) and the INT Seattle for its hospitality, and the DOE for partial support (N. A., A. K., C. A. S., and U. A. W.). J. L. A. is supported by MECD of Spain, Grant No. AP2001-3333. Useful discussions with R. Baier, E. Iancu, D. Kharzeev, Y. Kovchegov, P. Jacobs, and L. McLerran are gratefully acknowledged. We also thank M. A. Braun for discussions and a numerical cross-check.

Note added.—After appearance of this work, Refs. [9,10] were revised. Reference [10] no longer invokes the sum rule argument criticized above, and both now agree with our main conclusion.

[1] J. W. Cronin *et al.*, Phys. Rev. D **11**, 3105 (1975).
[2] PHENIX Collaboration, S. S. Adler *et al.*, Phys. Rev. Lett. **91**, 072303 (2003); STAR Collaboration, J. Adams *et al.*, *ibid.* **91**, 072304 (2003); PHOBOS Collaboration, B. B. Back *et al.*, *ibid.* **91**, 072302 (2003); BRAHMS Collaboration, I. Arsene *et al.*, *ibid.* **91**, 072305 (2003).
[3] PHENIX Collaboration, S. S. Adler *et al.*, Phys. Rev. Lett. **91**, 072301 (2003); STAR Collaboration, J. Adams *et al.*, *ibid.* **91**, 172302 (2003); PHOBOS Collaboration, B. B. Back *et al.*, Phys. Lett. B **578**, 297 (2004).
[4] D. Kharzeev, E. Levin, and L. McLerran, Phys. Lett. B **561**, 93 (2003).
[5] X. N. Wang, Phys. Lett. B **579**, 299 (2004).
[6] A. H. Mueller, Nucl. Phys. **B335**, 115 (1990).
[7] L. D. McLerran and R. Venugopalan, Phys. Rev. D **49**, 2233 (1994); **49**, 3352 (1994).
[8] F. Gelis and J. Jalilian-Marian, Phys. Rev. D **67**, 074019 (2003).
[9] R. Baier, A. Kovner, and U. A. Wiedemann, Phys. Rev. D **68**, 054009 (2003).
[10] D. Kharzeev, Y.V. Kovchegov, and K. Tuchin, Phys. Rev. D **68**, 094013 (2003).
[11] J. Jalilian-Marian, Y. Nara, and R. Venugopalan, Phys. Lett. B **577**, 54 (2003).
[12] Y.V. Kovchegov, Phys. Rev. D **54**, 5463 (1996).
[13] J. Jalilian-Marian, A. Kovner, L. D. McLerran, and H. Weigert, Phys. Rev. D **55**, 5414 (1997).
[14] D. Kharzeev and M. Nardi, Phys. Lett. B **507**, 121 (2001); D. Kharzeev and E. Levin, Phys. Lett. B **523**, 79 (2001); D. Kharzeev, E. Levin, and M. Nardi, hep-ph/0111315.
[15] E. Wang and X. N. Wang, Phys. Rev. C **64**, 034901 (2001); K. J. Eskola and H. Honkanen, Nucl. Phys. **A713**, 167 (2003); B. Z. Kopeliovich, J. Nemchik, A. Schafer, and A.V. Tarasov, Phys. Rev. Lett. **88**, 232303 (2002); A. Accardi, hep-ph/0212148; I. Vitev, Phys. Lett. B **562**, 36 (2003).
[16] I. Balitsky, Nucl. Phys. **B463**, 99 (1996).
[17] Y.V. Kovchegov, Phys. Rev. D **60**, 034008 (1999).
[18] M. Braun, Eur. Phys. J. C **16**, 337 (2000).
[19] K. Golec-Biernat and M. Wüsthoff, Phys. Rev. D **59**, 014017 (1999).
[20] N. Armesto and M. A. Braun, Eur. Phys. J. C **20**, 517 (2001).
[21] M. Lublinsky, Eur. Phys. J. C **21**, 513 (2001); K. Golec-Biernat, L. Motyka, and A. M. Stasto, Phys. Rev. D **65**, 074037 (2002).
[22] E. Iancu, K. Itakura, and L. McLerran, Nucl. Phys. **A708**, 327 (2002).
[23] A. H. Mueller and D. N. Triantafyllopoulos, Nucl. Phys. **B640**, 331 (2002).
[24] M. A. Braun, Phys. Lett. B **483**, 105 (2000).
[25] L.V. Gribov, E. M. Levin, and M. G. Ryskin, Phys. Rep. **100**, 1 (1983).
[26] Y.V. Kovchegov and A. H. Mueller, Nucl. Phys. **B529**, 451 (1998).
[27] Y.V. Kovchegov and K. Tuchin, Phys. Rev. D **65**, 074026 (2002).

Numerical analysis of the Balitsky-Kovchegov equation with running coupling: Dependence of the saturation scale on nuclear size and rapidity

J. L. Albacete,[1,2] N. Armesto,[2] J. G. Milhano,[2,3] C. A. Salgado,[2] and U. A. Wiedemann[2]

[1]*Departamento de Física, Módulo C2, Planta baja, Campus de Rabanales, Universidad de Córdoba, 14071 Córdoba, Spain*
[2]*Department of Physics, CERN, Theory Division, CH-1211 Genève 23, Switzerland*
[3]*Instituto Superior Técnico (IST), CENTRA, Avenida Rovisco Pais, P-1049-001 Lisboa, Portugal*

(Received 20 August 2004; published 7 January 2005)

We study the effects of including a running coupling constant in high-density QCD evolution. For fixed coupling constant, QCD evolution preserves the initial dependence of the saturation momentum Q_s on the nuclear size A and results in an exponential dependence on rapidity Y, $Q_s^2(Y) = Q_s^2(Y_0)\exp[\bar{\alpha}_s d(Y - Y_0)]$. For the running coupling case, we rederive analytical estimates for the A and Y dependences of the saturation scale and test them numerically. The A dependence of Q_s vanishes $\propto 1/\sqrt{Y}$ for large A and Y. The Y dependence is reduced to $Q_s^2(Y) \propto \exp(\Delta'\sqrt{Y + X})$, where we find numerically $\Delta' \simeq 3.2$. We study the behavior of the gluon distribution at large transverse momentum, characterizing it by an anomalous dimension $1 - \gamma$, which we define in a fixed region of small dipole sizes. In contrast to previous analytical work, we find a marked difference between the fixed coupling ($\gamma \simeq 0.65$) and running coupling ($\gamma \sim 0.85$) results. Our numerical findings show that both a scaling function depending only on the variable rQ_s and the perturbative double-leading-logarithmic expression provide equally good descriptions of the numerical solutions for very small r values below the so-called scaling window.

DOI: 10.1103/PhysRevD.71.014003 PACS numbers: 12.38.Bx

I. INTRODUCTION

High-density QCD [1]—the regime of large gluon densities—provides an experimentally accessible testing ground for our understanding of QCD beyond standard perturbation theory. The Balitsky-Fadin-Kuraev-Lipatov (BFKL) equation [2,3] is the perturbative framework in which the evolution of parton densities with decreasing Bjorken-x (increasing energy) is usually discussed. In the BFKL equation it is implicitly assumed that the system remains dilute throughout evolution and, hence, correlations between partons can be neglected. The fast growth of the gluon density predicted by the BFKL equation and experimentally observed at the Hadron Electron Ring Accelerator (HERA) located at the Deutsches Elektronen-Synchrotron, eventually leads to a situation in which individual partons necessarily overlap and, therefore, finite density effects need to be included in the evolution. These effects enter the evolution nonlinearly, taming the growth of the gluon density.

The need for and role played by saturation effects was first discussed in Refs. [4,5]. It was later argued [6–8] that in the high-density domain a hadronic object (hadron or nucleus) can be described in terms of an ensemble of classical gluon fields and that the number of gluons with momenta smaller than the so-called saturation scale is as high as it may be (i.e., saturated). The quantum evolution of the hadronic ensemble can be written in terms of a nonlinear functional equation [9–15] where the density effects are treated nonperturbatively (see also [16,17]).

An alternative approach, followed by Balitsky [18], relies on the operator product expansion for high-energy QCD to derive a hierarchy of coupled evolution equations (see [19] for a more compact derivation). In the limit of a large number of colors, the hierarchy reduces to one closed equation. This equation was derived independently by Kovchegov [20] in the dipole model of high-energy scattering [21–23].

The relation between these two approaches has been extensively discussed [13–15,24–27]. Apart from possible differences between the evolution equations in the kinematical region where the projectile becomes dense [24], the different approaches yield the same result, usually known as the Balitsky-Kovchegov (BK) equation. This equation has served as the starting point for a large number of analytical and numerical studies. It has also been derived in the S-matrix approach of Ref. [28] and as the large-N_c limit of the sum of fan diagrams of BFKL ladders [29,30]. It corresponds, as BFKL, to a resummation of the leading terms in $\alpha_s \ln(s/s_0)$ (leading-log approximation).

Although the full analytical solution of the BK equation is not known, several of its general properties, such as the existence and form of limiting solutions, have been identified in both analytical [31–37] and numerical [29,38–43] studies. Most of them refer to the fixed coupling case without impact parameter dependence, but analyses of the effect of a running coupling [42,44–48] and of the dependence on impact parameter [49–51] have also been carried out. Besides, there have been attempts to go beyond the large-N_c limit, either by analytical arguments [52–54] or by numerically solving the full hierarchy of evolution equations [47]. In this latter work, nonleading N_c corrections are found to give a contribution smaller than 10%–15%, in qualitative agreement with what could be naively expected from a numerical correction of $\mathcal{O}(1/N_c^2)$. From a phenomenological point of view, studies of the BK equation are motivated by the geometrical scaling phenomenon observed in lepton-proton [55] and lepton-nucleus data

[56,57] which has been related to the scaling properties of the solution of the BK equation (see, e.g., [58,59] for recent numerical analyses of HERA data based on nonlinear evolution). Further interest comes from the study of nuclear collisions [60], where saturation physics is argued [61] to underlie a large body of data including multiplicity distributions [57,62–66] and the rapidity dependence of the Cronin effect [43,67–70].

Next-to-leading-log contributions [71,72] are known to have a strong impact on the BFKL equation [73–77]. Both the choice of scale in the coupling constant [78] and the implementation of kinematical cuts for gluon emission [42,79,80], together with physically motivated modifications of the kernel [81–83], have been proposed to mend some observed pathologies of next-to-leading-log BFKL. It is usually expected that the unitarity corrections included in the BK equation become of importance for parametrically smaller rapidities [74,75] than those for which running coupling effects must be included [84]. This can be definitively established only once next-to-leading-log contributions are fully computed for BK (see [85] for a first step in this direction). However, the inclusion of running coupling effects in BK may offer a hint of some of the effects induced at next-to-leading log, as has been previously the case for BFKL. It may also help to reconcile the results of the equation with phenomenology [45,57].

In this paper, we investigate numerically the influence of the running coupling on the solution of the BK equation without impact parameter dependence, leaving this last point for a future publication. We go beyond previous numerical studies [42,46,47] by making a detailed comparison between analytical estimates and our numerical solution of the BK equation and analyzing the Y and A dependence of the saturation scale. Our key results are the confirmation of the Y and A dependence of the saturation scale proposed analytically [32–34] and the novel finding that the anomalous dimension (extracted for dipole sizes smaller than the inverse saturation scale) is different in the fixed and running coupling cases. To compare to analytical results which have been derived for asymptotically large energies, we shall evolve numerically to very large rapidities (up to $Y \sim 80$), significantly beyond the experimentally accessible range.

The plan of the paper is as follows. We first introduce the BK equation in Sec. II and the different implementations of the running of the coupling constant in Sec. III. In Sec. IV we explain the numerical method used to solve the BK equation. In Sec. V we present our numerical results, and we compare with previous numerical works and with analytical estimates. Finally, we summarize and discuss our main conclusions.

II. THE BALITSKY-KOVCHEGOV EQUATION

The BK equation gives the evolution with rapidity $Y = \ln(s/s_0) = \ln(x_0/x)$ of the scattering probability $N(\vec{x}, \vec{y}, Y)$ of a $q\bar{q}$ dipole with a hadronic target, where $\vec{x}$ ($\vec{y}$) is the position of the q ($\bar{q}$) in transverse space with respect to the center of the target. We define

$$\vec{r} = \vec{x} - \vec{y}, \qquad \vec{b} = \frac{\vec{x} + \vec{y}}{2}, \qquad \vec{r}_1 = \vec{x} - \vec{z}, \qquad \vec{r}_2 = \vec{y} - \vec{z}. \tag{1}$$

If one neglects the impact parameter dependence (which is justified for $r \ll b$, i.e., an homogeneous target with radius much larger than any dipole size to be considered), the BK equation reads ($r \equiv |\vec{r}|$)

$$\frac{\partial N(r, Y)}{\partial Y} = \int \frac{d^2 z}{2\pi} K(\vec{r}, \vec{r}_1, \vec{r}_2)[N(r_1, Y) + N(r_2, Y) - N(r, Y) - N(r_1, Y)N(r_2, Y)], \tag{2}$$

where the BFKL kernel is

$$K(\vec{r}, \vec{r}_1, \vec{r}_2) = \bar{\alpha}_s \frac{r^2}{r_1^2 r_2^2}, \qquad \bar{\alpha}_s = \frac{\alpha_s N_c}{\pi}. \tag{3}$$

The coupling constant is fixed and the kernel is conformally invariant. This implies that no impact parameter can be generated if not present in the initial condition. Also, there is no divergence for $r_1, r_2 \to 0$ provided $N(r, Y) \propto r^\beta$ for $r \to 0$ with $\beta > 0$. This comes from the cancellation between real and virtual corrections inherited from the BFKL equation. The azimuthally symmetric form of the BFKL equation, which gives the dominant contribution at high energies, corresponds to Eq. (2) without the nonlinear term.

The BK equation has the following probabilistic interpretation [24] (see Fig. 1): When evolved in rapidity, the parent dipole with ends located at $\vec{x}$ and $\vec{y}$ emits a gluon, which corresponds in the large-N_c limit to two dipoles with ends $(\vec{x}, \vec{z})$ and $(\vec{z}, \vec{y})$, respectively. The probability of such emission is given by the BFKL kernel (3) and weighted by the scattering probability of the new dipoles minus the scattering probability of the parent dipole (as the variation with rapidity of the latter is computed). The nonlinear term is subtracted in order to avoid double counting. It is this nonlinear term which prevents, in contrast to BFKL, the amplitude from growing boundlessly with rapidity. The

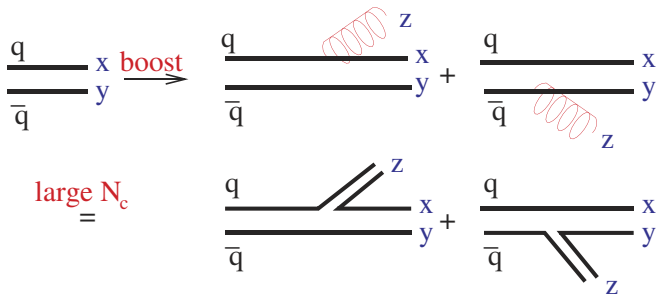

FIG. 1 (color online). Diagrams for gluon emission in the evolution of a dipole and its $N_c \to \infty$ limit.

BK equation ensures unitarity locally in transverse configuration space, $|N(r, Y)| \leq 1$. This is guaranteed since, for $N(r, Y) = 1$, the derivative with respect to Y in (2) cannot be positive.

III. RUNNING COUPLING

The BK equation (2) was derived at leading order in $\alpha_s \ln(s/s_0)$ for a fixed coupling constant α_s. An important part of the next-to-leading-log corrections is expected to come, as in BFKL, from the running of the coupling. The scale of the running coupling can be determined only when the next-to-leading-log calculation is available. In this paper, we introduce heuristically the running of the coupling, as done previously in BFKL (see, e.g., [86,87]); we will use different prescriptions for the scales in order to check the sensitivity of the results. To motivate our choices, we recall the interpretation of the BFKL kernel (3) as the Weizsäcker-Williams probability for gluon emission written in a dipolar form,

$$K(\vec{r}, \vec{r}_1, \vec{r}_2) \equiv K_0(\vec{r}, \vec{r}_1, \vec{r}_2) = \frac{\alpha_s N_c}{\pi} \frac{r^2}{r_1^2 r_2^2} = \frac{N_c}{4\pi^2} \left| \frac{g_s \vec{r}_1}{r_1^2} - \frac{g_s \vec{r}_2}{r_2^2} \right|^2, \quad (4)$$

with $g_s = \sqrt{4\pi\alpha_s}$.

Three distance scales appear in this kernel: an ''external'' one, the size of the parent dipole r, and two ''internal'' ones, the sizes of the two newly created dipoles r_1 and r_2. The latter depend on the transverse position of the emitted gluon $\vec{z}$ and on $\vec{r}$ through (1). We study three different prescriptions for implementing these scales in a running coupling constant in the BFKL kernel (4):

(1) In the first modified kernel, $K1$, the scale at which the running of the coupling is evaluated is taken to be that of the size of the parent dipole r. This choice amounts to the substitution $\alpha_s \to \alpha_s(r)$ in Eq. (4),

$$K_1(\vec{r}, \vec{r}_1, \vec{r}_2) = \frac{\alpha_s(r) N_c}{\pi} \frac{r^2}{r_1^2 r_2^2}. \quad (5)$$

(2) To implement the running of the coupling at the internal scale, we alternatively modify the emission amplitude in (4) before squaring it,

$$K_2(\vec{r}, \vec{r}_1, \vec{r}_2) = \frac{N_c}{4\pi^2} \left| \frac{g_s(r_1)\vec{r}_1}{r_1^2} - \frac{g_s(r_2)\vec{r}_2}{r_2^2} \right|^2. \quad (6)$$

(3) In order to check the sensitivity of the results to the Coulomb tails of the kernel, we further modify the kernel $K2$ by imposing short range interactions, so that the emission of large size dipoles is suppressed. To do this, we weight the gluon emission vertex by exponential (Yukawa-like) terms,

$$K_3(\vec{r}, \vec{r}_1, \vec{r}_2) = \frac{N_c}{4\pi^2} \left| \frac{e^{-\mu r_1/2} g_s(r_1)\vec{r}_1}{r_1^2} - \frac{e^{-\mu r_2/2} g_s(r_2)\vec{r}_2}{r_2^2} \right|^2, \quad (7)$$

with $\mu = \Lambda_{\rm QCD}$.

Let us anticipate that the different prescriptions $K1$, $K2$, and $K3$ lead to very similar results for the evolution. This can be traced back to the fact that all the geometrical dependence on $\vec{z}$ is integrated out so that only the r dependence in the running of the coupling survives. Even the introduction of the exponential damping has little effect, unless the range of the interaction is chosen unphysically small (i.e., $\mu \gg \Lambda_{\rm QCD}$). However, the inclusion of a short range damping effect is known [49,50] to alter significantly the solution of the BK equation with impact parameter dependence, which we do not consider in the present work.

For the qualitative properties of BK evolution studied in this paper, the precise value and running of the coupling constant is unimportant. To be specific, we use the standard one-loop expression

$$\alpha_s(r) = \alpha_s(k = 2/r) = \frac{12\pi}{\beta_0 \ln(\frac{4}{r^2\Lambda_{\rm QCD}^2} + \lambda)}, \quad (8)$$

where λ is an infrared regulator and $\beta_0 = 11N_c - 2N_f$ with $N_f = 3$. Both λ and $\Lambda_{\rm QCD}$ are determined from the conditions $\alpha_s(r = \infty) = \alpha_0$, $\alpha_s(r = 2/M_{Z^0}) = 0.118$, where M_{Z^0} is the mass of the Z^0 boson. In our work, this choice is not motivated by phenomenology but by its use in related works, e.g., [32,45], to which we want to compare. From now on, when comparing fixed and running coupling results, it will be understood that the value for the fixed coupling is the same as the one at which the running coupling is frozen, α_0.

IV. NUMERICAL METHOD AND INITIAL CONDITIONS

To solve the integro-differential equation (2), we employ a second-order Runge-Kutta method with a step size $\Delta Y = 0.1$. We discretize the variable $|\vec{r}|$ into 1200 points equally separated in logarithmic space between $r_{\rm min} = 10^{-12}$ and $r_{\rm max} = 10^2$. The numerical values of these limits are dictated by the initial conditions and $\Lambda_{\rm QCD}$. Throughout this paper, the units of r will be GeV^{-1} and those of Q_s will be GeV. The integrals in (2) are performed with the Simpson method. Inside the grid, a linear interpolation is used. For points lying outside the grid with $r < r_{\rm min}$, a power-law extrapolation is used, while for points with $r > r_{\rm max}$, the saturated value of the scattering probability is held constant, $N(r) \equiv N(r_{\rm max}) = 1$. While the initial conditions of $N(r)$ give negligible values for r small but much larger than $r_{\rm min}$, the evolution leads to a gradual filling of values close to $r_{\rm min}$ with increasing rapidity, which would result even-

tually in numerical inaccuracies. To solve this problem and push the evolution to very large rapidity, we rescale, in the fixed coupling case, the variable r in the solutions at intermediate values of Y and use them as initial condition (a power-law extrapolation is used for small values of r in order to cover the r range lost in the rescaling procedure). In this way, we are able to evolve initial conditions with $Q_s \sim 1$ GeV up to $Y \sim 36$ for $\bar{\alpha}_s = 0.4$ and up to $Y \sim 72$ for $\bar{\alpha}_s = 0.2$. In the running coupling case, the evolution is much slower and this rescaling is not needed to get to large rapidities. The accuracy of our numerical solution for all r values inside the grid is better than 4% up to the largest rapidities. It is much better than 4% in most of the r region studied. We have checked this numerical accuracy by varying the step size in Y by comparing our results to those of a fourth-order Runge-Kutta method, by varying the limits of the grid, by doubling the number of points used to discretize the function in the grid, and by using different integration, extrapolation, and interpolation methods.

We evolve three different initial conditions starting from some fixed value of x_0 (in practice, one usually takes $x_0 \sim 0.01$). The first initial condition we refer to as GBW since it shows at fixed x_0 the same r dependence as the Golec-Biernat–Wüsthoff model [88]:

$$N^{\mathrm{GBW}}(r) = 1 - \exp\left[-\frac{r^2 Q_s'^2}{4}\right]. \tag{9}$$

However, in contrast to the GBW model [88], our x dependence comes from BK evolution and we do not impose a power-law parametrization of the x dependence of Q_s'. Here and in the other initial conditions (10) and (11) below, we denote as Q_s' what is usually called the saturation scale. Our definition of the saturation scale Q_s is somewhat different [see Eq. (13) below] but the relation between both scales is straightforward, e.g., in GBW, $Q_s'^2 = -4\ln(1-\kappa)Q_s^2$. The second initial condition takes the form given by the McLerran-Venugopalan (MV) model [6,7]:

$$N^{\mathrm{MV}}(r) = 1 - \exp\left[-\frac{r^2 Q_s'^2}{4}\ln\left(\frac{1}{r^2\Lambda_{\mathrm{QCD}}^2} + e\right)\right]. \tag{10}$$

These initial conditions have been used in previous works, e.g., [39,43]. For transverse momenta $k \sim 1/r \geq \mathcal{O}(1\ \mathrm{GeV})$, the sensitivity to the infrared cutoff e is negligible. The amplitudes N^{GBW} and N^{MV} are similar for momenta of order Q_s' but differ strongly in their high-k behavior. The corresponding unintegrated gluon distribution $\phi(k) = \int (d^2r/2\pi r^2) e^{i\vec{r}\cdot\vec{k}} N(r)$ decays exponentially for N^{GBW} but has a power-law tail $\sim 1/k^2$ for N^{MV}. As a third initial condition, which we denote as AS in the following, we consider

$$N^{\mathrm{AS}}(r) = 1 - \exp[-(rQ_s')^c]. \tag{11}$$

The interest in this ansatz is that the small-r behavior $N^{\mathrm{AS}} \propto r^c$ corresponds to an anomalous dimension $1 - \gamma = 1 - c/2$ of the unintegrated gluon distribution at large transverse momentum. This anomalous dimension can be chosen to differ significantly from that of the initial conditions N^{GBW} and N^{MV}. Our choices $c = 1.17$ and $c = 0.84$ are somewhat arbitrary. They can be motivated *a posteriori* by the observation that the anomalous dimension of the evolved BK solution for both fixed and running coupling lies between the anomalous dimension of the initial conditions N^{AS} and N^{GBW} (or N^{MV}). Thus, the choice of N^{AS} is very convenient to establish generic properties of the solution of the BK equation. The values of Q_s' in Eqs. (9)–(11) are 1.4 GeV for GBW, 4.6 GeV for MV, 0.7 GeV for AS with $c = 1.17$ and 0.6 GeV for AS with $c = 0.84$. These values have been used in all our studies except in those on the A dependence in Sec. V D, where Q_s' has been rescaled with the nuclear size as discussed in that section.

V. RESULTS

In this section, we discuss our numerical results and how they compare to previous numerical work and analytical estimates.

A. Evolution: Insensitivity to details of running coupling prescription

Figure 2 shows the evolution of the dipole scattering probability for GBW initial condition with fixed and running coupling. The evolution is much faster for fixed coupling than for running coupling, as already known from previous numerical studies [42,46,47]. Remarkably, the solution is rather insensitive to the precise prescription with which running coupling effects are implemented in the modified BFKL kernels $K1$, $K2$, and $K3$. These differences are very small compared to those between fixed and running coupling.

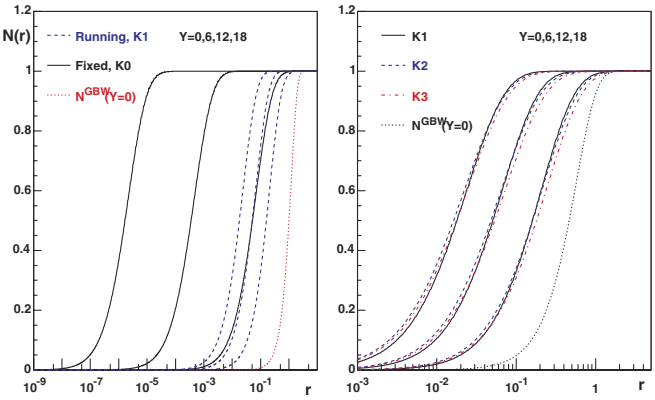

FIG. 2 (color online). Solutions of the BK equation for GBW initial condition (dotted line) for rapidities $Y = 6$, 12, and 18 with $\bar{\alpha}_0 = 0.4$. Left plot: Evolution with fixed ($K0$, solid lines) and running coupling ($K1$, dashed lines). Right plot: evolution with running coupling for kernel modifications $K1$ (solid lines), $K2$ (dashed lines), and $K3$ (dashed-dotted lines).

The small differences arising from the use of different kernels can be understood qualitatively. For example, compared to $K1$, the results obtained for $K2$ are enhanced at small values of r and suppressed at large values of r. This is due to the fact that, e.g., for a typical size $\sim 1/Q_s$ of the emitted dipoles r_1, r_2, a larger size $r > 1/Q_s$ of the parent dipole amounts to a larger coupling $g_s(r)$ entering the kernel $K1$ than the couplings $g_s(r_1)$, $g_s(r_2)$ entering $K2$. Thus, at large r the evolution is slower for $K2$, which results in the observed relative suppression. The analogous argument implies a relative enhancement obtained from the kernel $K2$ for small $r < 1/Q_s$.

Figure 2 also shows that the effects of imposing short range interactions, $K3$, are very small (unless the range of the interaction is unphysically small). As expected, effects from short range interactions included in $K3$ are larger for larger values of r. It is conceivable that the main next-to-leading-log effects on the original BK kernel are those of the running of the coupling constant included here and that further modifications, such as kinematical constraints [42,79,80], are comparatively small [89].

B. Scaling

In the limit $Y \to \infty$, the solutions of the BK evolution are no longer functions of the variables r and Y separately, but instead they depend on a single scaling variable

$$\tau \equiv r Q_s(Y). \tag{12}$$

Here the saturation momentum $Q_s(Y)$ determines the transverse momentum below which the unintegrated gluon distribution is saturated. It can be characterized by the position of the falloff in $N(r)$, e.g., via the definition

$$N[r = 1/Q_s(Y), Y] = \kappa, \tag{13}$$

where κ is a constant which is smaller than, but of order, one. We have checked that different choices such as $\kappa = 1/2$ and $\kappa = 1/e$ lead to negligible differences in the determination of $Q_s(Y)$. The results given below have been obtained for $\kappa = 1/2$.

In the fixed coupling case, the scaling property $N(r, Y) \to N(\tau)$ has been quantified in previous numerical works [39,41,43] and confirmed by analytical calculations [35–37]. In the running coupling case, the scale invariance of the BFKL kernel is broken by the scale $\Lambda_{\rm QCD}$ and it is *a priori* unclear whether scaling persists. However, when the two scales in the problem are separated widely due to evolution to large rapidity, $Q_s(Y) \gg \Lambda_{\rm QCD}$, one may expect that the scaling property of the BK solution is restored. In agreement with previous numerical works [46,47], we confirm this expectation: for all modifications $K1$, $K2$, and $K3$ of the BFKL kernel, the solutions tend to universal scaling forms as rapidity increases. Moreover, with increasing rapidity the sensitivity to the choice of scales in the kernel and its short range modification, as well as to the initial condition and to the value of the coupling constant in the infrared, becomes eventually negligible (see Fig. 3).

As seen in Fig. 3, the shape of the scaling solution differs significantly for fixed and running coupling as observed already in Ref. [46]. The running of the coupling suppresses the emission of dipoles of small transverse size (i.e., small τ and large transverse momenta). This leads to an enhancement in the large τ region of $N(\tau)$ which is seen for the running coupling case in Fig. 3.

The accuracy of scaling at small r has been studied in a previous work [43] for the fixed coupling case. Here we check scaling for both fixed and running coupling by comparing our numerical results to the scaling forms proposed in Ref. [33]. There it was argued that, in the so-called scaling window $\tau_{\rm sw} < \tau < 1$, the asymptotic solution of $N(r, Y)$ takes the following scaling forms for fixed and running coupling, respectively [33]:

$$f^{1)}(\tau) = a\tau^{2\gamma}(\ln\tau^2 + \delta), \tag{14}$$

$$f^{2)}(\tau) = a\tau^{2\gamma}\left(\ln\tau^2 + \frac{1}{\gamma}\right). \tag{15}$$

Here $1 - \gamma$ is usually called the anomalous dimension which governs the leading large-k behavior of the unintegrated gluon distribution. We define γ from a fit of our numerical results to the functions (14) and (15) in the Y-independent region $10^{-5} < \tau < 10^{-1}$, i.e., for $10^5 Q_s > 1/r > 10 Q_s$, with a, γ, and δ as free parameters. The

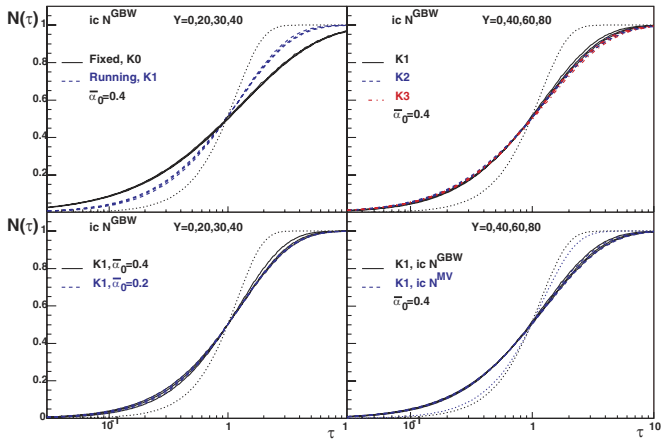

FIG. 3 (color online). Scaling solutions of BK for $Y = 0$, 20, 30, and 40 (plots on the left) and $Y = 0$, 40, 60, and 80 (plots on the right). Upper left: evolution for fixed (solid line) and running coupling ($K1$, dashed line) for GBW initial conditions. Upper right: solutions for the kernels $K1$ (solid line), $K2$ (dashed line), and $K3$ (dashed-dotted line). Lower left: scaling function for $K1$ with two different values of frozen coupling, $\bar{\alpha}_0 = 0.4$ (solid line) and $\bar{\alpha}_0 = 0.2$ (dashed line). Lower right: scaling solutions with running coupling ($K1$) for two different initial conditions, GBW (solid line) and MV (dashed line). In all plots the initial conditions correspond to the dotted lines and $\bar{\alpha}_0 = 0.4$ unless otherwise stated.

results given below were found to be insensitive to a variation of the lower limit of this fitting range.

For the case of fixed coupling constant, we find that the function $f^{1)}$ provides a very good fit to the evolved solutions. In Fig. 4, we show the fit values of the parameter γ, obtained for fixed coupling constant from the evolution of different initial conditions N^{GBW}, N^{MV}, and N^{AS} for different values of c. At initial rapidity, these distributions have widely different anomalous dimensions but evolution drives them to a common value, $\gamma \simeq 0.65$, which lies close to the theoretically conjectured one [32,33] of 0.628. For a small fixed coupling constant $\bar{\alpha}_0 = 0.2$, this asymptotic behavior is reached at $Y \sim 70$, while for a larger coupling constant $\bar{\alpha}_0 = 0.4$ the approach to this asymptotic value takes half the length of evolution (results not shown). For fixed coupling solutions, $f^{2)}$ does not provide a good fit to our numerical results.

We have repeated this comparison for all running coupling solutions. We found that both $f^{1)}$ and $f^{2)}$ provide good fits and yield very similar values of γ. The results for $K3$ are numerically indistinguishable from those for $K2$ and will not be shown in what follows. Also, the value of γ was found to be independent of the coupling constant $\bar{\alpha}_0$ at $r \to \infty$. As a fitting function, $f^{1)}$ is more general than $f^{2)}$ and describes well the solutions of BK in all considered cases. To avoid possible differences in the determination of γ due to the use of different fitting forms in the fixed and running coupling cases, in Fig. 4 we show the γ values extracted in both cases from a fit to $f^{1)}$. Irrespective of the initial condition, they approach a common asymptotic value $\gamma \sim 0.85$. While our numerical findings for N^{AS} with $c = 0.84$ are not inconsistent with the approach to this asymptotic value, no firm conclusions can be drawn. This initial condition just starts too far away from the asymptotic scaling solution to reach it within the numerically accessible rapidity range. In this case, the monotonic increase of γ with rapidity at large Y is smaller than the increase for N^{AS} with $c = 1.17$ at comparable values of γ, indicating that the rapidity evolution of the anomalous dimension depends, in general, not only on the small-r behavior but on the full shape of the scattering probability.

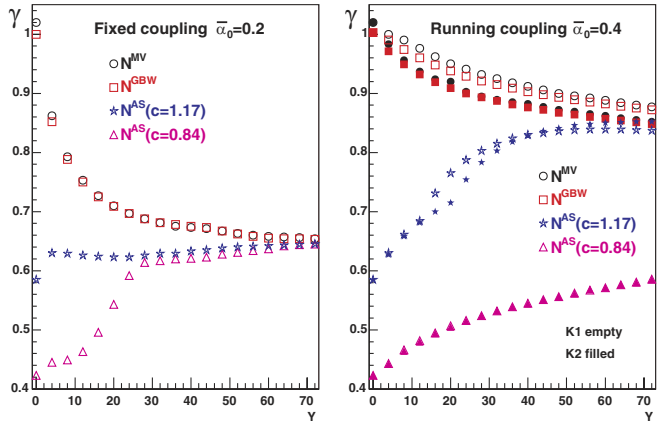

FIG. 4 (color online). The rapidity dependence of the parameter γ, characterizing the anomalous dimension $1 - \gamma$, as determined by a fit of (14) to the BK solutions for different initial conditions: GBW (squares), MV (circles), and AS with $c = 1.17$ (stars) and $c = 0.84$ (triangles). Left plot: results for fixed coupling with $\bar{\alpha}_0 = 0.2$. Right plot: results for running coupling with $\bar{\alpha}_0 = 0.4$ and two versions of the kernel $K1$ (empty symbols) and $K2$ (solid symbols).

The value $\gamma \sim 0.85$ is considerably larger than the one found in fixed coupling evolution. This is in agreement with previous numerical results [46] but in contrast to theoretical expectations [32,33,45] which predict the same value of γ for the fixed and running coupling cases. As an additional check, we have performed running coupling evolution from an initial condition given by the solution at large rapidity of fixed coupling evolution (for which $\gamma \simeq 0.65$). We find that, even with this initial condition, running coupling evolution leads to a value of $\gamma \sim 0.85$.

It has been argued [32,33] that expressions (14) and (15) are valid only for values of τ inside the scaling window, $\tau_{\mathrm{sw}} \sim \Lambda_{\mathrm{QCD}}/Q_s(Y) < \tau \lesssim 1$ with Y_0 the initial rapidity, and that the dipole scattering probability returns to the double-leading-log (DLL) expression

$$N^{\mathrm{DLL}}(r) = a(Y) r^2 [-\ln(r^2\Lambda^2)]^{-3/4} \times \exp\left[b(Y)\sqrt{-\ln(r^2\Lambda^2)} \right], \qquad (16)$$

with $a(Y) \propto Y^{1/4}$ and $b(Y) \propto \sqrt{Y}$, for values $\tau < \tau_{\mathrm{sw}}$. We have checked that this form provides a good fit (fit and numerical solution differ by less than $\pm 10\%$) to the fixed coupling solution of BK for $\tau < \tau_{\mathrm{sw}} = \Lambda/Q_s(Y)$, $\Lambda \sim 0.2$ GeV; see Fig. 5. Our comparison is limited to rapidities $Y \leq 20$, since the scaling window starts to extend over the entire numerically accessible r space for $Y > 20$. Up to $Y = 20$, the coefficients $a(Y)$ and $b(Y)$ follow the expected DLL Y behavior; see Fig. 5. However, the scaling ansatz $f^{1)}$ provides an equally good fit to the BK solutions for $\tau < \tau_{\mathrm{sw}}$. This is the reason why in previous numerical studies [43] no upper bound for a scaling window was found. When the solutions of BK are fitted to $f^{1)}$ within the scaling window, the values of γ at $Y = 0$ for both initial conditions are $\lesssim 20\%$ smaller than those found when the fit is done within a fixed τ window. But for larger Y the values of γ extracted from fits within either the scaling window or some fixed τ window approach each other and quickly coincide.

C. Rapidity dependence of the saturation scale

In the scaling region, for large Y where $Q_s(Y) \gg \Lambda_{\mathrm{QCD}}$, the BK equation (2) for fixed coupling constant can be written in terms of the rescaled variables $\vec{\tau} = Q_s(Y)\vec{r}$, $\vec{\tau}_1 = Q_s(Y)\vec{r}_1$, and $\vec{\tau}_2 = Q_s(Y)\vec{r}_2$. The Y dependence of

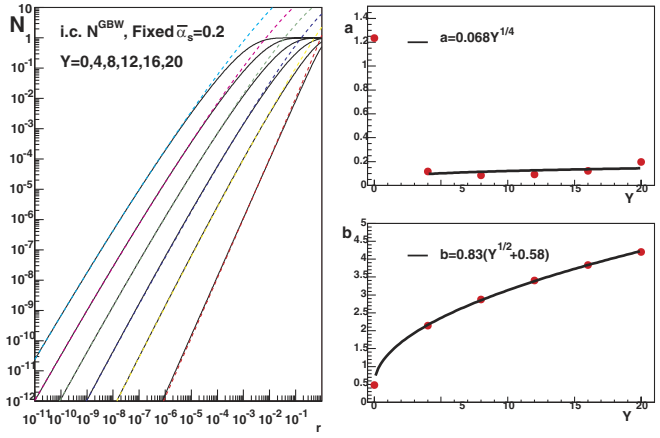

FIG. 5 (color online). Plot on the left: solutions of the BK equation (solid lines) with GBW initial condition and fixed coupling $\bar{\alpha}_s = 0.2$ compared to fits (dashed lines) to the DLL expression (16), for rapidities $Y = 0$, 4, 8, 12, 16, and 20 (curves from right to left). Plots on the right: values of the coefficients $a(Y)$ and $b(Y)$ (circles) in the DLL expression versus Y, compared to fits (curves) to the functional form suggested by DLL.

$N(r, Y) \equiv N(\tau)$ is then contained in $Q_s(Y)$. Rewriting the derivative on the left-hand side of (2),

$$\frac{\partial N(\tau)}{\partial Y} = \frac{\partial Q_s(Y)}{\partial Y} r \frac{\partial N}{\partial \tau} = \frac{\partial \ln[Q_s^2(Y)/\Lambda^2]}{\partial Y} r^2 \frac{\partial N}{\partial r^2}, \quad (17)$$

one finds [32]

$$\int \frac{d^2r}{r^2} \frac{\partial N(\tau)}{\partial Y} = \pi \frac{\partial \ln[Q_s^2(Y)/\Lambda^2]}{\partial Y} [N(\infty) - N(0)] = \pi \frac{\partial \ln[Q_s^2(Y)/\Lambda^2]}{\partial Y}. \quad (18)$$

Performing the same integration over $d^2r/r^2 = d^2\tau/\tau^2$ on the right-hand side of (2), one finds a number

$$d = \int \frac{d^2\tau d^2\tau_1}{2\pi^2} \frac{1}{\tau_1^2 \tau_2^2} [N(\tau_1) + N(\tau_2) - N(\tau) - N(\tau_1)N(\tau_2)], \quad (19)$$

which is independent of Y. The numerical value of d cannot be obtained without the knowledge of the scaling solution $N(\tau)$, and several approximations have been proposed [32,33] which we will compare with our numerical results. Combining Eqs. (2), (18), and (19), the Y dependence of the saturation scale is determined [32] by

$$\frac{\partial \ln[Q_s^2(Y)/\Lambda^2]}{\partial Y} = d\bar{\alpha}_s. \quad (20)$$

Thus, for the case of a fixed coupling constant, the saturation scale grows exponentially with rapidity,

$$Q_s^2(Y) = Q_0^2 \exp[\Delta Y], \quad (21)$$

where $\bar{\alpha}_s = \bar{\alpha}_0 =$ constant, $\Delta = d\bar{\alpha}_0$, and $Q_0^2 = Q_s^2(Y = 0)$ (i.e., the evolution starts at $Y = 0$).

For running coupling, the momentum scale is expected to be $\sim Q_s(Y)$. This suggests the substitution $\bar{\alpha}_s \to \bar{\alpha}_s[Q_s(Y)]$ in Eq. (20). To see this explicitly, let us include, as in $K1$, the coupling constant $\bar{\alpha}_s(r)$ in the integrand of (19), which leads to

$$d\bar{\alpha}_s \to \frac{12N_c}{\beta_0} \int \frac{d^2\tau d^2\tau_1}{2\pi^2} \frac{1}{\tau_1^2(\vec{\tau} - \vec{\tau}_1)^2} \times \frac{1}{\ln[Q_s^2(Y)/\Lambda_{\rm QCD}^2] - \ln(\tau^2/4)} \times [N(\tau_1) + N(|\vec{\tau} - \vec{\tau}_1|) - N(\tau) - N(\tau_1)N(|\vec{\tau} - \vec{\tau}_1|)]. \quad (22)$$

For $\tau \gg 1$, the integrand vanishes. For $\tau \ll 1$, the integral in $d^2\tau_1$ is finite and the remaining $d^2\tau$ suppresses the contribution of small τ. So we conclude that the dominant region is that of $\tau \sim 1$ and thus it is legitimate to approximate

$$\frac{12N_c}{\beta_0} \int \frac{d^2\tau d^2\tau_1}{2\pi^2} \frac{1}{\tau_1^2(\vec{\tau} - \vec{\tau}_1)^2} \times \frac{1}{\ln[Q_s^2(Y)/\Lambda_{\rm QCD}^2] - \ln(\tau^2/4)} \times [N(\tau_1) + N(|\vec{\tau} - \vec{\tau}_1|) - N(\tau) - N(\tau_1)N(|\vec{\tau} - \vec{\tau}_1|)] \simeq d\bar{\alpha}_s[Q_s(Y)]. \quad (23)$$

This approximation is also supported by numerical results [29,39,42] which show that in momentum space the typical transverse momentum of the gluons is $\sim Q_s$. Because of the similarities in the evolution shown previously, this should also hold for other implementation of the scale of the coupling constant such as $K2$ and $K3$. The logarithmic dependence of the coupling constant on $Q_s(Y)$ in (23), combined with Eq. (20), leads to [32]

$$Q_s^2(Y) = \Lambda^2 \exp\left[\Delta' \sqrt{Y + X}\right], \quad (24)$$

where $(\Delta')^2 = 24N_c d/\beta_0$ and $X = (\Delta')^{-2} \ln(Q_0^2/\Lambda^2)$. This estimate indicates that the rapidity dependence of the saturation scale is much weaker for running than for fixed coupling constant.

Figure 6 shows the Y dependence of Q_s^2 for several initial conditions and different choices of $\bar{\alpha}_0$, calculated for all the kernels considered in this work. The rise of Q_s is much faster for fixed than for running coupling, as already observed in Refs. [42,44–48,83,89].

For fixed coupling constant, Q_s^2 exhibits with good accuracy an exponential behavior for high-enough values of Y. The value of the slope extracted from a fit to the function (21) is $\Delta \simeq 1.83$ for $\bar{\alpha}_0 = 0.4$. As expected, for

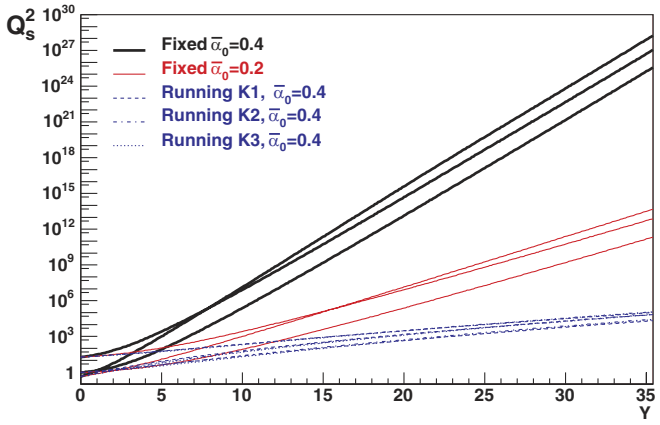

FIG. 6 (color online). The rapidity dependence of the saturation momentum Q_s^2 for fixed $\bar{\alpha}_s = 0.4$ (thick solid line), fixed $\bar{\alpha}_s = 0.2$ (thin solid line), and running coupling with $\bar{\alpha}_0 = 0.4$ for kernels $K1$ (dashed line), $K2$ (dashed-dotted line), and $K3$ (dotted line). For each group, lines from top to bottom in the rightmost side correspond to initial conditions AS with $c = 1.17$, MV, and GBW.

$\bar{\alpha}_0 = 0.2$ this value is reduced by a factor two, $\Delta \simeq 0.91$. For the constant (19), we find $d \simeq 4.57$, in agreement with previous numerical studies at very high rapidities [43] but slightly smaller than the theoretical expectation $d = 4.88$ [32,33]. In previous numerical studies [39,40,42], an even smaller value of $d \sim 4.1$ was obtained. We have checked that this is due to the fact that the rapidity region for the fit in our case corresponds to much larger Y.

For the case of a running coupling constant, an exponential fit can be done only for a very limited Y region. For example, for $Y \sim 10$ we find a logarithmic slope ~ 0.28 for GBW or MV initial conditions with $Q_0 \sim 1$ GeV, in agreement with the results of Ref. [45] but smaller than the values found in Ref. [83] (see also [48,89]). The exponential function (21) is unable to fit the full Y range. In contrast, the weaker rapidity dependence of (24) does provide a good fit in the full Y range. The fit to (24) yields $\Delta' \simeq 3.2$, while the theoretical expectation [32,33] is slightly larger, $\Delta' = 3.6$. We finally note that in Ref. [47] the Y derivative of $\ln Q_s^2(Y)$ has been found numerically to be proportional to $\sqrt{\alpha_s[Q_s(Y)]}$ in a much more restricted range of Y. We have been unable to fit our results over the full Y range to the corresponding Y dependence, $Q_s^2(Y) \propto \exp Y^{2/3}$.

We have found very little sensitivity of the values of Δ and Δ' to the fitting region, provided Y was chosen large enough. Our fits typically started at $Y \sim 15$, where the asymptotic behavior is approached, and explored the highest rapidities numerically accessible. Also, our results for running coupling do not depend on the choice of the kernel $K1$, $K2$, or $K3$, on the initial condition, or on the value of $\bar{\alpha}_0$. However, the AS initial condition with $c = 0.84$ is not included in our study since it does not approach the asymptotics within the numerically accessible rapidity range.

In Refs. [33,35–37,45] subleading terms in the Y behavior of Q_s have been presented. A form of the type $d \ln Q_s^2(Y)/dY = \bar{\alpha}_s a - bY^{-1} + cY^{-3/2}/(2\sqrt{\bar{\alpha}_s})$ has been proposed in the fixed coupling case, with $a = 4.88$, $b = 2.39$, and $c = 2.74$. This function contains all terms for the Y evolution of the saturation scale that are universal, i.e., independent of the initial condition (see also [90] for a comparison of solutions of BK to this functional form). The constant term corresponds to Eq. (21). We have used this functional form to fit the results of fixed coupling evolution on $d \ln Q_s^2(Y)/dY$ for different rapidity regions within $Y = 5$–40 (72) for $\bar{\alpha}_s = 0.4$ (0.2), for the GBW and MV initial conditions, respectively. First, we have used our definition of the saturation scale (13) with $\kappa = 1/2$. From a simple comparison to the proposed expression (using the theoretical coefficients provided in Ref. [37]), we are able to clearly identify in our numerical results the presence of the first two terms. On the contrary, the presence of the third term is disfavored. Fitting our numerical results to the first plus second terms, the value of a we find, $a \simeq 4.9$, is quite stable with respect to variations of the fitting region. It is higher than the value of d we extract with only the linear term (21), $d \simeq 4.57$, and closer to the theoretical expectation $d = 4.88$ [32,33]. In this two-parameter fit we get a value of $b \simeq 2.4$–2.5, varying slightly with the Y region of the fit. This value is quite close to the theoretical expectation 2.39. On the other hand, in a three-parameter fit the values of b and c we extract are very unstable (even changing signs) with respect to variations of the lower limit of the fitting region between $Y = 5$ and 20. We have also tried to get the value of c from a fit to $d/dY[Y d \ln Q_s^2(Y)/dY] = \bar{\alpha}_s a - cY^{-3/2}/(4\sqrt{\bar{\alpha}_s})$. While we find again a value of $a \simeq 4.9$, the value of c turns out to depend, as in the previous analysis, considerably on the fitted Y region. Second, we have used the definition of the saturation scale (13) but now with $\kappa = 0.01$ (i.e., we define Q_s in a point in which the dipole scattering probability is far from its unitarity limit). In this case, a simple comparison to the proposed expression using the theoretical coefficients provided in Ref. [37] allows us to clearly identify in our numerical results the presence of the three terms. Still, a three-parameter fit to our numerical results does not provide values of b and c stable with respect to changes in the fitting region. This influence of the definition of the saturation scale on the determination of the subleading corrections to its Y behavior is consistent with the finding in Ref. [90].

D. Nuclear size dependence of the saturation scale

The nuclear size enters the initial condition. The question is whether the BK evolution modifies or preserves this initial A dependence. For realistic nuclei, the impact parameter is likely to have an important effect on this A

dependence. This has been examined partially in Refs. [50,51]. However, the question is already of interest for the case without impact parameter dependence [34,39,40], which we study here.

Let us first assume some arbitrary A dependence, which we include in the initial condition by the rescaling factor

$$r^2 \to h r^2 \tag{25}$$

(this is true for GBW and AS initial conditions but not for MV due to the presence of the logarithm; however, the numerical results for the A dependence obtained with MV initial conditions are, for all purposes, equivalent to those with GBW). Here h contains the information about the nuclear size, and Eq. (20) reads

$$\frac{\partial \ln[Q_s^2(Y)/\Lambda^2]}{\partial Y} = d\bar{\alpha}_s\Big[\sqrt{h}Q_s(Y)\Big]. \tag{26}$$

In the case of a fixed coupling constant, the dilatation invariance of the BK equation (2) allows one to scale out any nuclear dependence included in the initial condition. Thus, the A dependence of the saturation scale is unaffected by evolution. To explore the case of a running coupling constant, we use the one-loop expression for α_s and write

$$Q_s^2(Y) = \frac{\Lambda^2}{h}\exp\sqrt{(\Delta')^2 Y + \ln^2\Big[\frac{hQ_s^2(Y=0)}{\Lambda^2}\Big]}. \tag{27}$$

Multiplying by h for the nucleus to undo the rescaling and setting $h = 1$ for the proton, we get

$$\frac{Q_{sA}^2(Y)}{Q_{sp}^2(Y)} = \exp\Bigg\{\sqrt{(\Delta')^2 Y + \ln^2\Big[\frac{hQ_s^2(Y=0)}{\Lambda^2}\Big]} - \sqrt{(\Delta')^2 Y + \ln^2\Big[\frac{Q_s^2(Y=0)}{\Lambda^2}\Big]}\Bigg\}. \tag{28}$$

If we assume the hierarchy

$$(\Delta')^2 Y \gg \ln^2\Big[\frac{hQ_s^2(Y=0)}{\Lambda^2}\Big] \gg \ln^2\Big[\frac{Q_s^2(Y=0)}{\Lambda^2}\Big], \tag{29}$$

so $A \gg 1$, we find

$$\ln\frac{Q_{sA}^2(Y)}{Q_{sp}^2(Y)} \simeq \frac{\ln^2[\frac{hQ_s^2(Y=0)}{\Lambda^2}]}{2\sqrt{(\Delta')^2 Y}}. \tag{30}$$

Here $hQ_s^2(Y=0)$ is the initial saturation momentum for the nucleus, and Eq. (30) coincides with Eq. (44) of Ref. [34] with $(\Delta')^2$ as defined below Eq. (24) (see also [47,64,91] for related discussions). This result suggests that any information about the initial A dependence of the saturation scale is gradually lost during evolution: albeit at extremely large rapidities, all hadronic targets look the same. Usually, one assumes an $A^{1/3}$ dependence of the saturation scale for the initial condition [6,7] $h \propto A^{1/3}$. However, other A dependencies have been proposed; see, e.g., [92].

Figure 7 shows that fixed coupling evolution preserves the A dependence of the saturation scale irrespective of whether this dependence is $\propto A^{1/3}$ as for the GBW or MV initial conditions (which produces numerical results for the A dependence which are very close to those obtained for GBW) or it differs from $\propto A^{1/3}$ due to an anomalous dimension included, e.g., in the AS initial condition. On the other hand, running coupling evolution is seen to reduce the A dependence with increasing rapidity. We find that, if fitted in a wide rapidity range, the dependence of $\ln[Q_{sA}^2(Y)/Q_{sp}^2(Y)]$ on Y is $\sim Y^{-0.4}$. However, for large values of A and Y, the decrease with increasing Y is $\propto 1/\sqrt{Y}$ and thus well described by (30) [34].

Combining the rescaling argument based in (25) with the observation that the DLL solution is approached for small r or large transverse momentum k, one is led to an interesting implication for the large-k behavior of the ratios of gluon densities in nuclei over nucleon (or central over peripheral nucleus) [43,68–70]. In fixed coupling evolution the rescaling of the initial condition (25) trivially implies the same rescaling in the evolved solution, which we will consider to be DLL for sufficiently large k. Thus, one gets for the ratio R of the gluon densities in transverse momentum space for nuclei over nucleon

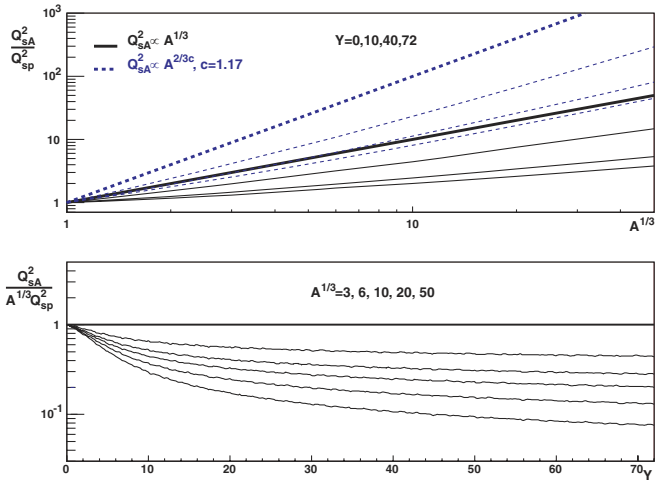

FIG. 7 (color online). Upper plot: Q_{sA}^2/Q_{sp}^2 versus $A^{1/3}$ for initial conditions GBW [$Q_{sA}^2(Y=0) \propto A^{1/3}$, solid line] and AS with $c = 1.17$ [$Q_{sA}^2(Y=0) \propto A^{2/3c}$, dashed line]; thick lines are the results for $Y = 0$ in the running coupling case and for all rapidities in fixed coupling; for running coupling, different rapidities $Y = 10$, 40, and 72 (thin lines) are shown from top to bottom for each initial condition. Lower plot: $Q_{sA}^2/(A^{1/3}Q_{sp}^2)$ versus Y for GBW with $A^{1/3} = 3$, 6, 10, 20, and 50 with the same line convention as the upper plot (the results for fixed coupling have been obtained for $Y < 36$ and extrapolated as a constant equal to 1). In all plots $\bar{\alpha}_0 = 0.4$ and, in the running coupling case, the kernel $K1$ has been used.

$$R \simeq \left[\frac{\ln(k^2/\Lambda^2) - \ln h}{\ln(k^2/\Lambda^2)}\right]^{-3/4} \exp\left\{b(Y)\left[\sqrt{\ln(k^2/\Lambda^2) - \ln h} - \sqrt{\ln(k^2/\Lambda^2)}\right]\right\}. \quad (31)$$

This ratio tends very slowly to one for $k \to \infty$. We have checked that the results of this formula agree with the numerical computations in Ref. [43] and thus it provides justification to the apparent absence of a return to the collinear limit, $R = 1$ at $k \to \infty$, found in this reference for the largest studied k values.

VI. CONCLUSIONS

The inclusion of a running coupling constant may be expected to account for important next-to-leading-log effects in the BK equation, as has been previously the case for BFKL. This motivates the present numerical study of the BK equation without impact parameter dependence. Our main results are insensitive to details of the implementation of running coupling effects, the infrared regulation of the coupling constant, and the choice of initial conditions which are evolved. They can be summarized as follows:

(1) The rapidity dependence of the saturation momentum is much faster for the fixed coupling constant than for the running one, as observed previously [42,44,46,47]. It is well described by $Q_s^2(Y) \propto \exp(\bar{\alpha}_s dY)$ for fixed coupling and by $Q_s^2(Y) \propto \exp(\Delta'\sqrt{Y + X})$ for running coupling. For large rapidities, we find $d \simeq 4.57$, which is slightly smaller than the theoretical expectation $d = 4.88$ [32,33]. For running coupling, we find $\Delta' \simeq 3.2$, slightly smaller than the expected value $\Delta' \simeq 3.6$ [32,33,45]. For a very limited region of Y, a fit to the exponential form $Q_s^2(Y) \propto \exp(DY)$ works even for running coupling, but it cannot account for the entire Y range. For the fixed coupling case, we have checked the existence of the subleading terms in the Y dependence of the saturation scale proposed in Refs. [33,35–37]. As found in Ref. [90], their precise determination depends on the definition of the saturation scale.

(2) For sufficiently large rapidity, the solution of the BK equation with fixed coupling is known to show scaling [39,41,43]. We confirm scaling for the running coupling case in agreement with Refs. [46,47]. The approach to the scaling solution is faster with fixed than with running coupling.

(3) As observed previously [46] and at variance with analytical estimates [32,33,45], the behavior of $N(r)$ at small r differs for the cases of fixed and running coupling. For small $r < 1/Q_s(Y)$, forms of the type $(rQ_s)^{2\gamma}\ln(CrQ_s)$ [33] describe the solutions at sufficiently high rapidity, where γ, defined in a Y-independent fitting region, is $\simeq 0.65$ for the fixed coupling constant but $\gamma \sim 0.85$ for running coupling. These values are for the limit $Y \to \infty$.

(4) Arguments in Refs. [32,33] suggest a lower limit to the scaling window $rQ_s(Y) \sim \Lambda_{\rm QCD}/Q_s(Y)$ below which $N(r)$ returns to the perturbative double-leading-logarithmic expression. Remarkably, the scaling forms (14) proposed in Refs. [33,45] give good fits to the solutions of BK even outside the scaling window, for $r < \Lambda/Q_s^2(Y)$, $\Lambda \sim 0.2$ GeV. Hence, it is not possible to establish numerically the limit of the scaling region as a deviation from scaling. However, the double-leading-log approximation provides an equally good description of the numerical solution in the r region below the scaling window.

(5) For fixed coupling, the scale invariance of the kernel preserves any A dependence of the initial condition during BK evolution. For running coupling and for very large energies and nuclear sizes, we have rederived and checked numerically Eq. (30): the A dependence decreases with increasing rapidity like $1/\sqrt{Y}$ [34].

The above results have been established by evolving over many orders of magnitude in energy. Thus, any phenomenological application of these findings has to assume that initial conditions can be fixed at (and perturbatively evolved from) a sufficiently small energy scale for the nonlinear evolution to be effective in an experimentally accessible regime. Moreover, phenomenology based on the BK equation will face at least some of the problems known from applications of BFKL such as the question of whether and how to implement kinematical cuts for gluon emission. Despite these caveats, it is interesting to compare the numerical results found here to the general trends in the data. A comparison of saturation-inspired parametrizations with data on lepton-proton, lepton-nucleus, and nuclear collisions at high energies suggests a saturation scale $Q_{sA}^2 \propto A^\alpha \exp(DY)$ with $D \simeq 0.29$ [88] and $\alpha \simeq 4/9 > 1/3$ [57] (for related phenomenological studies, see [55,56]).

Our results allow us to discuss to what extent existing data, showing geometric scaling, differ from the asymptotic BK scaling behavior. In particular, the strong A dependence of the saturation scale seen in the data indicates, at variance with the result from the BK scaling solution with running coupling, that the properties of the initial nuclear condition have not yet been washed out by nonlinear small-x evolution. The kinematic range of the lepton-nucleus data studied in Refs. [56,57] is too small to test this evolution. Also, the exponential Y dependence of the saturation scale with $D \sim 0.3$ seen in the data can appear naturally from BK evolution of reasonable initial conditions over some units in rapidity in the running coupling case. But this value of D is not a property of the asymptotic solution for running coupling. For fixed

coupling, it can be obtained only with unrealistically small values of the coupling constant.

None of these facts contradicts nonlinear BK evolution—they simply illustrate that the evolution observed in experimental data has not yet reached its asymptotic behavior. To further advance our understanding of saturation effects in QCD dynamics at high energies, both theoretical and experimental studies are required. In the context of the BK equation, this requires the study of solutions under more realistic conditions. In particular, the impact parameter dependence may have a significant effect on the A dependence of the saturation scale, a point which we plan to study in the future. On the experimental side, the forward rapidity measurements at the Relativistic Heavy Ion Collider located at the Brookhaven National Laboratory give access to a kinematic window interesting for small-x evolution studies. These studies are at the very beginning. Also, in the near future measurements at the CERN Large Hadron Collider will provide more stringent tests of small-x evolution, extending the kinematic reach by at least 3 orders of magnitude further down in the momentum fraction x.

ACKNOWLEDGMENTS

We thank R. Baier, J. Bartels, M. A. Braun, E. Iancu, A. H. Mueller, and A. Sabio Vera for useful discussions and comments. We are grateful to K. Golec-Biernat for a critical reading of the manuscript and many helpful remarks. Special thanks are due to A. Kovner, who participated in an early stage of this work and made numerous useful suggestions about the manuscript. J. L. A. and J. G. M. thank CERN Theory Division for hospitality and acknowledge financial support by the Ministerio de Educación y Ciencia of Spain (Grant No. AP2001-3333) and the Fundação para a Ciência e a Tecnologia of Portugal (Contract No. SFRH/BPD/12112/2003), respectively.

[1] *QCD Perspectives on Hot and Dense Matter*, NATO Science Series II: Mathematics, Physics and Chemistry Vol. 87, edited by J.-P. Blaizot and E. Iancu (Kluwer, Dordrecht, The Netherlands, 2002).
[2] E. A. Kuraev, L. N. Lipatov, and V. S. Fadin, Zh. Eksp. Teor. Fiz. **72**, 377 (1977) [Sov. Phys. JETP **45**, 199 (1977)].
[3] I. I. Balitsky and L. N. Lipatov, Yad. Fiz. **28**, 1597 (1978) [Sov. J. Nucl. Phys. **28**, 822 (1978)].
[4] L. V. Gribov, E. M. Levin, and M. G. Ryskin, Phys. Rep. **100**, 1 (1983).
[5] A. H. Mueller and J.-W. Qiu, Nucl. Phys. **B268**, 427 (1986).
[6] L. D. McLerran and R. Venugopalan, Phys. Rev. D **49**, 2233 (1994).
[7] L. D. McLerran and R. Venugopalan, Phys. Rev. D **49**, 3352 (1994).
[8] L. D. McLerran and R. Venugopalan, Phys. Rev. D **50**, 2225 (1994).
[9] J. Jalilian-Marian, A. Kovner, L. D. McLerran, and H. Weigert, Phys. Rev. D **55**, 5414 (1997).
[10] J. Jalilian-Marian, A. Kovner, A. Leonidov, and H. Weigert, Phys. Rev. D **59**, 014014 (1999).
[11] J. Jalilian-Marian, A. Kovner, A. Leonidov, and H. Weigert, Phys. Rev. D **59**, 034007 (1999); **59**, 099903(E) (1999).
[12] A. Kovner and J. G. Milhano, Phys. Rev. D **61**, 014012 (2000).
[13] E. Iancu, A. Leonidov, and L. D. McLerran, Nucl. Phys. **A692**, 583 (2001).
[14] E. Iancu, A. Leonidov, and L. D. McLerran, Phys. Lett. B **510**, 133 (2001).
[15] E. Ferreiro, E. Iancu, A. Leonidov, and L. McLerran, Nucl. Phys. **A703**, 489 (2002).
[16] W. Buchmuller and A. Hebecker, Nucl. Phys. **B476**, 203 (1996).
[17] A. L. Ayala, M. B. Gay Ducati, and E. M. Levin, Nucl. Phys. **B493**, 305 (1997).
[18] I. Balitsky, Nucl. Phys. **B463**, 99 (1996).
[19] H. Weigert, Nucl. Phys. **A703**, 823 (2002).
[20] Y. V. Kovchegov, Phys. Rev. D **60**, 034008 (1999).
[21] N. N. Nikolaev and B. G. Zakharov, Z. Phys. C **49**, 607 (1991).
[22] A. H. Mueller, Nucl. Phys. **B415**, 373 (1994).
[23] A. H. Mueller and B. Patel, Nucl. Phys. **B425**, 471 (1994).
[24] A. Kovner, J. G. Milhano, and H. Weigert, Phys. Rev. D **62**, 114005 (2000).
[25] A. H. Mueller, Phys. Lett. B **523**, 243 (2001).
[26] J. P. Blaizot, E. Iancu, and H. Weigert, Nucl. Phys. **A713**, 441 (2003).
[27] E. Iancu and A. H. Mueller, Nucl. Phys. **A730**, 460 (2004).
[28] A. Kovner and U. A. Wiedemann, Phys. Rev. D **64**, 114002 (2001).
[29] M. Braun, Eur. Phys. J. C **16**, 337 (2000).
[30] J. Bartels, L. N. Lipatov, and G. P. Vacca, hep-ph/0404110.
[31] E. Levin and K. Tuchin, Nucl. Phys. **B573**, 833 (2000).
[32] E. Iancu, K. Itakura, and L. McLerran, Nucl. Phys. **A708**, 327 (2002).
[33] A. H. Mueller and D. N. Triantafyllopoulos, Nucl. Phys. **B640**, 331 (2002).
[34] A. H. Mueller, Nucl. Phys. **A724**, 223 (2003).
[35] S. Munier and R. Peschanski, Phys. Rev. Lett. **91**, 232001 (2003).
[36] S. Munier and R. Peschanski, Phys. Rev. D **69**, 034008 (2004).
[37] S. Munier and R. Peschanski, Phys. Rev. D **70**, 077503 (2004).
[38] M. A. Kimber, J. Kwiecinski, and A. D. Martin, Phys. Lett.

B **508**, 58 (2001).
[39] N. Armesto and M. A. Braun, Eur. Phys. J. C **20**, 517 (2001).
[40] E. Levin and M. Lublinsky, Nucl. Phys. **A696**, 833 (2001).
[41] M. Lublinsky, Eur. Phys. J. C **21**, 513 (2001).
[42] K. Golec-Biernat, L. Motyka, and A. M. Stasto, Phys. Rev. D **65**, 074037 (2002).
[43] J. L. Albacete, N. Armesto, A. Kovner, C. A. Salgado, and U. A. Wiedemann, Phys. Rev. Lett. **92**, 082001 (2004).
[44] M. Lublinsky, E. Gotsman, E. Levin, and U. Maor, Nucl. Phys. **A696**, 851 (2001).
[45] D. N. Triantafyllopoulos, Nucl. Phys. **B648**, 293 (2003).
[46] M. A. Braun, Phys. Lett. B **576**, 115 (2003).
[47] K. Rummukainen and H. Weigert, Nucl. Phys. **A739**, 183 (2004).
[48] K. Kutak and A. M. Stasto, hep-ph/0408117.
[49] A. Kovner and U. A. Wiedemann, Phys. Rev. D **66**, 051502 (2002).
[50] K. Golec-Biernat and A. M. Stasto, Nucl. Phys. **B668**, 345 (2003).
[51] E. Gotsman, M. Kozlov, E. Levin, U. Maor, and E. Naftali, Nucl. Phys. **A742**, 55 (2004).
[52] E. Iancu and A. H. Mueller, Nucl. Phys. **A730**, 494 (2004).
[53] A. H. Mueller and A. I. Shoshi, Nucl. Phys. **B692**, 175 (2004).
[54] E. Iancu, A. H. Mueller, and S. Munier, hep-ph/0410018.
[55] A. M. Stasto, K. Golec-Biernat, and J. Kwiecinski, Phys. Rev. Lett. **86**, 596 (2001).
[56] A. Freund, K. Rummukainen, H. Weigert, and A. Schafer, Phys. Rev. Lett. **90**, 222002 (2003).
[57] N. Armesto, C. A. Salgado, and U. A. Wiedemann, hep-ph/0407018 [Phys. Rev. Lett. (to be published)].
[58] E. Gotsman, E. Levin, M. Lublinsky, and U. Maor, Eur. Phys. J. C **27**, 411 (2003).
[59] K. J. Eskola, H. Honkanen, V. J. Kolhinen, J.-W. Qiu, and C. A. Salgado, Nucl. Phys. **B660**, 211 (2003).
[60] N. Armesto, Acta Phys. Pol. B **35**, 213 (2004).
[61] M. Gyulassy and L. McLerran, nucl-th/0405013.
[62] D. Kharzeev and M. Nardi, Phys. Lett. B **507**, 121 (2001).
[63] D. Kharzeev and E. Levin, Phys. Lett. B **523**, 79 (2001).
[64] D. Kharzeev, E. Levin, and M. Nardi, hep-ph/0408050.
[65] M. A. Braun and C. Pajares, hep-ph/0405203.
[66] M. A. Braun, Phys. Lett. B **599**, 269 (2004).
[67] D. Kharzeev, E. Levin, and L. McLerran, Phys. Lett. B **561**, 93 (2003).
[68] R. Baier, A. Kovner, and U. A. Wiedemann, Phys. Rev. D **68**, 054009 (2003).
[69] D. Kharzeev, Y. V. Kovchegov, and K. Tuchin, Phys. Rev. D **68**, 094013 (2003).
[70] D. Kharzeev, Y. V. Kovchegov, and K. Tuchin, Phys. Lett. B **599**, 23 (2004).
[71] V. S. Fadin and L. N. Lipatov, Phys. Lett. B **429**, 127 (1998).
[72] M. Ciafaloni and G. Camici, Phys. Lett. B **430**, 349 (1998).
[73] D. A. Ross, Phys. Lett. B **431**, 161 (1998).
[74] Y. V. Kovchegov and A. H. Mueller, Phys. Lett. B **439**, 428 (1998).
[75] N. Armesto, J. Bartels, and M. A. Braun, Phys. Lett. B **442**, 459 (1998).
[76] J. R. Andersen and A. Sabio Vera, Phys. Lett. B **567**, 116 (2003).
[77] J. R. Andersen and A. Sabio Vera, Nucl. Phys. **B679**, 345 (2004).
[78] S. J. Brodsky, V. S. Fadin, V. T. Kim, L. N. Lipatov, and G. B. Pivovarov, JETP Lett. **70**, 155 (1999).
[79] C. R. Schmidt, Phys. Rev. D **60**, 074003 (1999).
[80] J. R. Forshaw, D. A. Ross, and A. Sabio Vera, Phys. Lett. B **455**, 273 (1999).
[81] M. Ciafaloni, D. Colferai, G. P. Salam, and A. M. Stasto, Phys. Lett. B **587**, 87 (2004).
[82] G. Altarelli, R. D. Ball, and S. Forte, Nucl. Phys. **B674**, 459 (2003).
[83] V. A. Khoze, A. D. Martin, M. G. Ryskin, and W. J. Stirling, Phys. Rev. D **70**, 074013 (2004).
[84] A. H. Mueller, Phys. Lett. B **396**, 251 (1997).
[85] A. Babansky and I. Balitsky, Phys. Rev. D **67**, 054026 (2003).
[86] L. N. Lipatov, Zh. Eksp. Teor. Fiz. **90**, 1536 (1986) [Sov. Phys. JETP **63**, 904 (1986)].
[87] J. C. Collins and J. Kwiecinski, Nucl. Phys. **B316**, 307 (1989).
[88] K. Golec-Biernat and M. Wusthoff, Phys. Rev. D **59**, 014017 (1999).
[89] G. Chachamis, M. Lublinsky, and A. Sabio Vera, hep-ph/0408333.
[90] K. Golec-Biernat, hep-ph/0408255.
[91] E. M. Levin and M. G. Ryskin, Yad. Fiz. **45**, 234 (1987) [Sov. J. Nucl. Phys. **45**, 150 (1987)].
[92] E. Levin and K. Tuchin, Nucl. Phys. **A693**, 787 (2001).